AN EXPERIMENTAL STUDY OF THE THREE DIMENSIONAL STRESS-STRAIN BEHAVIOR OF WHEAT EN MASSE

By

HARVEY BRIGHT MANBECK

Bachelor of Science
Pennsylvania State University
University Park, Pennsylvania
1963

Master of Science
Pennsylvania State University
University Park, Pennsylvania
1965

Submitted to the Faculty of the Graduate College
of the Oklahoma State University
in partial fulfillment of the requirements
for the Degree of
DOCTOR OF PHILOSOPHY
July, 1970

AN EXPERIMENTAL STUDY OF THE THREE DIMENSIONAL

STRESS-STRAIN BEHAVIOR OF

WHEAT EN MASSE

Thesis Approved:

G. L. Nelson
Thesis Adviser

E. W. Schroeder

George W. C. Dahlberg

Donald E. Boyd

D. Durham
Dean of the Graduate College

ACKNOWLEDGMENTS

This study was conducted as a part of Oklahoma Agricultural Experiment Station Project 1429.

The author is especially indebted to his major adviser, Dr. Gordon L. Nelson. This thesis could not have become reality without his capable guidance, assistance and encouragement throughout all phases of the study.

For their assistance throughout the study, my sincere appreciation is extended to the other members of the Advisory Committee: Professor E. W. Schroeder, Head of the Agricultural Engineering Department; Mr. G. W. A. Mahoney, Assistant Professor of Agricultural Engineering; and Dr. D. E. Boyd, Associate Professor of Mechanical and Aerospace Engineering. Their criticism and suggestions have been invaluable.

For providing facilities and assistantships during the study, I extend my appreciation to Professor E. W. Schroeder.

My thanks is extended to Jack Fryrear and Norman Griffin for assistance in preparation of the figures.

A special thanks is extended to Dr. B. L. Clary, Assistant Professor of Agricultural Engineering, for his encouragement throughout the study and for his critique of the manuscript.

I am grateful to Mrs. Rita Kreutziger for her efforts in typing the rough draft of the manuscript and to Mrs. Karen Metz for her efforts in typing the final draft of the manuscript.

TABLE OF CONTENTS

Chapter		Page

Chapter | Page

LIST OF TABLES

Table | Page

LIST OF FIGURES

Figure		Page

Figure Page

Figure Page

CHAPTER I

INTRODUCTION

Background Information

Design loads for grain and fertilizer storage structures are currently predicted by the grain pressure theories of Janssen (22), Airy (1), and Riembert (41). Janssen's theory has found the most widespread acceptance in the United States, while in Europe the solution of Riembert is most commonly used.

These theories are inadequate for the design of thin walled deformable storage structures now commonly found in agricultural enterprises. The inadequacies result directly from the following limitations.

All existing grain pressure theories are one or two dimensional approximations of a three dimensional state of stress. Jaky (21) proposed a two dimensional solution to grain bin loads, whereas the remaining theories are one dimensional solutions. None of the existing theories are general enough to allow the designer to consider the loads indueed by expansion and/or contraction of the stored granular media caused by changes in temperature and/or moisture content. This is of importance as most granular media encountered in agriculture are hygroscopic materials. Dale and Robinson (12) observed that lateral pressures in deep bins increased nearly six-fold with moisture increases of 1 to 4 percent in wheat.

The most severe limitation of these grain pressure theories is that they assume the confining structure to be an infinitely rigid body. It has been observed by Terzaghi (52) in studies of soils that confining wall deformations of only several hundredths of an inch resulted in large changes in the pressure distribution on the wall. Similarly, Hamilton (16) noted large increases in the pressures exerted by grain on circular cylindrical bins when the bin walls were displaced towards the grain. Jenike (23) in his work with grain hoppers also noted that small wall deformations resulted in large variations in the resulting pressure distributions. Collins (9), Saul (46), and Dabrowski (11) observed that bin wall flexibilities significantly altered the magnitude and distribution of the loads on bin walls.

The inadequacy of the existing theories is further demonstrated by the discrepancies observed between measured bin loads and those predicted by theory. The studies of Hamilton (16), Stewart (51), Collins (9), Jenike (23), Dabrowski (11), Saul (46), and Isaacson (20) indicated that large differences exist between measured and predicted loads in grain storage structures.

The stress distribution in an arbitrary storage system could be obtained by application of the three dimensional theory of continuum mechanics. Such an approach to the grain pressure problem would inherently include the interaction between the bin wall and granular medium and would allow for the consideration of the expansion and contraction of the granular medium with moisture content and temperature.

Employment of the theory of continuum mechanics to a grain storage system requires that the three basic conditions of mechanics be defined. These conditions are those of equilibrium, kinematics, and constituency. The first two conditions are dependent solely upon the geometry of the system and are defined in any standard text of continuum mechanics. Constituency, the stress-strain behavior, is independent of the geometry, but is dependent upon the material properties of the system.

Generally, the stress-strain behavior of the bin wall is known, whereas the three dimensional stress-strain behavior of the stored granular media en masse is unknown. Thus, it is necessary that the stress-strain behavior of granular media en masse be defined before a rational solution to the grain pressure problem can be attempted.

Objectives

Based on the background information, the literature review of the following chapter, and time limitations, the objectives of this study are:

1. To define methods and techniques adequate for evaluating the three dimensional static stress-strain behavior of granular media encountered in agricultural enterprises.
2. To evaluate the three dimensional static stress-strain behavior of a granular medium en masse.

Scope of the Study

The static stress-strain behavior of only one granular medium en masse, say wheat, at one physical state will be investigated. The initial venture into this field of study would become too unwieldy if variations in moisture contents and/or physical properties of the medium were considered. It is more important that the feasibility of the techniques be demonstrated for one set of conditions. Generalization should be the goal of subsequent studies.

All stress levels are assumed to be below the level at which macroscopic failure occurs. Macroscopic failure stress is defined as the stress level at which flow commences. That is, the stress level at which strain continues to increase without bounds--without any increase in stress level. This type of failure is differentiated from microscopic failure which occurs continuously in the form of arrested slips as individual grains slide over one another during the deformation process.

Only normal stresses and strains were considered in the investigation. No attempt was made to study the effects of shear stresses.

Prediction equations for strain have been developed for normal strains for the stress paths anticipated in grain storage systems. The equations are also limited to the first cycle of loading and to stress paths in which the ratio of normal stresses, $\sigma_1:\sigma_2:\sigma_3$, remain constant during loading and unloading.

Definition of Symbols

Many quantities appear repeatedly throughout the report, and therefore, are designated by symbols. Unless otherwise noted in the text, the symbols are defined according to the following list.

Symbol	Quantity
A_i	Dimensionless function of π_2 and π_3
a_i	Slope of loading curve in log-log space in the ith direction
D	Approach of the centers of two contacting bodies under contact forces, in.
ΔV	Corrected volumetric deformation, cu. cm.
ΔV_c	Volumetric deformation due to membrane compression, cu. cm.
ΔV_{corr}	Volumetric deformation due to membrane indentation and compression, cu. cm.
ΔV_g	Volumetric deformation due to grain deformation, cu. cm.
ΔV_I	Volumetric deformation due to membrane indentation, cu. cm.
ΔV_t	Volumetric deformation due to membrane indentation, membrane compression and grain deformation, cu. cm.
ΔV_{raw}	Raw volumetric deformation, cu. cm.
e	Base of natural logarithms
e_o	Initial voids ratio
ϵ_1	Principal strain in a horizontal direction, in./in.
ϵ_2	Principal strain in a horizontal direction perpendicular to ϵ_1, in./in.
ϵ_3	Principal strain in the vertical direction, in./in.
$\epsilon_i)_e$	Elastic component of strain in the ith direction, in./in.
$\epsilon_i)_H$	Strain in ith direction due to contact stresses, in./in.
ϵ_{im}	Strain level in the ith direction at which unloading commenced, in./in.
$\epsilon_i)_p$	Plastic component of strain in the ith direction, in./in.
$\epsilon_i)_R$	Strain in ith direction due to particle reorientation, in./in.
$\epsilon_i)_T$	Total strain in the ith direction, in./in.
ϵ_{oi}	Instantaneous strain in the ith direction in a creep test, in./in.

f_i	Designation of an arbitrary function
G	Shear modulus, psi.
H	Height of a wheat kernel, in.
i	Subscript designating principal stress directions
L	Subscript designating a loading function
$\bar{n}_h$	Mean slope of the unloading curve in log-log space in any horizontal direction
n_i	Slope of the unloading curve in log-log space in the ith direction
$\bar{n}_v$	Mean slope of the unloading curve in log-log space in the vertical direction
p	Pressure applied to the stress plate, psi.
ϕ	Angle of internal friction, degrees
ϕ_i	Dimensionless coefficient in prediction equations
π_1	The dependent pi-term. The principal strain in the ith direction, in./in.
π_2	Stress ratio σ_1/σ_3
π_3	Stress ratio σ_2/σ_3
π_4	Stress ratio σ_1/σ_c
R	Correlation coefficient
r	Radial distance the load cylinder is located from the centroid of the stress plate, in.
S	Standard deviation from regression
σ_o	Hydrostatic compressive stress, psi.
σ_1	Principal stress in a horizontal direction, psi.
σ_2	Principal stress in a horizontal direction perpendicular to σ_1, psi.
σ_3	Principal stress in the vertical direction, psi.
σ_c	The characteristic stress level for wheat en masse, psi.
σ_{im}	Stress level in the ith direction at which unloading commenced, psi.

t	Time from application of a load, min.
τ_i	Characteristic time in the ith direction, min.
θ	Counterclockwise angle of rotation from the y-axis to the location of the load cylinder on the stress plate, degrees
U	Subscript designating an unloading function

CHAPTER II

LITERATURE REVIEW

Stress-Strain Behavior of Granular Soils

Theoretical Considerations

Evaluation of stresses within granular media has long been accomplished by the limiting stress approach. This approach is discussed in standard texts on earth pressure theory such as Terzaghi (53). The theory does not center upon the constitutive behavior of the granular medium, but it is concerned with the limiting, or the active and passive, states of stress in the medium. That is, the theory is dependent upon the stress levels at which failure occurs, but says nothing about the path between the two limiting cases.

Recently, soil mechanicians have taken a more fundamental approach to the determination of stresses within granular media. Cox, et.al. (10) summed up the deficiencies of the limiting stress approach to the problem of earth pressures.

> "Until quite recently, an important deficit in the theory of earth pressure lay in its development without reference to stress-strain relationships, the theory being based upon the concept of states of limiting equilibrium satisfying Coulomb's law of soil failure in conjunction with a conjectural extremum principle. This procedure altogether neglects the important fact that stress-strain relations are an essential constituent of a complete theory of any branch of the continuum mechanics of deformable bodies."

Cox, et.al. (10) investigated the deformation of granular media with particle sizes ranging from clay to sand and for a range of soils from saturated clay to dry sand. It was found theoretically that under quasi-static axially symmetric deformation, the behavior of natural soil is approximated by an ideal soil which obeys Coulomb's yield criterion and associated flow rule. The soil deformations were found to be characterized by a rigid-perfectly plastic stress-strain relationship.

Other investigators studied the stress-strain relationships of granular and cohesive medium by assuming different idealized deformation relationships. For example, Biot (5) assumed that the relationship was viscoelastic in nature; Shield (48) assumed, as did Cox (10), that the relationship was rigid-perfectly plastic; and Drucker, et.al (13) assumed that the relationship was elastic-plastic with work hardening before failure and perfectly plastic after failure.

Brown (6) cited limitations of the work hardening theory presented by Drucker, et.al. (13) since the mechanical strength of the soil due to friction is not included in work hardening. Based on the assumptions that: (1) Sand is a structure consisting of elastic grains of known geometry and properties; (2) Coulomb friction is developed at points of particle contact; (3) Changes in internal geometry in an incremental displacement are insignificant; and (4) Sand is isotropic and homogeneous, Brown developed an incremental stress-strain theory for sand and an associated yield function. Of interest in his study are two hypotheses relating to the behavior of sand under deformation: (1) A purely deviatoric external agency must do positive work on the displacements it causes (for stable deformation); and (2) The effect of straining on a sand aggregate is to transform it from one randomly disordered configuration to another. The consequences of these hypotheses are that the hydrostatic component of the external agency is zero and continuing macroscopic isotropy exists in the mass of sand.

Roscoe, et.al. (42), in discussing the yielding of clays, assumed the soil to be an elastic-plastic continuously isotropic medium. Further, he pointed out that if stress-strain relationships of soils are desired, it is necessary to define both hydrostatic and deviatoric stress parameters. These parameters are defined, respectively, by the volumetric strain and the shear strain relationships.

The Hertz theory (19) of contact stresses for spherical points of contact has been used by various authors to help define the stress-strain relationship of noncohesive granular medium. Briefly, this theory states that the radius of the area of contact of the two spheres is given by the relationship:

$$a = \sqrt[3]{\frac{3\pi}{4} \quad \frac{P(k_1 + k_2)\ R_1 R_2}{R_1 + R_2}} \tag{1}$$

where a = radius of contact area between spheres, in.

P = applied normal load between the spheres, lb_f.

R_1 = radius of curvature of sphere 1, in.

R_2 = radius of curvature of sphere 2, in.

$k_1 = \dfrac{1 - \nu_1^2}{\pi E_1}$, sq.in./$lb_f$.

$k_2 = \dfrac{1 - \nu_2^2}{\pi E_2}$, sq.in./$lb_f$.

ν_1 = Poisson's ratio for sphere 1.

ν_2 = Poisson's ratio for sphere 2.

E_1 = Young's modulus for sphere 1, psi.

E_2 = Young's modulus for sphere 2, psi.

Also, the Hertz method predicts that the compressive displacement, D, of two points along the normal to the points of contact is

$$D = \sqrt[3]{\frac{9\pi^2}{16} \quad \frac{P^2(k_1 + k_2)^2 \ (R_1 + R_2)}{R_1R_2}} \tag{2}$$

Ko and Scott (27) measured the volumetric strain of a granular noncohesive material and found that it did not vary linearly with the 2/3 power of external pressure as predicted by Equation 2. They concluded that the discrepency was due to an increasing number of points of contact within the mass as the pressure increased. A "holey" model was suggested to describe this effect. The use of the "holey" Hertzian theory supported Ko's experimental results for hydrostatic states of stress.

The Hertzian theory and Ko's results did not consider the effects of tangential forces between spheres. Mindlin, (33), in a theoretical study of the displacement of two spheres in contact subjected to a monotonically increasing tangential load, found that at a point of contact slip occurs on an annulus of outer radius, a (same radius as defined in Equation 1), and inner radius,

$$c = a(1 - \frac{T}{fN})^{1/3} \tag{3}$$

where c = inner radius of annulus of slip, in.

a = outer radius of annulus of slip, in.

T = tangential contact force, lb_f.

N = normal contact force, lb_f.

$f = dT/dN$.

Mindlin (33) also developed an expression for the relative displacement of the centers of two spheres

$$\delta = \frac{3fN(2-\nu)\left[1-\left(1-\frac{T}{fN}\right)^{2/3}\right]}{8\,Ga} \tag{4}$$

where δ = relative displacement of centers of two spheres, in.

ν = Poisson's ratio of the spheres

G = shear modulus of the spheres, psi.

The tangential compliance of spheres in contact was also developed by Mindlin (33) and may be represented by the equation

$$S = \frac{d\delta}{dT} = \frac{2(1-\nu)}{8\,Ga\left(1-\frac{T}{fN}\right)^{1/3}} \tag{5}$$

where S = the tangential compliance, in./lb_f.

Mindlin, et.al. (35) studied the behavior of granular particles when subjected to an oscillating tangential contact force where $T \leq fN$ and found that a stable cycle was obtained after the first quarter cycle of loading.

Mindlin and Deresiewicz (34) studied the same problem discussed above, but included the effect of a varying tangential contact force of constant obliquity superimposed over a constant initial normal contact force N_o. They developed a theory for the first loading and unloading cycle and the subsequent stabilized cycle of loading. For the stabilized cycle, if the tangential force varies from +T* to -T*, the tangential compliance is defined by S_R for the loading cycle.

$$S_R = \frac{d\delta}{dT} = \frac{2 - \nu}{4\ Ga} \left\{ \theta + (1 - \theta)\left[1 - (1 + \theta)\frac{L^* + L}{2(1 + \theta L)}\right]^{-1/3} \right\} \tag{6}$$

where $\theta = f/\beta$

$L = T/fN_o$

$L^* = T^*/fN_o$

$\beta = dT/dN \geq f$

T^* = maximum value of the tangential force, lb_f.

For the unloading cycle they found the compliance to be obtained by reversing the signs of θ and L in Equation 6.

Duffy and Mindlin (14) derived the differential stress-strain relation for a medium composed of a face centered cubic array of elastic spheres in contact. The theory was based on the theory of elastic bodies in contact and includes the effects of both normal and tangential components of contact forces. They concluded that the relation between strain and the normal contact force is nonlinear, but elastic; and that the relation between the tangential component of force and displacement is inelastic and nonlinear. They concluded further that the stress-strain relationship is dependent upon the loading history of the medium and is necessarily incremental in nature.

Duffy and Mindlin (14) derived the governing differential equations for granular media by considering the equilibrium conditions and the conditions of the compatability of relative displacements. The equilibrium equations (Equations 7) were obtained by considering each sphere to have twelve points of contact with two tangential and one normal component of force at each contact point.

In Equations 7 the following notation is used. dN_{ij}, dT_{ij}, and dT_{kk} are the force increments for a contact with its normal in the i-j plane. Consequently, dN_{ij} and dT_{ij} lie in the i-j plane, whereas dT_{kk} is normal to the i-j plane. The symbol dP_{ij} is the force increment applied to the face of a cubical element of particles.

For each cubical element there are 36 contact force components; only 18 of which are independent since they are diametrically opposite 18 other force components. Also, since each sphere and portion of a sphere are in equilibrium, as well as is the entire cubical element, there are only 9 independent equations of equilibrium.

Note that in Equations 7 the primed elements indicate that the contact normal is opposite in sign to the unprimed contact normal; and that the 9 equations of equilibrium are obtained by selecting any three of the four equations in Equation set 7 and cycling the subscripts.

$$
\begin{aligned}
&4dT_{xx} + 2\sqrt{2}\,(dN_{xx} + dN_{xy} - dT_{zx} + dT_{xy}) = dP_{xx} + dP_{xy} + dP_{zx} \\
&4dT'_{xx} + 2\sqrt{2}\,(dN'_{xz} + dN_{xy} + dT'_{zy} + dT_{xy}) = dP_{xx} + dP_{xy} - dP_{zx} \\
&4dT_{xx} - 2\sqrt{2}\,(dN'_{zx} + dN'_{xy} - dT'_{zx} + dT'_{xy}) = -dP_{xx} + dP_{xy} - dP_{zx} \\
&4dT'_{xx} - 2\sqrt{2}\,(dN_{zx} + dN'_{xy} - dT_{zx} + dT'_{xy}) = -dP_{xx} + dP_{xy} - dP_{zx}
\end{aligned}
\qquad (7)
$$

Similarly, Duffy and Mindlin (14) wrote the set of equations for compatability of relative displacements. Note that $d\alpha_{ij}$ is the displacement corresponding to dN_{ij}, $d\delta_{ij}$ is the displacement corresponding to dT_{ij}, and $d\delta_{kk}$ is the displacement correspondong to dT_{kk}. Any three of the set of Equations 8 plus six more obtained by cyclic permutation of the subscripts define the relative displacement conditions.

$$
\begin{aligned}
\sqrt{2}\, d\delta_{zz} &= -d\alpha'_{yz} + d\alpha_{zx} + d\delta'_{yz} + d\delta_{zx} \\
\sqrt{2}\, d\delta_{zz} &= +d\alpha_{yz} - d\alpha'_{zx} - d\delta_{yz} - d\delta'_{zx} \\
\sqrt{2}\, d\delta'_{zz} &= -d\alpha_{yz} + d\alpha_{zx} + d\delta_{yz} + d\delta_{zx} \\
\sqrt{2}\, d\delta'_{zz} &= +d\alpha'_{yz} - d\alpha'_{zx} + d\delta'_{yz} + d\delta'_{zx}
\end{aligned}
\tag{8}
$$

Since the number of equations is less than the number of unknowns, the constitutive relationships are required. Duffy and Mindlin (14) chose to express these in terms of normal and tangential compliances, C_{ij} and S_{ij}, as shown in the set of Equations 9.

$$
\begin{aligned}
d\alpha_{ij} &= C_{ij}\, dN_{ij} & \qquad d\alpha'_{ij} &= C'_{ij}\, dN'_{ij} \\
d\delta_{ij} &= S_{ij}\, dT_{ij} & \qquad d\delta'_{ij} &= S'_{ij}\, dT'_{ij} \\
d\delta_{kk} &= S_{kk}\, dT_{kk} & \qquad d\delta'_{kk} &= S'_{kk}\, dT'_{kk}
\end{aligned}
$$

These three sets of equations, Equation 7, 8, and 9, are sufficient conditions for solving for the stress distributions within a granular medium. However, Mindlin (33) has pointed out earlier that the 19 equations are not linear in components of contact forces since: the equations contain compliances; the compliances are dependent upon the contact forces through the radius, a, of the contact circle; and the compliances are dependent upon the load history of the element. Thus, analytical solution of the system becomes extremely difficult, if not impossible.

Experimental Considerations

Ko and Scott (25) commented on the direction taken by soil mechanists with regard to establishing a valid earth pressure theory.

> "The analytic solutions which have been employed represent situations which are extremely idealized versions of real life counterparts. The solutions referred to are those for various simple stress distributions of linearly elastic isotropic homogeneous media on the one hand; and certain results derived from the upper bounds methods of ideally plastic analysis on the other. It seems to the authors (Ko and Scott) that this situation has inhibited the study of the real stress-strain behavior, or constitutive relations of soils, and that work has consequently tended to concentrate on the stress conditions at failure."

Ko and Scott (25) developed a cubical soil test box which permitted independent control of stress in three directions for determining the stress-strain characteristics of soils in general. The apparatus consists primarily of a 4 inch hollow aluminum cube which serves as a housing for six rubber membranes; each of which is mounted on one inside face of the cube. Each membrane, and subsequently the granular medium, is loaded by hydraulic pressure.

The loading of the stress box is controlled by a mechanical-hydraulic analog. Ko showed that there exists an exact analog between the location of a concentrated load on a triangular plate supported at its vertices and the position of the stress point, defined by the support reactions, on the octahedral stress plane. The reactions at the vertices correspond to the three principal stresses which are transmitted to the cubical element by means of hydraulic lines.[1]

The advantages of this test apparatus are that: (1) Stresses are controlled in three orthogonal directions; (2) The hydrostatic and deviatoric components of stress can be separated; (3) A particular stress history can be reproduced exactly by simultaneous and proportional changes of the stresses in three orthogonal directions; and (4) More homogeneous states of stress and strain are obtained in the soil sample than in a triaxial shear test sample.

Two other attempts to test cubical samples of soil have been made by Kjellman (24) and Bell (4). However, the testing apparatus developed by these investigators contained deficiencies ranging from mechanical complexity in the former to stress inhomogeneity in the latter. Presently, Ko and Scott's apparatus is the most sophisticated and manageable cubical soil testing apparatus available.

Ko and Scott (26, 27, 28) conducted three dimensional load-deformation tests on sand in which they considered hydrostatic stresses only, deviatoric stresses only, and a combination of hydrostatic and deviatoric components of stress. A summary of their findings follows: (1) A sand sample never before subjected to shear stress is nonlinearly elastic and isotropic at all void ratios when subjected to hydrostatic compression; (2) The compressibility of the sand was not influenced by the shear stress history; (3) The sand remained elastic and isotropic when hydrostatic and deviatoric stress components were superimposed; (4) For straight shear stress paths in an octahedral plane deformations varied

---

[1]This apparatus is described in more detail in Chapter III.

logarithmically with octahedral shear stress; (5) Shear unloading along the same path as loading indicated that the elastic and plastic components of deformation were nearly equal in magnitude; and (6) Shear loading and reloading along straight line stress paths in an octahedral plane produced deformations which varied roughly linearly with octahedral shear stress.

Hardin and Richart (17) determined the dynamic shear modulus of sand using a resonating triaxial column. The tests were conducted by applying an initial confining pressure and torque and then imposing an additional oscillating torque to the sample. The authors concluded that the octahedral shear stress is a measure of the deviatoric stress component. Hardin and Black (18) recorded the following equations for the shear modulus of clean, dry, round grained sand for vibrating loads of small amplitude. σ_o is taken as being equal to the isotropic component of initial static stress independent of the deviatoric component of stress, stress history, and rate of loading. The amplitude of oscillation of shear strain was 2.5×10^{-5}; and the constants in the numerator of Equations 10 and 11 are necessarily dimensional.

$$G = \frac{(32.17 - 14.80e)^2}{1 + e} (\sigma_o)^{1/2} \text{ for } \sigma_o \geq 2000 \text{ psf} \quad (10)$$

$$G = \frac{(22.15 - 10.60e)^2}{1 + e} (\sigma_o)^{3/5} \text{ for } \sigma_o < 2000 \text{ psf} \quad (11)$$

where e = voids ratio

σ_o = isotropic confining pressure, psf.

G = shear modulus, psi.

Saada (45) developed and tested a stress controlled triaxial testing apparatus. The true stress was applied pneumatically and could be controlled either manually or automatically. The apparatus has been recommended primarily for use in rheological studies of sensitive clays.

Rowe (44) conducted shear box and triaxial shear tests on cohesionless soils in which he studied the effects of the parameters: sample thickness, soil type, length of the slip line, type of test, soil density, confining pressure, direction of loading, and strain history of the soil. He hypothesized that the slip line theory can be used for intermediate states of deformation (those states between the active and passive states); and contended that ϕ, the internal angle of friction, varies with load and approaches an ultimate value, ϕ_u. He concluded that in a cohesionless soil which is not failing, ϕ is dependent mainly upon the movement of a unit length of the plane subjected to maximum shear and is dependent to a lesser degree upon soil grading and rate of shear. ϕ, he concluded, varies largely with confining pressure, density, strain history and strain direction.

In a more recent study Rowe (43) extended his approach and applied the principle of least work to a random mass of irregular particles. He hypothesized that deformation of a granular medium consists of a number of arrested slides. Equation 12 represents his stress-strain relationship for intermediate stresses.

$$\frac{\sigma_1}{\sigma_3 \left(1 + \frac{dV}{V\epsilon_1}\right)} = \mathrm{Tan}^2 \left(45 + \frac{\phi_u}{2}\right) \tag{12}$$

where σ_1 = axial stress, psi.

σ_3 = lateral stress, psi.

V = initial volume of the sample, cu. in.

$d\dot{V}$ = incremental rate of change in volume, cu. in.

$\dot{\epsilon}_1$ = incremental axial strain rate.

ϕ_u = ultimate angle of internal friction.

Stress-Strain Behavior of Small Grains

Small grains implies agricultural particulate materials such as wheat, corn, and sorghum. Most studies of the load-deformation behavior of small grains have been confined to the behavior of individual kernels. Furthermore, the load-deformation behavior was usually used only as a tool to define some other property of the grain such as the modulus of elasticity or Poisson's ratio of the individual kernel. Nevertheless, the results of these investigations provide some useful insight into the more general three-dimensional stress-strain behavior of small grains en masse.

Mohsenin (36) made the observation that biological materials are generally nonelastic. Instead, they are elastic-plastic with strain hardening since the hysteresis losses associated with most biological materials were observed to decrease with repeated cycles of loading. In the case of the load-deformation behavior of corn kernels, he reported that the mechanical behavior was nonlinearly elastic-plastic. The hysteresis losses associated with the first and second load cycles were 45.3 and 15.6 percent, respectively.

Shpolyanskaya (49) evaluated the modulus of elasticity of wheat grains by applying the Hertz theory of contact stresses and assuming the grains to be spherical. Upon loading the individual grain between two flat plates and measuring the resultant deformations, he determined the modulus of elasticity of wheat grains to be between 5.37 x 10^5 psi and 6.64 x 10^5 psi. Repeated loading and unloading of the kernel showed that after several cycles, the load-deformation behavior approached that of an elastic body.

Zoerb (54, 55) studied the load-deformation behavior of soft winter wheat using small core samples of a kernel. Nonlinear elastic-plastic behavior with strain hardening tendencies were observed. The hysteresis losses decreased from 46.3 in the first load cycle to 26.4 percent in the second load cycle. It was also observed that hysteresis losses increased with the moisture content of the grain. Similar trends were noted for both kernels of corn and pea beans.

Shelef and Mohsenin (47) loaded wheat kernels in various manners to obtain the elastic modulus of wheat. Whole grains were loaded between two flat plates, whole grains were loaded by a spherical indenter 0.016 inch in diameter, whole grains were loaded with a cylindrical indenter, and core samples were compressed between two parallel plates. In each test the load-deformation behavior was found to be elastic-plastic with strain hardening. They reported moduli of elasticity of wheat in the range of 1.57 x 10^5 and 8.30 x 10^5 psi.

Arnold and Roberts (3) also loaded wheat core samples between parallel plates. Their observations confirmed the elastic-plastic nature of cereal grains.

It has been suggested by Stewart (50) that the triaxial compression test be used to evaluate the physical properties of small grains. He used the triaxial compression test method successfully to study the effect of moisture content and specific weight upon the internal friction properties of sorghum grain. The triaxial compression test, however, would not suffice for obtaining the generalized stress-strain behavior of small grains en masse, because it is confined to the case where $\sigma_1 \neq \sigma_2 = \sigma_3$ (The symbols refer to the three principal stresses.), and the stresses and strains in triaxial samples have been shown [See Lambe (31).] to be nonhomogeneous throughout the sample.

The uniaxial compression of wheat en masse in a circular cylindrical testing chamber was studied by Narayan and Bilanski (38). Vertical pressures up to 3000 psi were applied to the sample. The vertical stress-strain behavior was found to be logarithmic at stresses below 500 psi, but tended toward a linear relationship above a vertical stress of 500 psi. This suggested that two modes of deformation were involved. At low stresses the controlling mechanism of deformation was particle reorientation; whereas, at higher stress levels, the predominant mechanism was individual particle deformation. They observed that unloading behavior proceeded along parallel paths with successive load cycles. Also, the unloading paths were parallel even when the stress level at which unloading commenced was varied.

Discussion

It has been observed that only limited studies have been made of the stress-strain behavior of small grains. To be sure no attempts have been made to define the three dimensional stress-strain behavior of small grains en masse.

The three dimensional stress-strain behavior of granular soils en masse has been investigated both theoretically and experimentally. The theoretical approach has not proved to be very successful, because of the complex mechanisms controlling stress-strain behavior.

Among the factors affecting the behavior are particle shape, particle size, mechanical properties of the particles, and the orientation of the particles within the mass. Even if elastic spherical particles of uniform size are assumed to make up the particulate array, the theoretical evaluation of the general stress-strain behavior becomes a formidable task. Since most granular media encountered in agriculture are nonspherical, nonuniform in size, and nonlinearly inelastic, the possibility of attaining a theoretical description of the stress-strain behavior of, say, wheat is remote.

In view of the complex nature of the stress-strain behavior of granular media en masse, and in view of the conclusion reached by Ko and Scott (25) (See page 16.) for granular soils, it has been concluded that an experimental evaluation of the stress-strain behavior of small grains en masse is more feasible than an analytical approach. Furthermore, the experimental apparatus designed by Ko and Scott (25) for evaluating the three dimensional stress-strain behavior of granular soils appears to be adaptable to the study of the mechanical behavior of granular media encountered in agricultural storage systems.

CHAPTER III

EXPERIMENTAL APPARATUS

Composite Description

The primary experimental apparatus used in this investigation is the system developed by Ko and Scott (25) for the study of the static stress-strain behavior of sand. Only minor changes were made to adapt it to use in investigating the static stress-strain behavior of agricultural materials.

Figure 1 is a photograph of the apparatus, sans the air compressor, in the agricultural engineering laboratory at Oklahoma State University. The apparatus was located in a temperature controlled room.

The function of the apparatus is to independently and simultaneously apply uniform stresses to the three pairs of opposite sides of a cubical element of a granular medium and to measure the deformations encountered in each of the three principal stress directions. The resulting strains are assumed to be uniform and homogeneous throughout the sample thickness in each of the three principal stress directions. The application of stresses is accomplished by a mechanical-hydraulic analog. This analog will be discussed in more detail in the section describing the method of operation.

The apparatus consists of eight major components. These components may be located in Figure 1 according to the letter

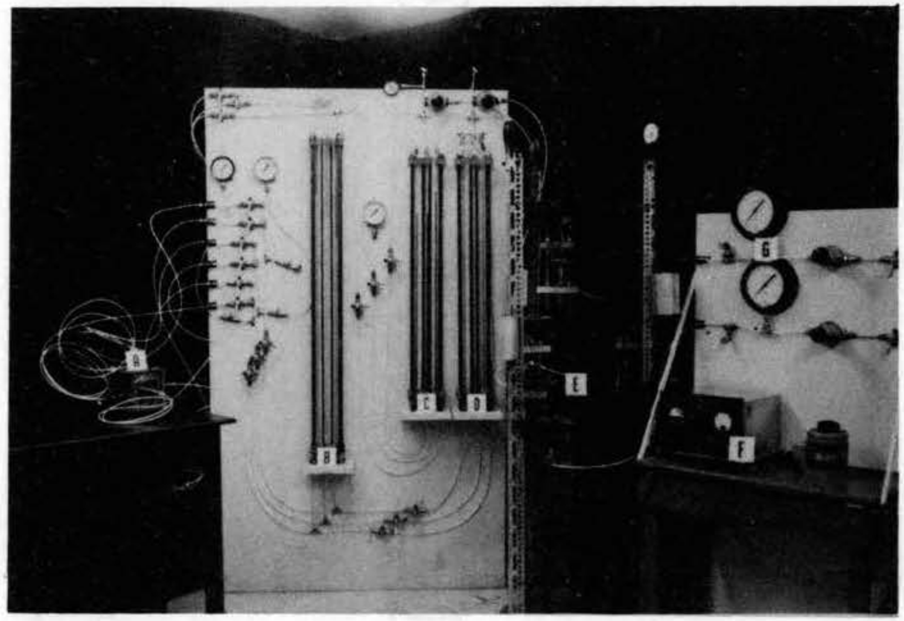

Figure 1. Composite View of the Experimental Apparatus

designations listed below.

A - Stress box

B - Calibrated oil-water tubes

C - Oil reservoirs

D - Water reservoirs

E - Stress control device

F - Rectifier for the electromagnet

G - Pressure gauges for the load cylinders

Another representation of the components and their relationship to one another is given in the schematic diagram in Figure 2. A description of each component and its function is discussed in the following sections.

Stress Control Device

The function of the stress control device is to provide means for simultaneous, continuous, and independent application of stresses in three directions. A photograph and schematic diagram of the stress control device are presented in Figures 3 and 4. The device is supported by three 16 gauge punched steel angle sections which are tied together at the base to form vertices of an equilateral triangle 21 inches on a side.

Three 1/4 inch thick steel triangular plates 21 inches on a side are located inside the triangular frame. These plates are labeled 1, 2, and 3 in Figure 4. Plates 1 and 3 are rigidly fastened to the frame. The distance between the fixed plates is determined only by the size of the cylinders between them. Plate 2 is a free, or

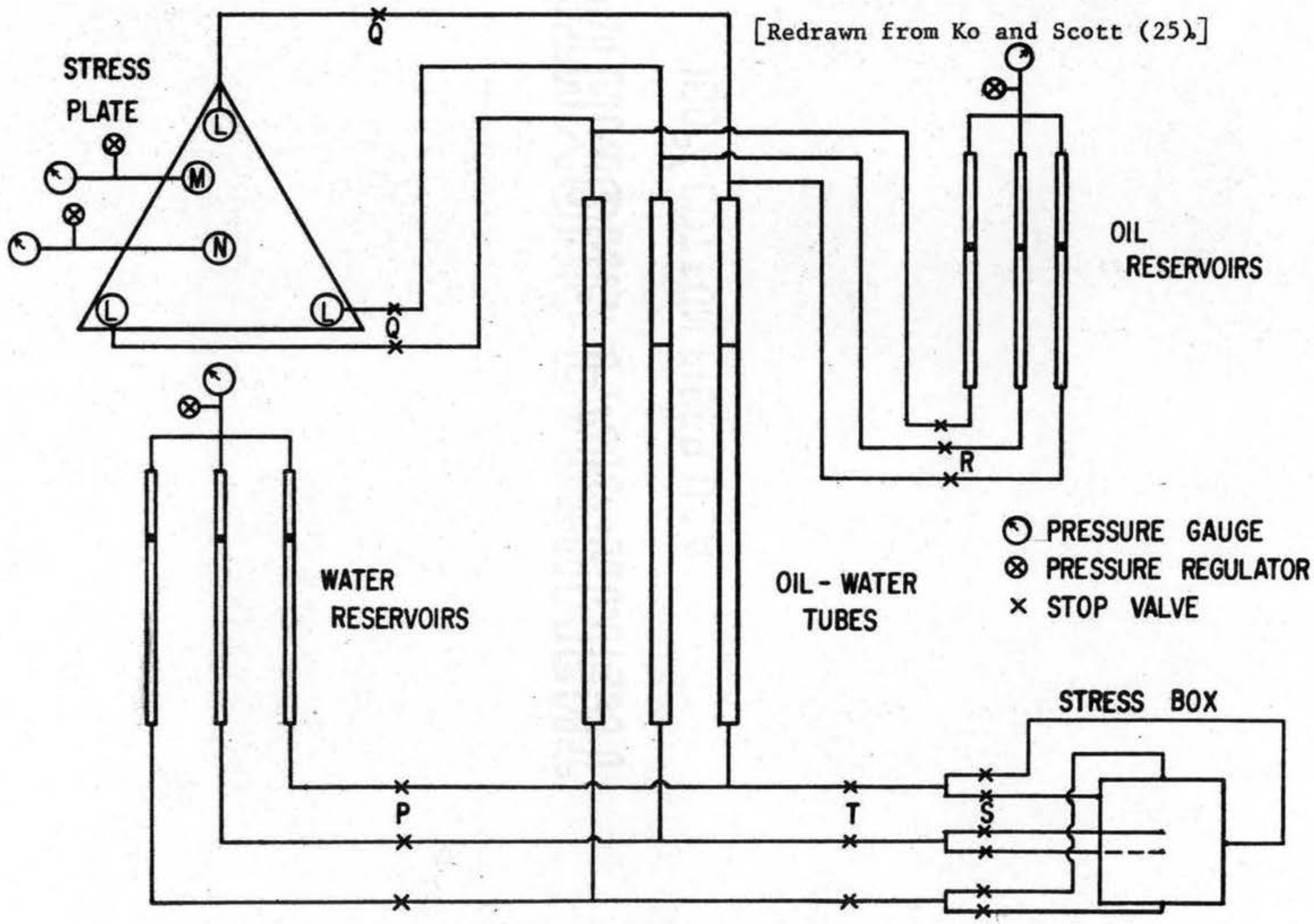

Figure 2. Schematic Diagram of the Experimental Apparatus

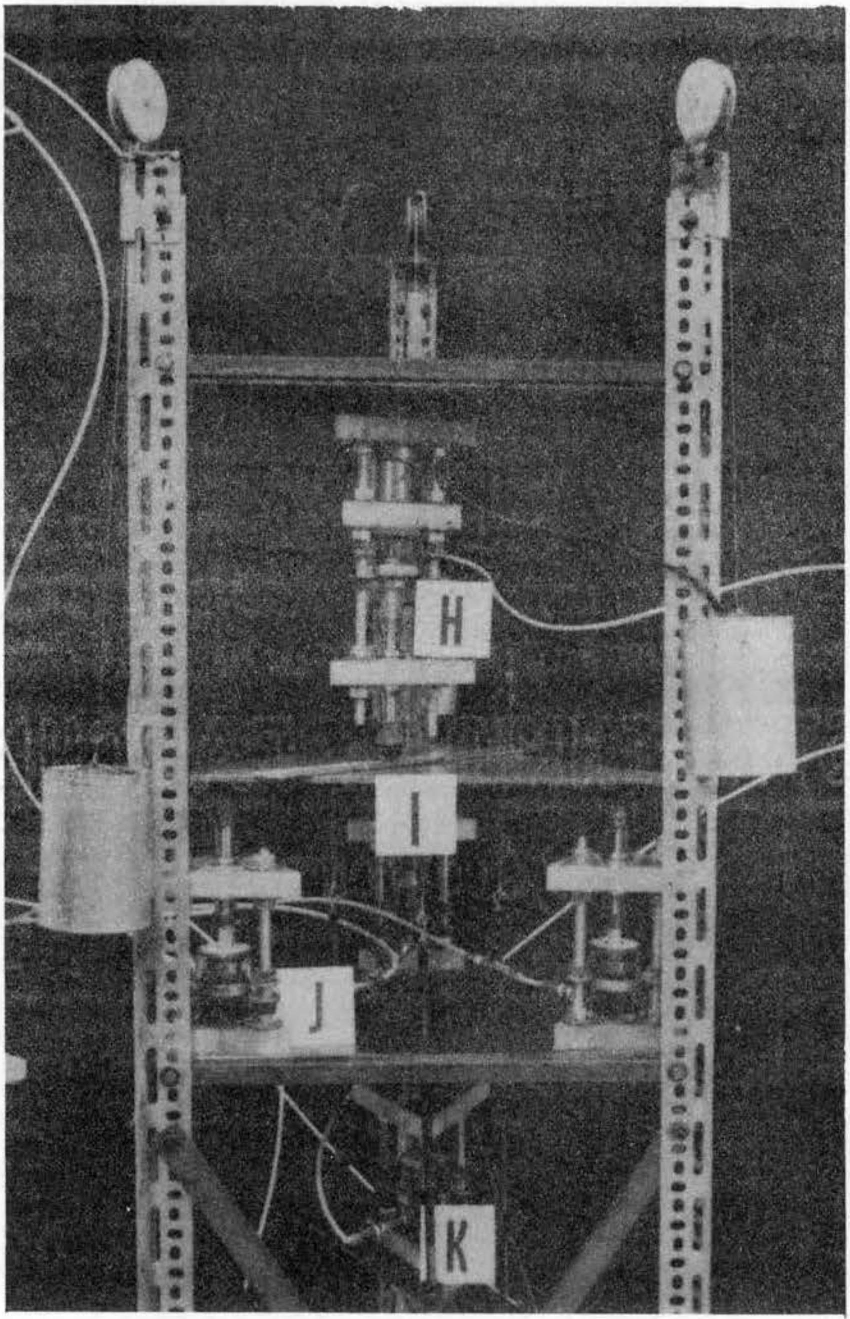

Figure 3. The Stress Control Device

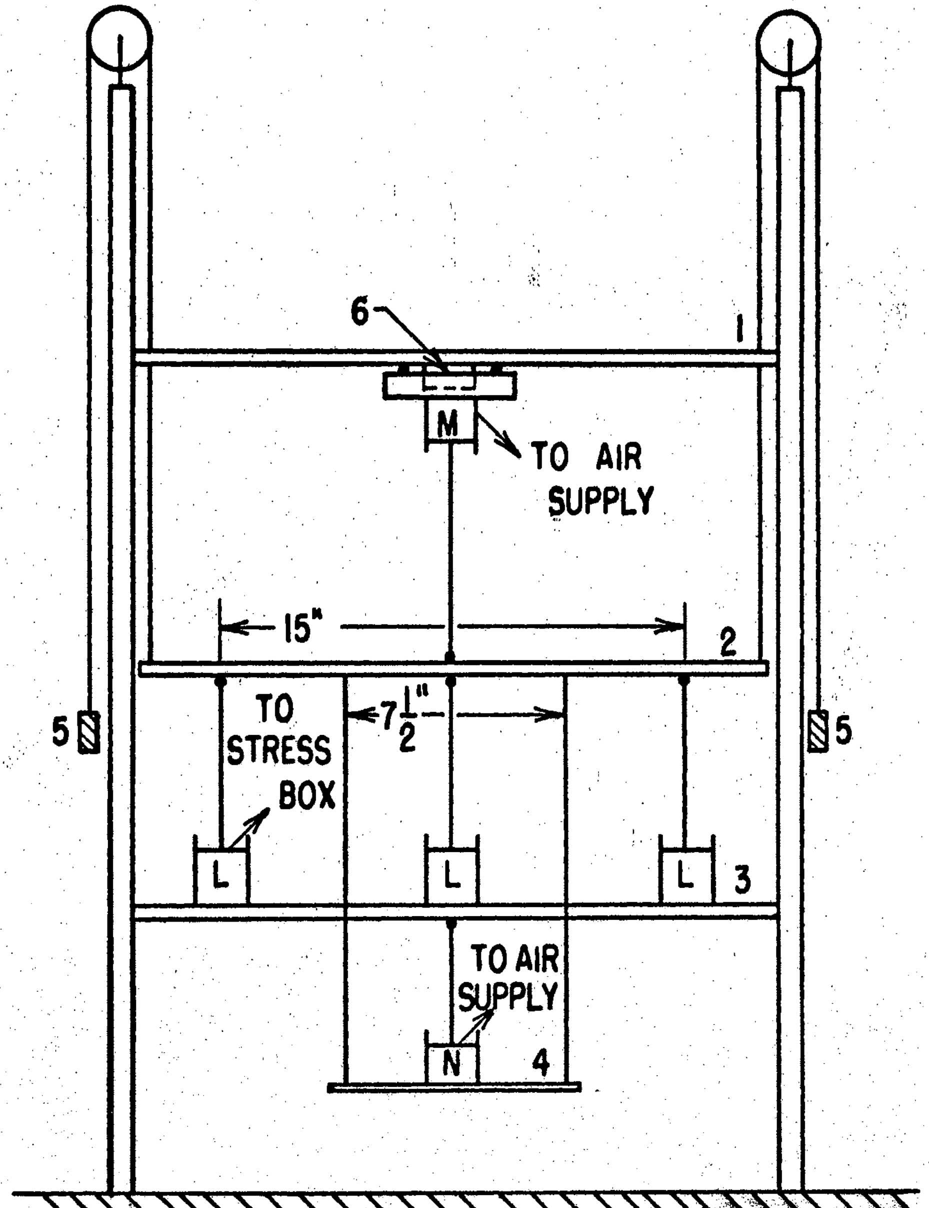

Figure 4. Schematic Diagram of the Stress Control Device [Redrawn from Ko and Scott (25).]

floating, plate. The counterweights, 5, are fastened to plate 2 and exactly balance the weight of the floating plate and any components attached to it. Three ball seats have been machined in plate 2 at the vertices of a 15 inch equilateral triangle. The ball seats serve as sockets for the piston rods of the three middle cylinders.

The cylinders L and M, which have a maximum rated pressure of 60 psi, are all Bellofram Type 10-100 actuators. These cylinders have a stroke of 1.03 inches, a cross sectional area of 2.26 square inches, and a nearly frictionless movement. Cylinders L and N were mounted as shown in Figure 5.

The cylinder mounting served to support and align the cylinder and piston rods. The linear ball bushing in the aligning lucite plate provided a nearly frictionless support for the piston rod. The ball transfer mounted on the piston rod end fits into a ball seat appropriately located on plate 2.

Cylinders L were bolted to plate 3 by means of the threaded rods, whereas the load cylinder M was not fastened to any plate. Instead, it was free to be moved from one location to another between plates 1 and 2.

The mounting for cylinder M varied from that of cylinders L and N in that another one inch thick lucite plate was mounted below the base plate shown in Figure 5. This plate served as a housing for an electromagnet (Item 6 in Figure 4) which was used to hold the load cylinder M in place during a loading test.

Plate 4, which is suspended symmetrically from plate 2, is a 3/16 inch thick triangular steel plate 9 inches on a side. The suspension rods were located at the vertices of a 7 1/2 inch equilateral

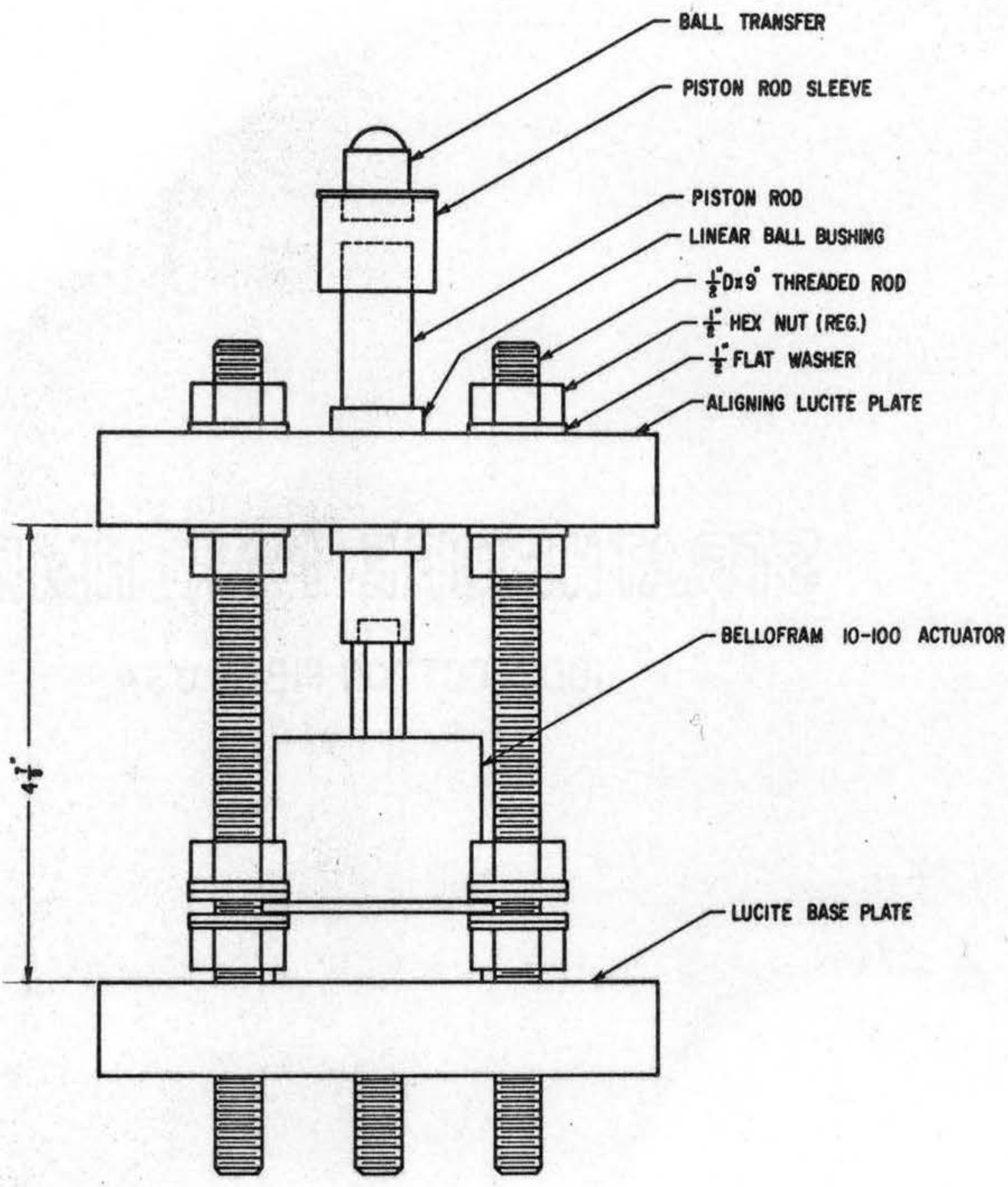

Figure 5. Drawing of the Load Cylinder Mounting

triangle. Cylinder N, which is identical to cylinders L, was bolted rigidly to plate 4. The ball transfer on the piston rod end was aligned with the centroid of plate 2 and fit into a ball seat on the underside of plate 3.

Stress Boxes

Basic Construction

The stress box is the cubical container in which the granular samples are held and loaded. For the study two sample boxes were constructed; one which had inside dimensions of 4 inches on a side and one which had internal dimensions of 6 inches on a side. Other than for size differences, the two boxes were identical in design.

Each stress box was constructed of six 5/8 inch thick aluminum plates. Each plate was square with 45 degree bevelled edges as shown in the vertical section of the box in Figure 6. In each bevelled surface was machined a rectangular groove for a 0.139 inch O-ring. Also, clearance holes for 10-24 machine screws were drilled through each bevelled surface. In two edges of the side plates holes were drilled and tapped for 4-40 machine screws. At the center of each plate a 1/4 inch NPT was drilled and tapped.

The plates for the top and bottom of the box were 9/32 inch smaller on a side than the plates for the sides of the box. The difference in the size of these plates is a consequence of the retaining frame which rests on the top and bottom edges of the side plates.

The retaining frames are made of 0.200 inch thick aluminum and are provided with drilled and tapped holes to accommodate 4-40 machine screws. The retaining frames are fastened, one each, to the top and

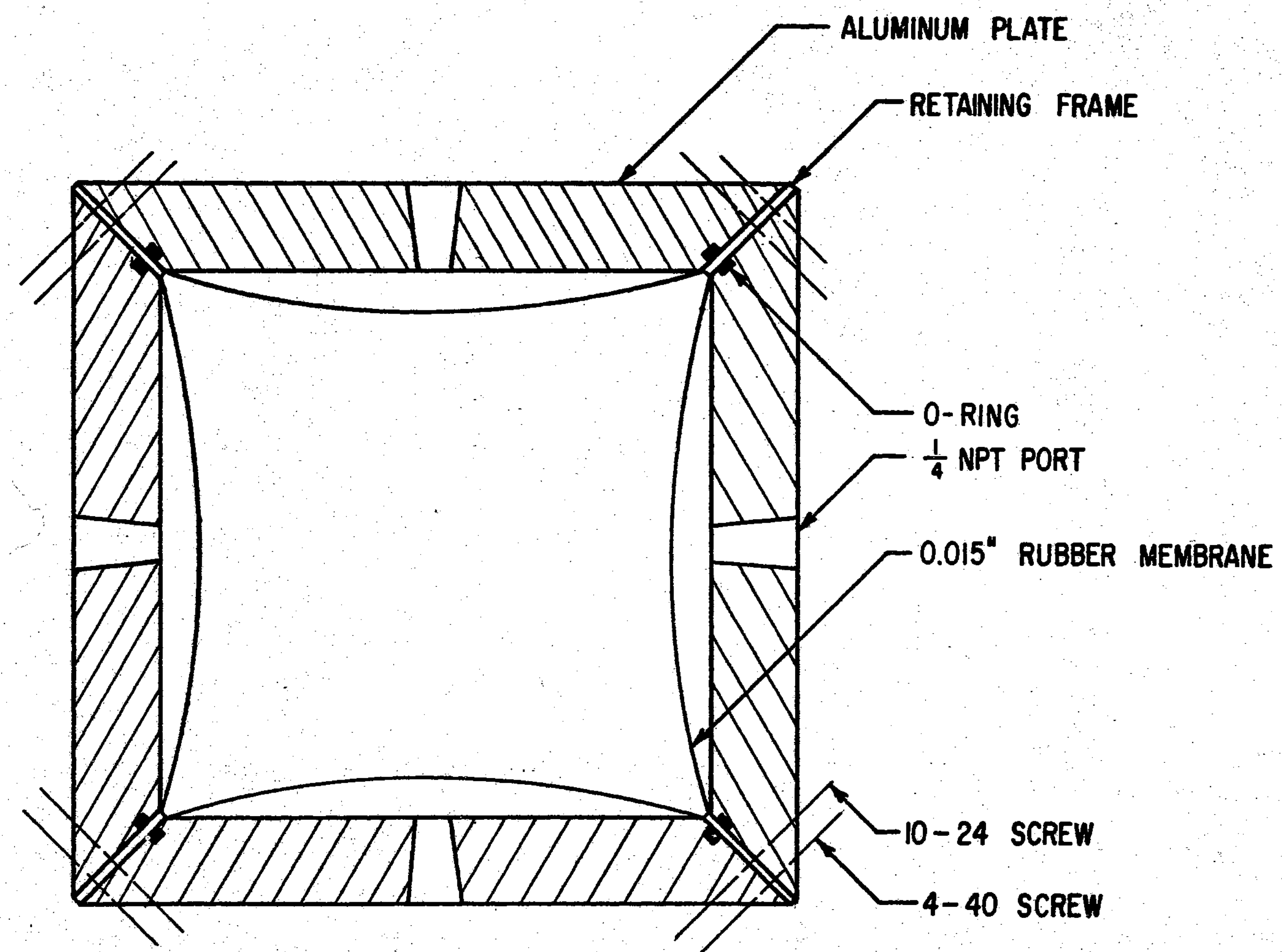

Figure 6. Vertical Section of the Assembled Stress Box [Redrawn from Ko and Scott (25).]

bottom bevelled edges of the side plates in order to separate the top and bottom plates from the side plates. This is desirable, since only the top or bottom plate need be disassembled when preparing a sample. Thus, the latex rubber membranes mounted on the side plates are held in place by the retaining frame when either the top or bottom plate is removed.

On each plate is placed a latex rubber membrane. The membranes were fabricated by a dip process described in a Latex Technical Bulletin entitled "Natural Latex Dipping Process" (30). Molds for the membrane fabrication were made of lucite and were of the same size and shape as the aluminum plates of the stress box sans O-ring grooves. The thickness of the membranes was nearly uniform and was within the range of 0.014 to 0.018 inches.

The membranes were held in place on the plates by means of the 0.139 inch O-rings. Figure 7 shows a view of the top plate with the membrane and O-ring in place.

Adherence to the following assembly procedures assured a water-tight mating of the stress box. A thin coat of low viscosity gasket sealer was applied to the O-ring grooves. Upon mounting the membranes and O-rings onto each plate, the retaining frame components were fastened to each of the side plates. The four side walls were loosely fastened with 10-24 machine screws. Before tightening the screws, the bottom plate was loosely attached to the side plates. Tightening of the screws commenced sequentially until all the screws were secure. It is important that the screws not be turned in the holes or the membranes will tear during the tightening process. The top plate is attached to the box after a sample has been prepared. Again the screws holding the top plate in place must be sequentially tightened. An assembled 4 inch and 6 inch box are both shown in Figure 8.

Auxiliary Components

Apparatus for measuring the uniformity of the strain within the stress box was also constructed. Five micrometer depth gauges were mounted to one of the side plates on each stress box. The 1/8 inch diameter pointers on the depth gauges protruded through clearance holes in the plate.

A series electrical circuit was mounted on the latex rubber membrane. The circuit consisted of 3/16 inch diameter pieces of 0.001 inch brass shim stock connected by fine insulated conducting wire. The wire was brought outside the box by compressing it between the aluminum plate and rubber membrane along the bevelled edge. The locations of the micrometer depth gauges on the plates and the brass shim stock on the membranes are shown in Figure 9.

An ohm meter was placed in series between the circuit and the depth gauges. When all the gauges were backed away from the shim stock circuit, an open circuit resulted. By sequentially lowering the depth gauges until a finite electrical resistance was recorded on the ohm meter, the distance of the membrane from a datum could be determined at any measuring station. An assembled 4 inch stress box with the micrometer depth gauges in place is shown in Figure 10.

Oil-Water Tubes

The oil-water tubes were constructed of thick walled high strength glass tubes 3/8 inch I. D. by 1/2 inch O. D. The tubes were calibrated

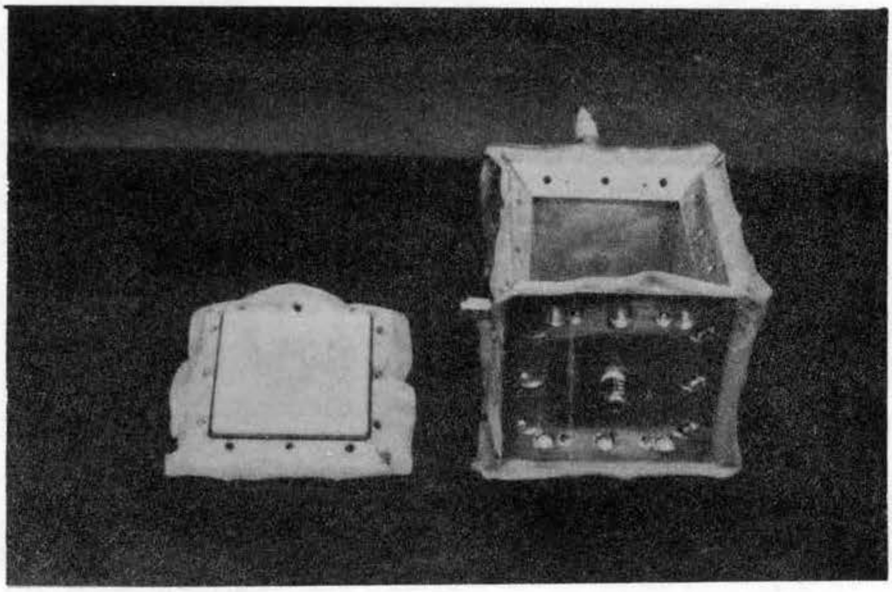

Figure 7. Partially Assembled Four Inch Stress Box

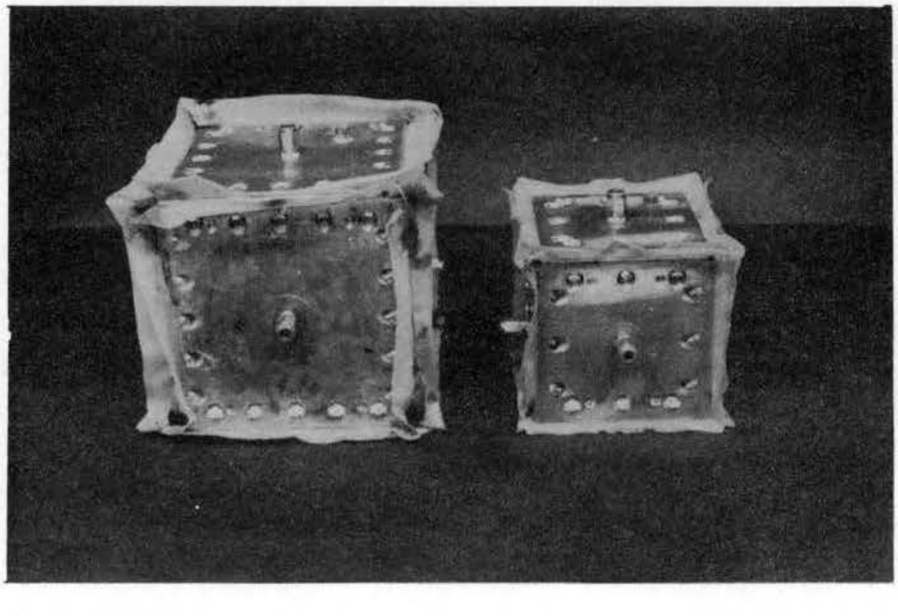

Figure 8. Assembled Four and Six Inch Stress Boxes

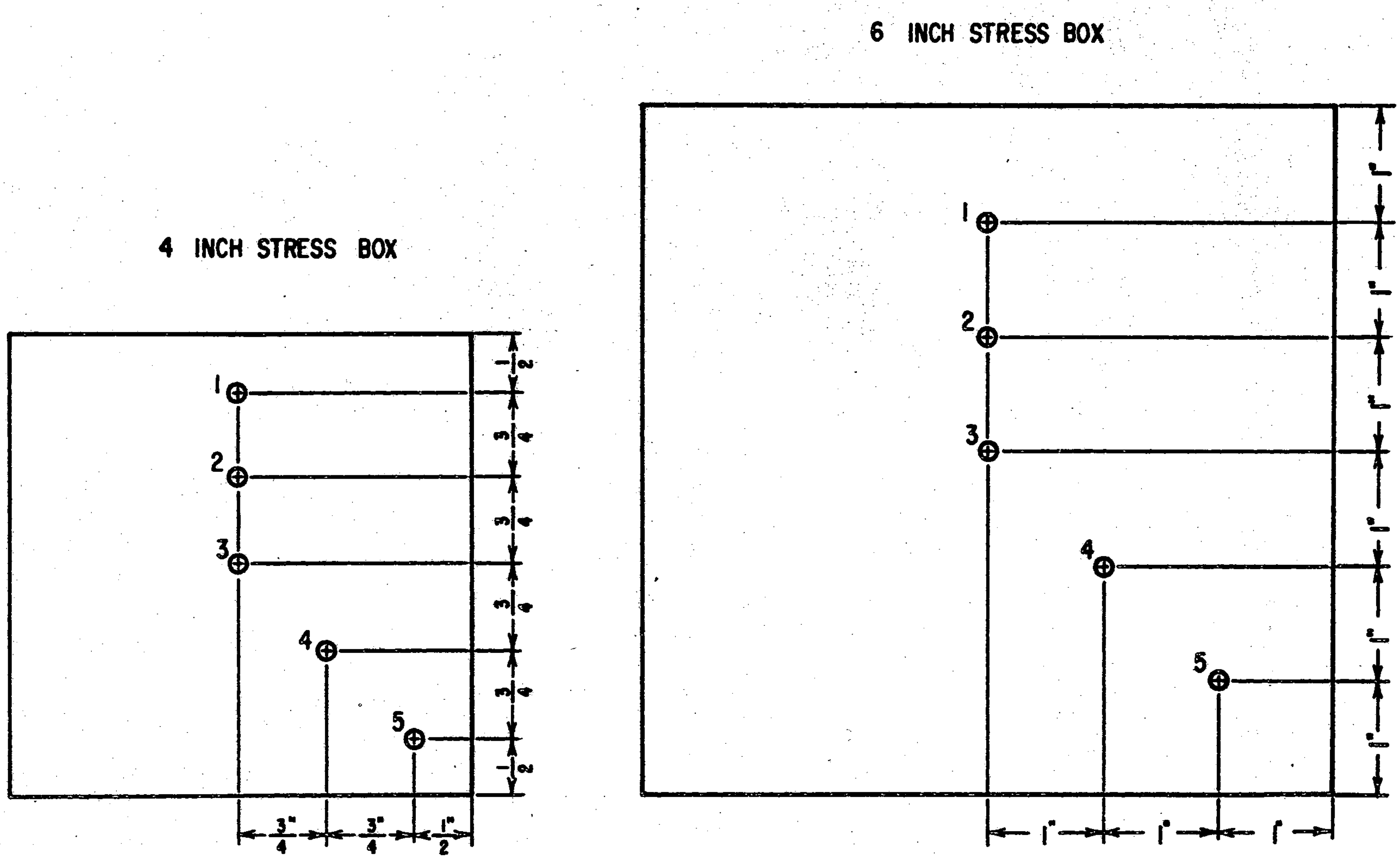

Figure 9. Location of Depth Gauges on the Rubber Membranes

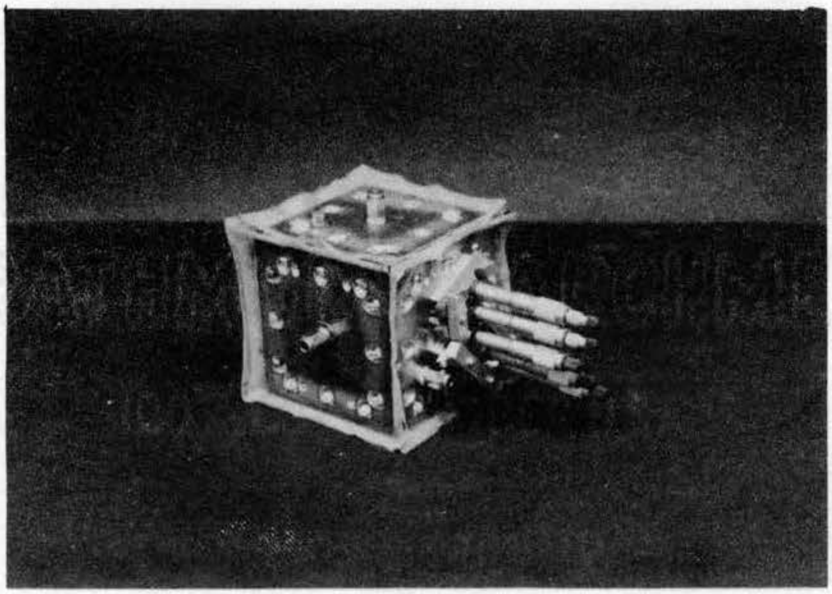

Figure 10. Four Inch Stress Box With Micrometer Depth Gauges in Place

to the nearest 0.1 cubic centimeter and had a range of 0 to 58 cubic centimeters.

The function of these tubes was to measure the change in volume behind the membranes of the stress box. A change in the volume would be accompanied by a change in the oil-water level in the calibrated tube. The oil used in the tube was Mobil D.T.E. oil. Care was taken to remove as much air as possible from both the oil and the water contained in the hydraulic lines.

Oil and Water Reservoirs

These reservoirs were made of regular strength 1/2 inch O.D. glass tubing. The oil reservoirs were not calibrated, but the water reservoirs were calibrated to within 0.1 cubic centimeter and had a capacity of 120 cubic centimeters apiece.

The oil reservoirs served only to supply extra oil when required. The water reservoirs were used as a supply source and also as a means for measuring the amount of water admitted between the plates and membranes of the stress box during sample preparation. This was of importance in evaluating the volume and voids ratio of the test samples.

Auxiliary Equipment

The pressures applied to the load cylinders M and N were controlled by a pressure regulator and measured with bourdon tube pressure gauges. Marshalltown Test Gauges with a 6 inch dial, a least reading of 0.5 psi and an accuracy of 1/4 of one percent of the full scale reading of 100 psi was used for this purpose. A pressure gauge was placed in each of the hydraulic lines extending from the cylinders L.

These gauges were also Marshalltown Test Gauges with an accuracy of 1/4 of one percent of full scale of 100 psi. However, these gauges only had a 3 inch dial and a least reading of 1 psi. They served as a means for periodically checking the line pressures for a given location of the load cylinder M on the floating stress plate. During a load-deformation test each of these gauges was separated from the test apparatus by means of a small gate valve. The entrapped air inside the bourdon tube would have compressed under load, thereby inducing an error in the volumetric deformations.

The rectifier was constructed in the agricultural engineering laboratory. It served to condition the power source for the electromagnet attached to load cylinder M.

Various gate valves were located as shown in the schematic diagram of Figure 2. These valves served to isolate portions of the hydraulic system both while preparing and loading the sample.

Method of Operation

The apparatus described can be used to test the load-deformation behavior of any granular medium which can be placed into the stress box. After a sample is placed into the stress box and the hydraulic lines are connected as shown in either Figure 1 or Figure 2, the method of application of stress is accomplished by only a few simple steps.

First, a stress state and a stress path must be selected. Then the location or locations of the load cylinder M on the stress plate 2 must be determined. Ko and Scott (25) have derived the relationship between the pressure in each of the hydraulic lines leaving cylinders L, the location of the load cylinder, and the magnitude of the pressure in load cylinder M.

Figure 11 is a sketch of the stress plate (Plate 2 in Figure 4). The pressures in the cylinders at the vertices of the stress plate are the principal stresses, σ_1, σ_2, and σ_3. If the distance between vertices of the plate is given by 2ℓ, if a set of coordinates, x and y, is established with origin at the centroid of the stress plate, and if the y-axis is oriented such that it passes through the σ_1-vertex, then the expressions for the principal stresses can be written as:

$$\sigma_1 = \frac{P}{3} (1 + \sqrt{3}\,\bar{y}) \tag{13}$$

$$\sigma_2 = \frac{P}{3} (1 + \frac{3}{2}\bar{x} - \frac{\sqrt{3}}{2}\bar{y}) \tag{14}$$

$$\sigma_3 = \frac{P}{3} (1 - \frac{3}{2}\bar{x} - \frac{\sqrt{3}}{2}\bar{y}) \tag{15}$$

where $P = \sigma_1 + \sigma_2 + \sigma_3$

= pressure applied to the load cylinder M, psi.

$\bar{x} = \frac{x}{\ell}$

$\bar{y} = \frac{y}{\ell}$

σ_i = principal stress in the ith direction, psi.

Equations 13, 14, and 15 can be more conveniently expressed in terms of the angle θ measured counterclockwise from the y-axis, and the distance r from the centroid of the stress plate.

Noting that

$$x = r \sin\theta \tag{16}$$

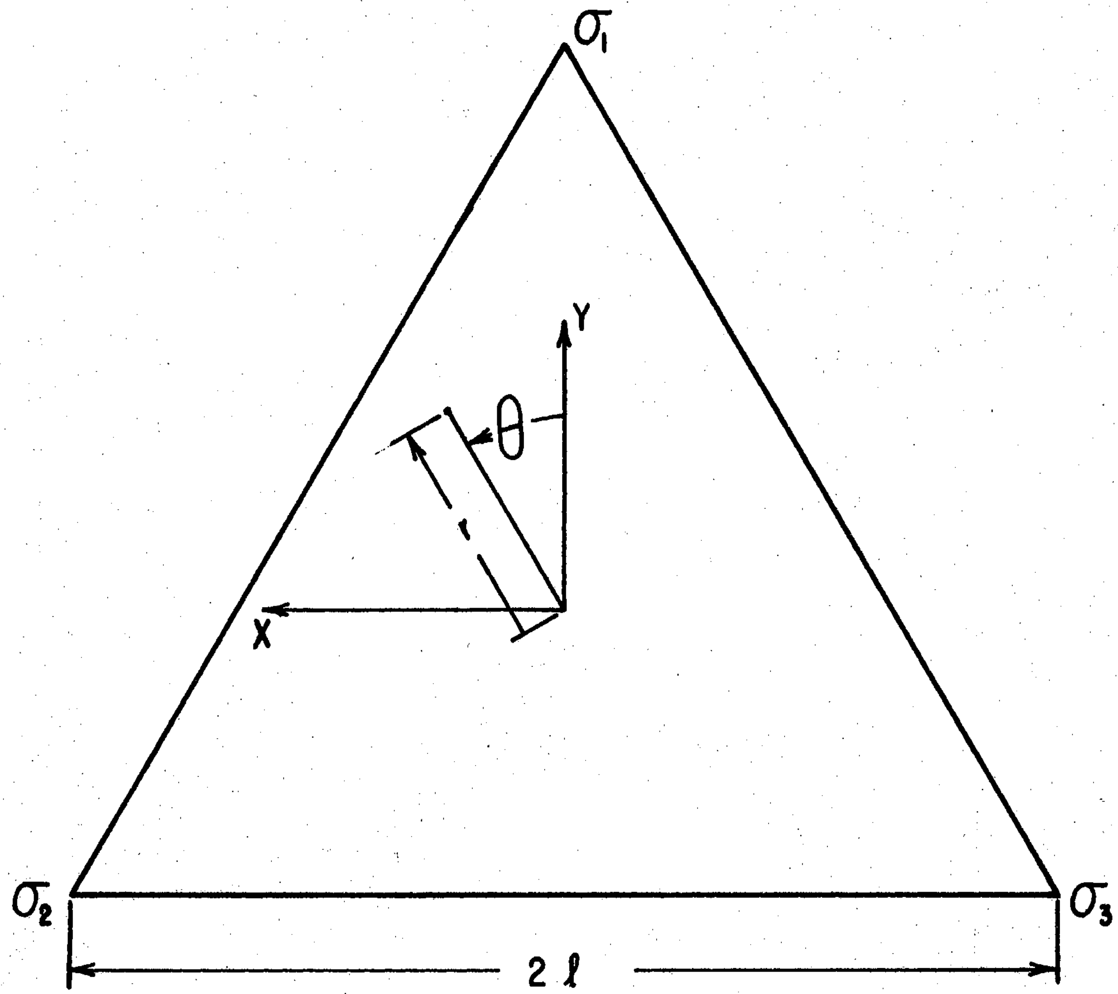

Figure 11. Definition Sketch of the Stress Plate

$$y = r \cos \theta \tag{17}$$

$$\bar{x} = \frac{r}{\ell} \sin \theta = \bar{r} \sin \theta \tag{18}$$

and
$$\bar{y} = \frac{r}{\ell} \cos \theta = \bar{r} \cos \theta, \tag{19}$$

the equations for principal stresses become:

$$\sigma_1 = \frac{P}{3} (1 + \sqrt{3}\, \bar{r} \cos \theta) \tag{20}$$

$$\sigma_2 = \frac{P}{3} (1 + \frac{3}{2} \bar{r} \sin \theta - \frac{\sqrt{3}}{2} \bar{r} \cos \theta) \tag{21}$$

$$\sigma_3 = \frac{P}{3} (1 - \frac{3}{2} \bar{r} \sin \theta - \frac{\sqrt{3}}{2} \bar{r} \cos \theta) \tag{22}$$

The values for the principal stress, σ_1, σ_2, and σ_3, are tabulated in Appendix A-I for selected values of r and θ for a load cylinder pressure of 1 psi. Angles above 90 degrees are not included because of symmetry of the stresses in the other quadrants. Also included in Appendix A-I are the stress ratios σ_1/σ_3 and σ_2/σ_3 for each set of coordinates r and θ.

Knowing the relationship between stress plate coordinates and principal stresses, it is an easy chore to locate the load cylinder and apply the desired magnitude of stress. For example, if a hydrostatic state of stress is desired, (σ_1:σ_2:σ_3 = 1:1:1) the load cylinder is simply placed at the centroid of the stress plate. If a deviatoric state of stress is desired, the load cylinder is moved away from the centroid of the stress plate.

The stresses in cylinders L are transmitted through the hydraulic lines, through the oil-water tubes, and to the six sides of the stress box. Each hydraulic line is divided at the stress box with one line going to each of a pair of opposite faces. Deformation of the granular medium under load causes water to flow into the space between the membrane and aluminum plate. The resulting change in the oil-water level in the oil-water tubes is a measure of the deformation of the granular medium.

Separation of the hydrostatic and deviatoric stress states is the function of load cylinder N. Since plate 4 is suspended symmetrically from plate 2, and since cylinder N is located at the centroid of plate 4, any load applied to cylinder N transmits a hydrostatic state of stress to cylinders L. If cylinders M and N are both loaded with cylinder M located away from the centroid of plate 2, then both a hydrostatic and deviatoric state of stress can be applied to the stress box. The value of this feature of the stress control device becomes clear when it is realized that any arbitrary state of stress can be separated into a hydrostatic and a deviatoric component of stress.

CHAPTER IV

GENERAL PROCEDURES

The procedures discussed in this chapter are general in that they apply to all the testing programs in this study. Except where otherwise noted, it is to be assumed that these procedures have been followed throughout the testing program.

Stress Control Device Calibration

Periodically, it was required that the line pressures, σ_1, σ_2, and σ_3, be calibrated to assure that they complied with the line pressures predicted by Equations 20 to 22.

For various locations, r and θ, on the stress plate the line pressures were computed for several values of load cylinder pressure p_i. The top load cylinder was placed at the various locations and loaded from 0 to p_{max}. At each pressure level, p_i, the line pressures were recorded and compared to the computed line pressures. When a discrepancy between measured and computed pressures occurred, the line pressure was adjusted to the computed pressure by altering the magnitude of the counterweights fastened to the stress plate. The counterweights consisted of lead shot to facilitate the calibration procedure.

The above procedure was repeated during loading and unloading of the top cylinder from 0 to p_{max} to 0 until the computed and measured line pressures agreed to within 0.25 psi. Then the load cylinder was moved to a new location and the procedure was repeated.

Test Sample Preparation

Strict adherence to the following methods of test sample preparation was required to assure that: (1) Variations between test samples were minimized; (2) The test sample was homogeneous; and (3) The shape of the sample was nearly cubical.

The first step was to remove all the entrapped air from the space between the membranes and the aluminum plates. This was done to each side of the stress box with the exception of the top side. Only after the sample was prepared and the top plate was in place could the air space be evacuated.

The stress box was next filled with water. A clear lucite plate which had the same size and shape as the top plate was placed on top of the stress box. Water was siphoned through a hole in the lucite plate until the water level touched the plate bottom. The weight and volume of water required to fill the stress box was recorded. This volume was designated by the symbol V_B.

The box was emptied and dried with tissue paper before the hydraulic lines were connected to the stress box. Precautions were taken to assure that the hydraulic lines were void of any air bubbles. Also, all the gate valves on the apparatus were closed before connecting the hydraulic lines. Reference will be made to Figure 2 in the following discussion.

The water level in each of the three water tubes was recorded. Valves P and T were opened and approximately 16 cu. cm. of water was admitted behind the bottom membrane. A visual check was made for air bubbles behind the membrane. Enough water, approximately 4 cu. cm., was admitted behind each of the side membranes to fill the membrane to a depth of 1 inch. The granular medium was then funnelled into the box in such a manner as to fill the box uniformly to a depth of 1 inch. Water and grains were admitted in this sequence until the box was filled to a level even with the bottom of the lucite plate. About 4 lifts were required to fill the 4 inch stress box, whereas the 6 inch stress box required 6 lifts. It was necessary to use this filling procedure, because the side membranes would have bulged excessively near the bottom if completely filled in one lift. Thus, the grain sample would not have been a cubical.

When the box is filled, the water levels in the water reservoirs and the total weight of the grain sample, W_S, are recorded, the volume of water admitted behind the membranes, V_A, is computed and recorded, and the sample volume, V_T, is determined by subtracting V_A from V_B. Thus,

$$V_T = V_B - V_A \tag{23}$$

where V_T = total sample volume, cu. cm.

V_B = volume of the empty stress box, cu. cm.

V_A = volume of water admitted behind the membranes, cu. cm.

The voids ratio of the sample is computed during the sample preparation procedures to insure that the voids ratio of the sample is within the limits defined for the test being conducted. Equation 24 is the expression which related the sample volume and weight to the initial voids ratio.

$$e_o = \frac{(V_T)\ (S.G.)\ (\gamma_w)}{W_s} - 1 \tag{24}$$

where e_o = initial voids ratio of the sample.

W_s = total sample weight, gms.

γ_w = density of water, gms./cu. cm.

If the sample voids ratio was within the desired range, the top plate was fastened to the stress box and the air space behind the membrane was evacuated by circulating water into the center port of the plate and out of a second port located in a corner of the plate. The stress box was tilted during this operation to allow air bubbles to escape. The sample was ready to be tested as soon as the hydraulic line was connected to the top plate.

Before a test was begun the following additional steps had to be completed: (1) The load cylinder had to be properly located on the stress plate; (2) Valves P and R had to be closed; (3) Valves Q, T, and S had to be opened; and (4) The initial oil-water level had to be recorded.

Data Collection

The load cylinder pressure was varied from 0 to p_{max} in 3 psi increments of pressure at uniform time intervals. The rate of loading will be determined by some preliminary investigations. At the end of each time interval, the oil-water level in each oil-water tube and the three stress levels were recorded. The same procedure was followed during unloading of the sample from p_{max} to 0.

At the conclusion of a loading test valves S were closed and the oil-water level was recorded in each oil-water tube. Then the pressure in the load cylinder was loaded along the same path followed with valves S open. At each pressure level the oil-water levels were recorded. The change in the oil-water level with valves S closed was the error introduced to the volumetric deformations of the grain sample due to the combined effect of compression of entrapped air in the fluid lines and expansion of the hydraulic tubes under load.

Reduction of Data

In this study all compressive deformations are assumed positive. This is in agreement with the standard sign conventions adopted in the area of soil mechanics.

The raw volumetric deformations in the ith direction at any given pressure level were obtained by calculating the difference between the oil-water levels at the given pressure level and at 0 psi in the ith direction. The resulting volumetric deformation was designated by the symbol, $\Delta V_{raw})_i$. This is called the raw volumetric deformation, because several volumetric corrections must be applied to $\Delta V_{raw})_i$.

Corrections to Deformation Measurements

Two volumetric corrections must be applied to the raw volumetric deformations. These are:

a. Corrections to compensate for the compressibility of entrapped air in the hydraulic lines and the expansion of the hydraulic lines under load.

b. Corrections to compensate for the tendency of the rubber membranes to fill the voids between individual grains under load; and corrections to compensate for the compressibility of the rubber membrane under load.

These corrections have been evaluated experimentally.

The first source of error has already been discussed in the section entitled "Data Collection." The correction term applied to the raw deformations to compensate for the compressibility of entrapped air and expansion of the hydraulic lines is designated by the symbol ΔV_L. The magnitude of ΔV_L is simply the difference between the oil-water levels at load cylinder pressure p and 0 psi when the hydraulic system is isolated from the test sample by the valves S in Figure 2.

The correction curve for the effects of membrane compression and indentation are required because it is assumed that the membrane deforms as a plane. The curve was developed on the following basis. It is asserted that any volumetric deformation behind a membrane adjacent to a single layer of granules is composed of three components: (1) Deformation of individual particles; (2) Compression of the membrane; and (3) Indentation of the membrane. In equation form the total volumetric deformation under load of a membrane adjacent to a single layer of particles is:

$$\Delta V_t = \Delta V_c + \Delta V_I + \Delta V_g \tag{25}$$

where ΔV_t = total volumetric deformation, cu. cm.

ΔV_c = volumetric deformation due to compressibility of the membrane, cu. cm.

ΔV_I = volumetric deformation due to grain indentation, cu. cm.

ΔV_g = volumetric deformation due to grain deformation, cu. cm.

Manipulation of Equation 25 yielded the correction term desired.

$$\Delta V_{corr} = \Delta V_c + \Delta V_I = \Delta V_t - \Delta V_g \qquad (26)$$

Thus, it was required that ΔV_g and ΔV_t be defined.

The apparatus used for evaluating ΔV_g is shown in Figure 12. The deformation of the grains at load P was evaluated from the change in the dial gauge reading. The stresses were evaluated simply by dividing P by the cross-sectional area of the aluminum block. For convenience in future calculations the grain deformations were converted to volumetric deformation per square inch of area.

The apparatus used to determine the total deformation of a membrane adjacent to a single layer of particles, ΔV_t is diagrammed in Figure 13. The apparatus consists of a hollow steel box which has its bottom side open. The open side is a 6 1/2 inch square. A rubber membrane is placed over the open end and is secured to the sidewalls by a watertight compression fit. In the top of the box is an NPT connection for admitting water and a bleed valve for removing any entrapped air. A hydraulic line connected to the NPT fitting runs to a calibrated water tube which is connected to an air compressor.

ΔV_t is obtained by the following procedure. A single layer of grain is placed on the base plate. The box with the membrane in place is located on the four supports and then slowly lowered by adjusting

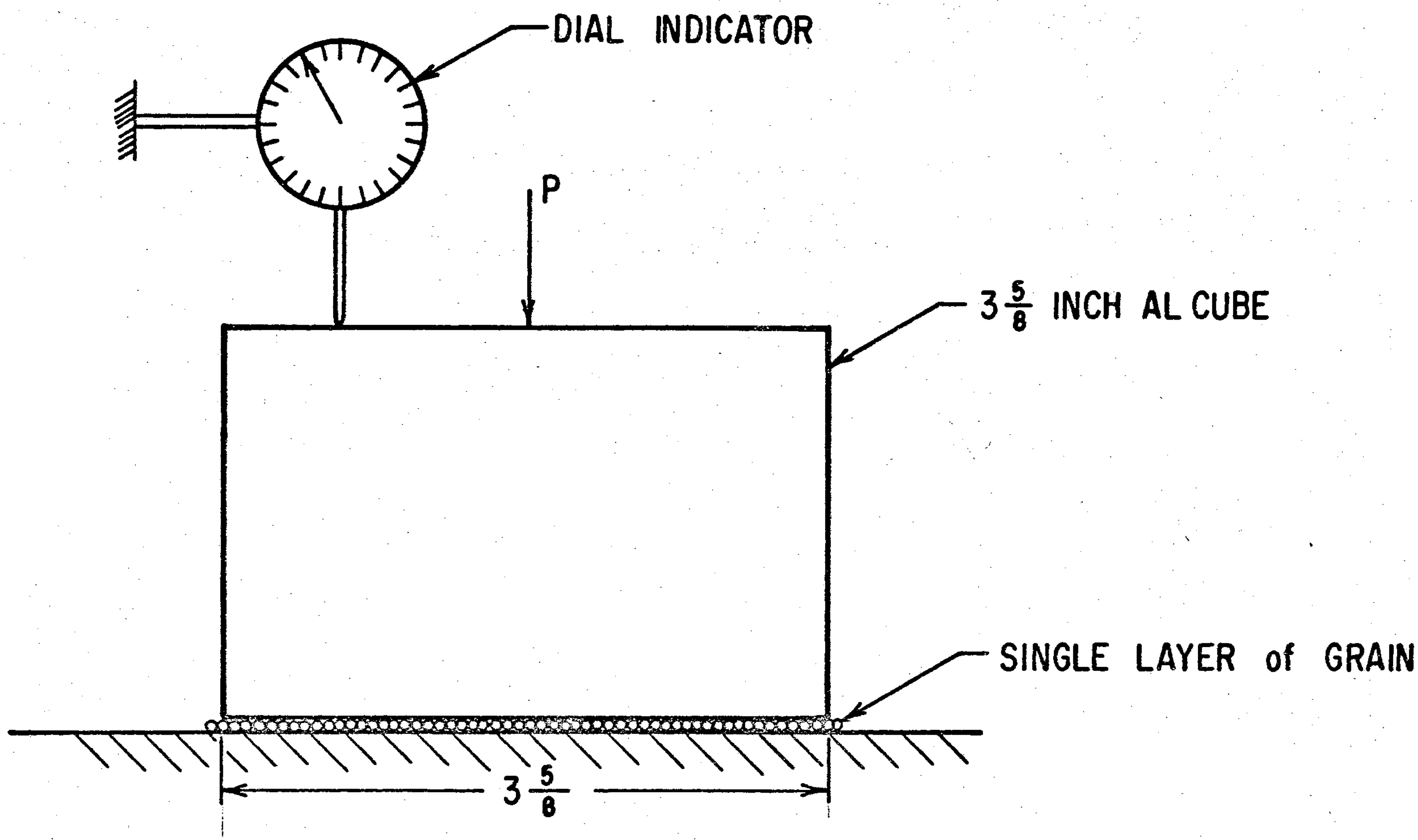

Figure 12. Sketch of Apparatus for Determination of the Deformation of a Single Layer of Grain

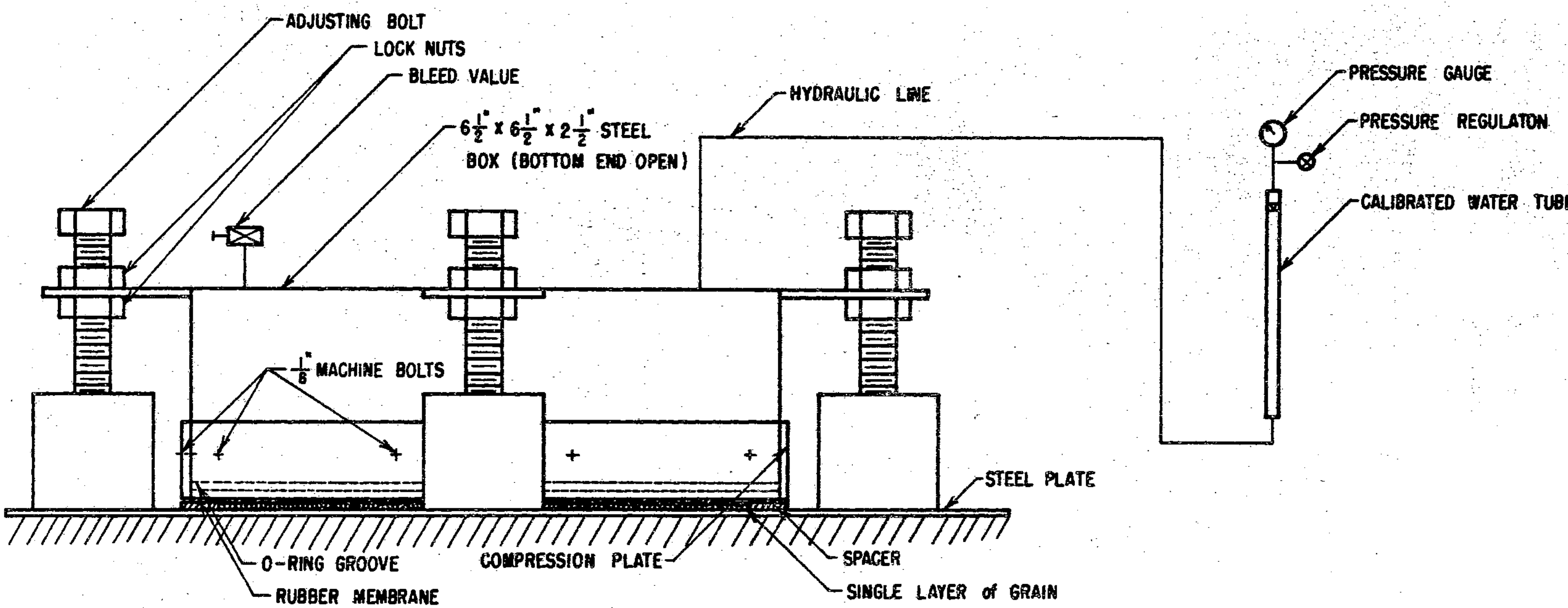

Figure 13. Sketch of Apparatus for Determination of the Total Membrane Deformation Behind a Single Layer of Grain

the bolts on the four supports until the membrane just touches the layer of wheat. The lock nuts are then tightened and the box is filled with water. Care must be taken to remove all the air from the box. After connecting the hydraulic lines and recording the initial water level in the calibrated tube, the test commenced.

The pressure was increased from 0 to 60 psi in 5 psi increments. At each increment the change in the liquid level in the water tube was recorded. The difference between the water level at pressure p and 0 psi was the desired ΔV_t at pressure p. The deformation, ΔV_t, was also converted to the volume change per square inch of membrane area.

By the procedures outlined above, an expression for ΔV_{corr} per square inch of membrane area as a function of stress level, σ_i, was developed. To apply the correction to a membrane on a stress box, it was required to multiply the value for ΔV_{corr}/sq. in. by the area of the membrane. In Appendix B-II the correction curve for the wheat grains used in the testing program is given as a function of pressure level.

Reduction of Raw Volumetric Deformations to Strains

Equipped with the correction curve for membrane indentation, the reduction of data is straight forward. The true volumetric deformation behind the two membranes in the ith direction is given by the equation:

$$\Delta V)_i = \Delta V_{raw})_i - \Delta V_L)_i - \Delta V_{corr})_i \tag{27}$$

The strain in the ith direction is evaluated by Equation 28.

$$\epsilon_i = \frac{\Delta V)_i}{\Delta V_T} \tag{28}$$

Sensitivity of the Computed Strains

The least reading of any volumetric deformation measurement is 0.1 cu. cm. Since three volumetric deformations are required to compute the corrected volumetric deformation in the ith direction in the stress box, the least reading of the corrected volumetric deformation is 0.3 cu. cm.

If the least reading for the corrected volumetric strain is substituted for $\Delta V)_i$ in Equation 28, a measure of the sensitivity of the computed strains is obtained.

$$S = \pm \frac{0.3}{V_T} \tag{29}$$

where S = strain sensitivity, cm./cm.

V_T = volume of test sample, cu. cm.

For a 4 inch stress box the sample volume was approximately 1000 cu. cm. For a 6 inch stress box the sample volume was approximately 3330 cu. cm. Thus, the sensitivity of the strains for the 4 and 6 inch stress boxes were, respectively, $\pm$ 0.030 x 10^{-2} and $\pm$ 0.010 x 10^{-2} cm./cm.

Variations in Procedures

Uniformity of Strain Measurements

The micrometer dials and the electrical circuit described in Chapter III under the subheading "Auxiliary Components" were mounted and in place before the test sample was prepared. The test was conducted as described in this chapter. However, before loading commenced, the deformation of the membrane was recorded at each of the five depth gauge stations. Then, at each increment of load, the linear displacement at each station on the membrane was recorded by lowering the depth gauge until it closed the electrical circuit, recording the micrometer dial reading, and backing the depth gauge from the membrane.

By subtraction it was possible to determine the linear displacement of the membrane at each station for any level of stress. The uniformity of the membrane deformation was observed by comparing the linear displacement of the five stations.

Creep Tests

The only change in procedure concerned the mode of load application and the recording of data. The maximum desired stress level was applied to the stress box at the beginning of the creep test. The oil-water levels were then recorded at time intervals.

Radial Stress Path

In these tests the magnitude of the pressure in the load cylinder remained constant. However, the location of the load cylinder was moved from the centroid of the stress plate outward along a straight line path. That is, p and θ remained constant throughout the test, but the distance from the centroid, r, was varied. This had the effect of holding the sum, $\sigma_1 + \sigma_2 + \sigma_3$, constant, but causing a variation in the stress ratios, σ_1/σ_3 and σ_2/σ_3.

CHAPTER V

THE PARTICULATE MATERIAL

The particulate material investigated in this study was hard winter wheat. The physical properties of the wheat which were deemed important to the stress-strain behavior of wheat en masse are presented in this chapter.

Properties Evaluated and Methods

The physical properties evaluated are: (1) The size and shape of the individual grains; (2) The specific gravity of the grains; (3) The angle of internal friction; (4) The moisture content; (5) The coefficient of static friction between the wheat and latex rubber; (6) The coefficient of static friction between wheat and aluminum; and (7) The voids ratio. Five samples were randomly selected from the wheat used in the testing program. Each sample was subjected to the physical tests described below.

The size and shape of the particles were determined by measurement of three orthogonal dimensions of the wheat grain. This technique was suggested by Mohsenin (36). The dimensions measured were the lengths of the maximum axis, a, the minimum orthogonal axis, c, and the maximum axis orthogonal to both a and c, b. The dimensions were obtained using a Wilder Opto-M Model A Optical Comparator with a 10X magnification and a 0.05 millimeter grid. The grain was rotated in the comparator until the maximum dimension was observed. Then the grain was rotated about the major axis until the minimum axis was observed. The grain was finally rotated 90 degrees about the major axis to obtain the intermediate dimension. Five kernels were selected and measured from each of the five wheat samples.

The specific gravity of the wheat kernels was determined by the large pycnometer method as described by Mohsenin (36). The angle of internal friction was evaluated by standard confined triaxial shear tests in which confining stresses of 20.84 and 27.72 psi were employed. A discussion of the confined triaxial shear test for cohesionless soils is described in Lambe (31). The coefficients of static friction were determined by the methods outlined by Brubaker and Pos (7) for grains on structural surfaces.

The grain moisture content was determined by oven drying the samples for 24 hours at 180 degrees Fahrenheit. The moisture content of the wheat was checked periodically during the testing program to insure that the moisture content was not significantly altered. Any variation in the moisture content could have been critical since the physical properties of wheat, such as the coefficient of static friction and internal friction, were reported by Brubaker and Pos (7) and Lorenzen (32) to vary with moisture content.

The voids ratio of the wheat varied between samples and was evaluated independently for each sample tested. The procedure for obtaining the initial voids ratio was presented in Chapter IV under the subheading "Test Sample Preparation."

Summary of the Physical Properties

The three axial dimensions of twenty-five wheat grains are presented in Appendix C-I. In Appendix C-II are summarized the results of the other physical properties tests.

The mean physical properties of the wheat are compared to published physical properties for wheat in Table I. The size of the wheat grains were smaller than the published values. The size difference could be due to seasonal and/or varietal differences. The ratio of the axial dimensions, a/b and a/c, are nearly equal; and both the measured and published results agree with Shelef and Mohsenin's (47) observation that the major axis is approximately twice as long at the other two orthogonal axes.

The observed specific gravity was only 1.4 percent lower than the published value of 1.42. The coefficient of static friction of wheat on aluminum or latex rubber has not been published, however, Lorenzen (32) reported the static coefficient of friction between wheat at a moisture content of 11.0 percent and steel to be 0.39. The observed value of 0.253 appears to be in the proper range since the aluminum used was extremely smooth. No comparison could be made for the friction coefficient between latex rubber and wheat.

The angle of internal friction for wheat at 11.0 percent moisture has been published by Lorenzen (32). The observed and published friction angle differed by only +2.0 percent.

TABLE I

MEAN VALUES OF THE PHYSICAL PROPERTIES OF THE WHEAT USED IN THE TESTING PROGRAM

Property	Measured Value and Std. Dev.	Published Value and Std. Dev.
Length of Major Axis (in.)	0.196 0.002	0.224[1] 0.010
Length of Interm. Axis (in.)	0.098 0.001	0.129[1] 0.010
Length of Minor Axis (in.)	0.091 0.001	0.123[1] 0.008
Specific Gravity	1.396 0.013	1.42[1] --
Internal Friction Angle (degrees)	25.0 0.1	24.5[2] --
Moisture Content	11.38 0.28	7.80[1] --
Static Coef. of Friction on Latex Rubber	0.477 0.007	(Not available)
Static Coef. of Friction on Aluminum	0.253 0.003	(Not available)

[1]Published values are from Mohsenin (36).
[2]Published values from Lorenzen (32).

CHAPTER VI

PRELIMINARY INVESTIGATIONS

Size Effect and Strain Uniformity

Purpose and Nature of the Tests

The purposes of this series of investigations were to determine the influence of test sample size upon the stress-strain behavior of wheat en masse, to determine the degree of uniformity of the strains encountered in the stress boxes, and to select the size stress box to be used in subsequent testing programs for wheat en masse.

Hydrostatic compression tests, in which the applied stresses varied from 0 to 20 to 0 psi, were conducted with both the 4 and 6 inch test boxes. Volumetric deformation readings were taken at stress levels of 0, 1, 2, 3, 5, 8, 11, 14, 17, and 20 psi. The stress increments were applied at one minute intervals. A stress level of 20 psi was considered large enough to span both mechanisms of deformation encountered in particulate media en masse; namely particle deformation and particle reorientation. At each stress increment the linear deformation of one of the side membranes was also measured by means of the five micrometer depth gauges. Three replications were run for each stress box.

Test Results

A summary of the voids ratios of the test samples is presented in Table II. The range of the voids ratio was 0.739 to 0.781. This indicated that with careful sample preparation the initial voids ratio of the test samples could be closely controlled.

TABLE II

INITIAL VOIDS RATIOS FOR THE SIZE EFFECT TEST SAMPLES

Test Sample	Initial Voids Ratio
Hydrostatic Compression - 4 inch box	Rep 1 - 0.761 Rep 2 - 0.781 Rep 3 - 0.765
Hydrostatic Compression - 6 inch box	Rep 1 - 0.739 Rep 2 - 0.764 Rep 3 - 0.766

The stress-strain curves for wheat in a 4 inch and a 6 inch sample under hydrostatic compression are presented in Figures 14 through 19. The data for these curves are tabulated in Appendix D-I. In each of these figures the σ_1 and σ_2 directions correspond to the stresses applied in the horizontal direction, whereas σ_3 always refers to the stress applied in the vertical direction.

The $\sigma_1 - \epsilon_1$ and the $\sigma_2 - \epsilon_2$ curves were nearly identical in every test, while the $\sigma_3 - \epsilon_3$ curve was displaced to the left of the other two. The maximum difference observed between ϵ_1 and ϵ_2 at a stress

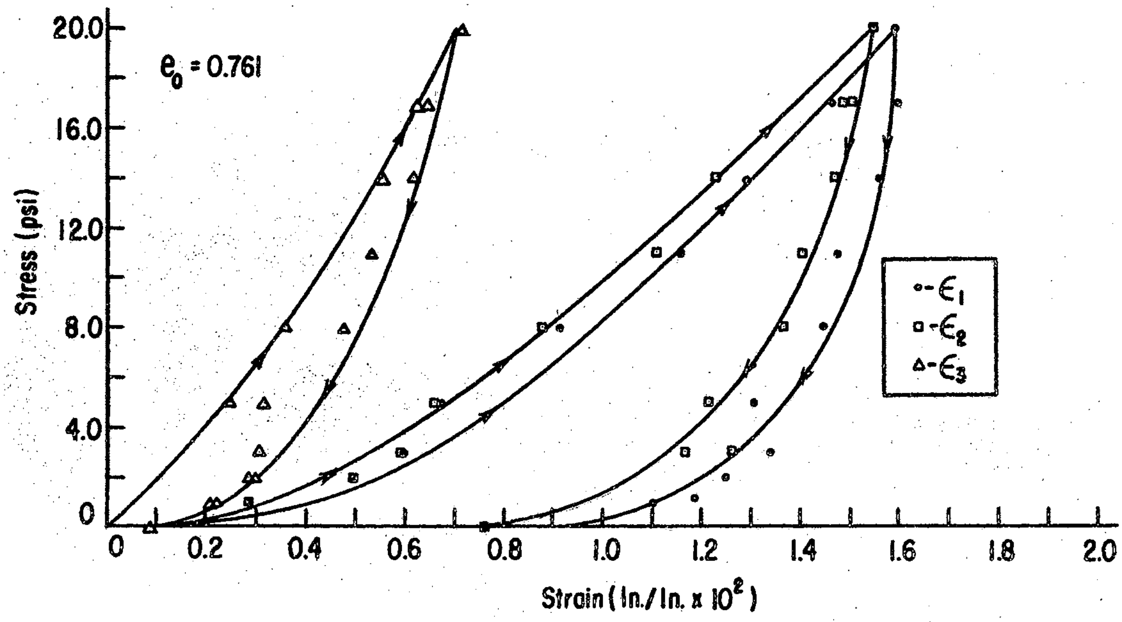

Figure 14. Hydrostatic Stress-Strain Curves Obtained with the Four Inch Stress Box - Rep 1

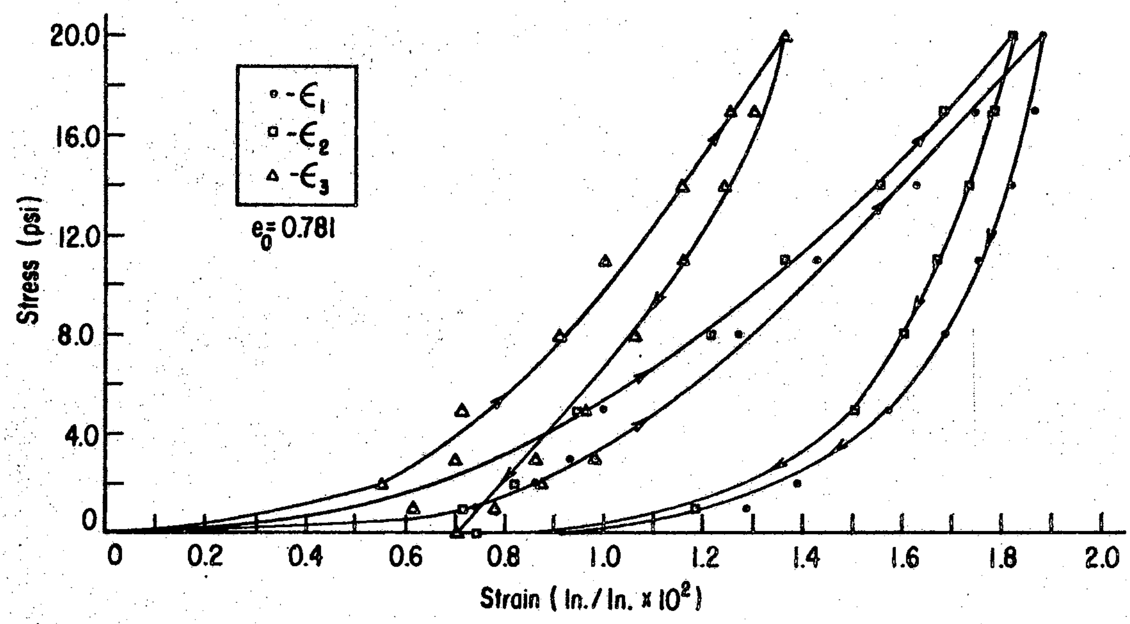

Figure 15. Hydrostatic Stress-Strain Curves Obtained with the Four Inch Stress Box - Rep 2

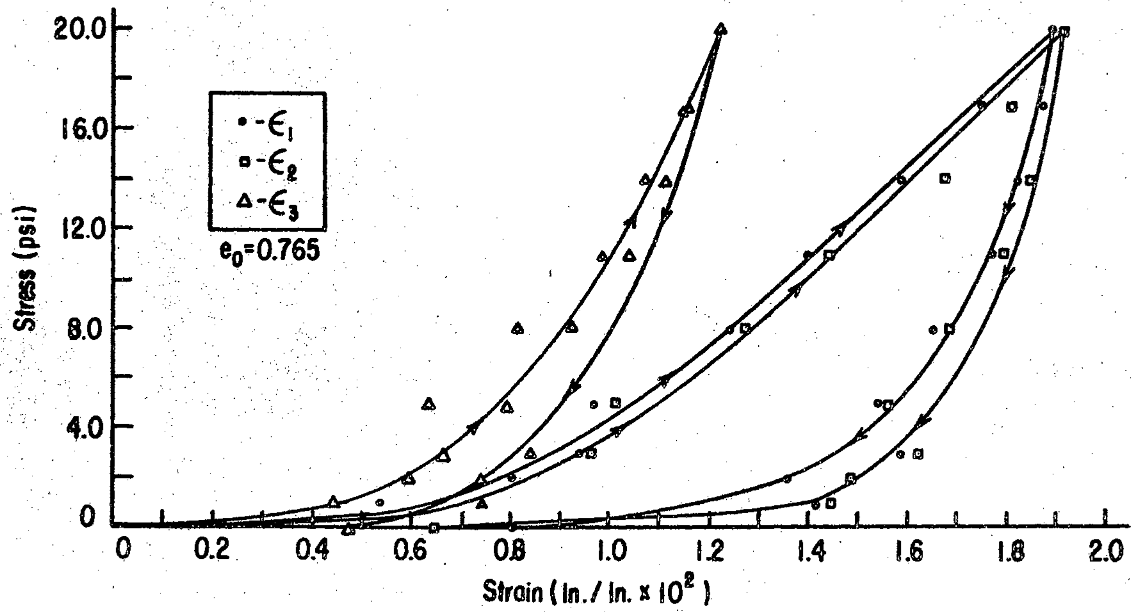

Figure 16. Hydrostatic Stress-Strain Curves Obtained with the Four Inch Stress Box - Rep 3

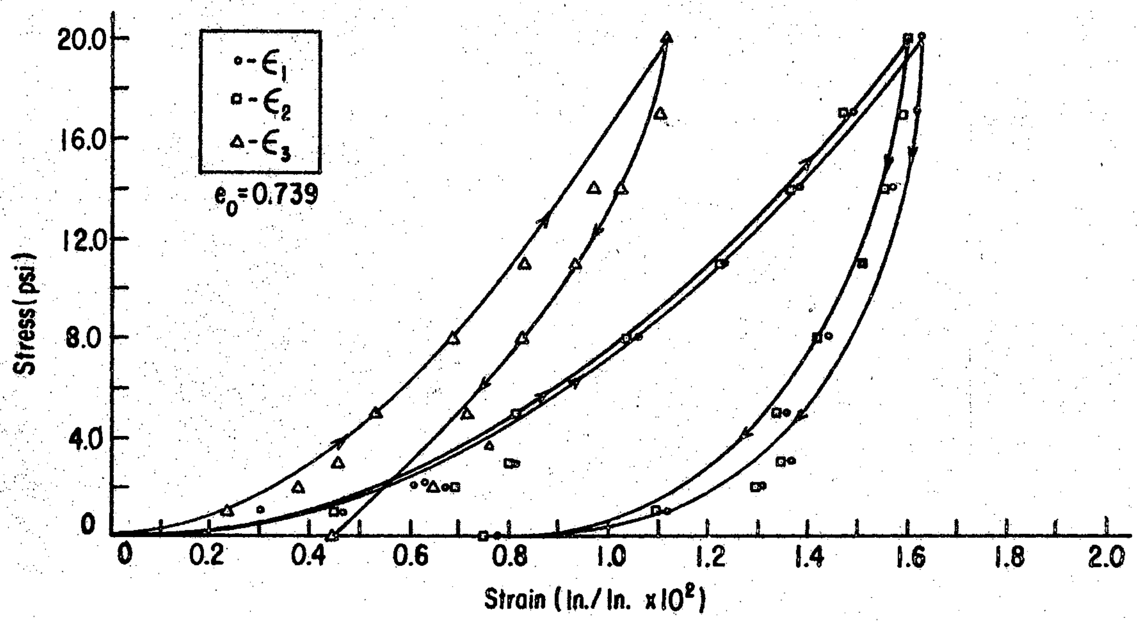

Figure 17. Hydrostatic Stress-Strain Curves Obtained with the Six Inch Stress Box - Rep 1

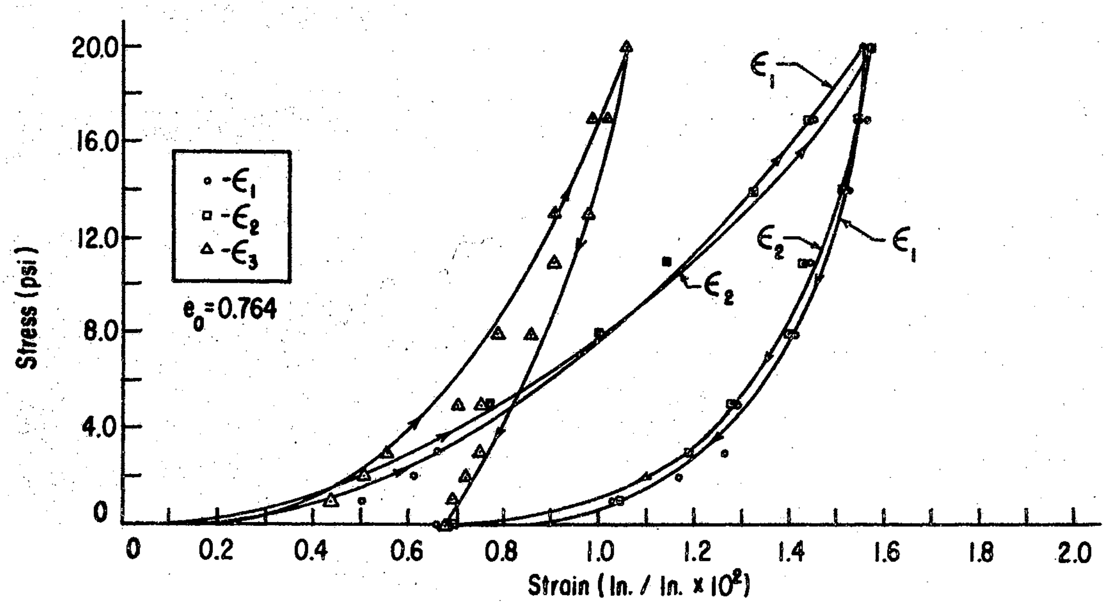

Figure 18. Hydrostatic Stress-Strain Curves Obtained with the Six Inch Stress Box - Rep 2

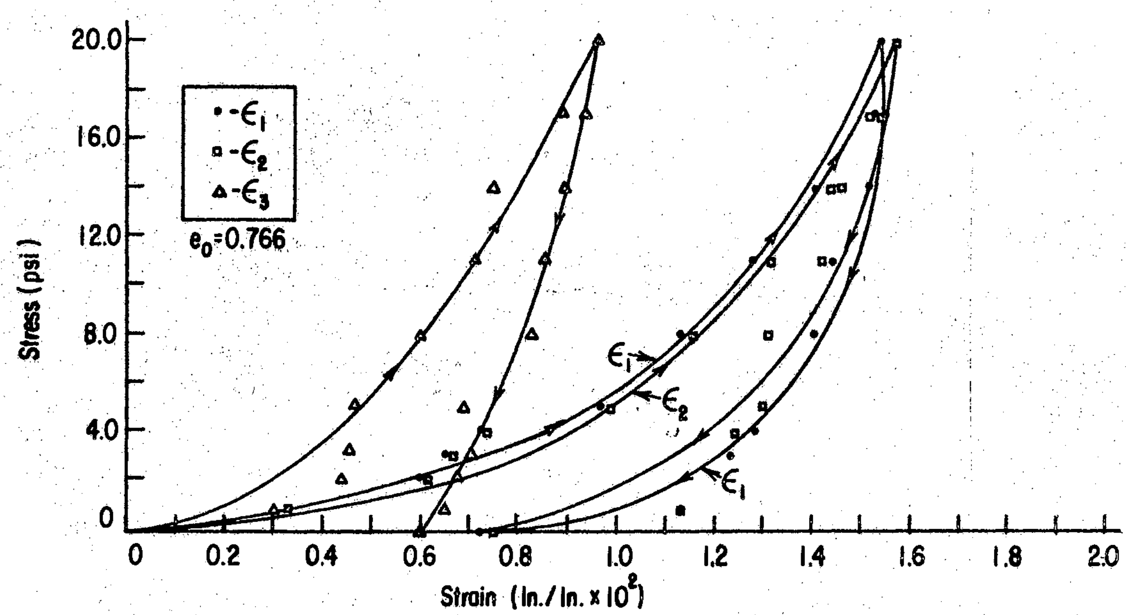

Figure 19. Hydrostatic Stress-Strain Curves Obtained with the Six Inch Stress Box - Rep 3

level of 20 psi was 3 percent, whereas ϵ_3 was consistently 20 to 30 percent lower than either of the horizontal strains. Hysteresis losses of about 25 and 65 percent were observed in the vertical and horizontal directions, respectively.

The stress-strain curves for the 4 inch and 6 inch stress box all exhibited the same characteristic shape. At stresses below approximately 8 psi the $\sigma_i - \epsilon_i$ relationship was nonlinear and large deformations were experienced for small increments of pressure, but at stresses above 8 psi the $\sigma_i - \epsilon_i$ relationship tended toward a linear relationship. The wheat began to behave as a much stiffer material as stress level increased. The shape of the curves, therefore, lend support to the contention that two distinct mechanisms of deformation are present: one in which particle reorientation is predominant and one in which particle deformation is predominant.

The stress-strain behavior obtained with the 4 inch cubical sample of grain is shown in Figures 14, 15, and 16. The following observations were made upon superimposing the stress-strain diagrams for these three replications. The $\sigma_i - \epsilon_i$ curves for rep 2 and rep 3 nearly coincided in the respective directions of stress. In rep 1, however, the unit strains in each direction were about 12 percent lower than the strains at a corresponding stress level in reps 2 and 3. The deviation of the results of rep 1 from those of reps 2 and 3 resulted from the rep 1 sample being accidentally preconsolidated to a stress level of 2 psi and unloaded before the hydrostatic compression test was conducted. Thus, the initial voids ratio of the sample in rep 1 was reduced by the preconsolidation. As expected, the curves for rep 1 tended towards linear at a lower unit strain than in reps 2 and 3.

The stress-strain diagrams obtained with the 6 inch samples are plotted in Figures 17, 18, and 19. Superposition of the diagrams for the three replications indicated that the respective curves were nearly identical for the three replications.

It was concluded that the strains measured by both the 4 inch and the 6 inch sample are repeatable. Thus, repeatability of results played no role in the selection of an adequate sample size for subsequent testing.

A comparison of the $\sigma_i - \epsilon_i$ behavior of the 4 and 6 inch samples indicated that the unit strains for the 4 inch sample were consistently higher than the corresponding unit strains for the 6 inch samples. The magnitude of these differences are shown in Table III for rep 2 of the respective sample sizes.

Inspection of the stress-strain curves and the percent differences listed in Table III suggested that the unit strains were considerably and consistently higher in the 4 inch sample than in the 6 inch sample. Furthermore, the differences were larger at the lower levels of stress than at the higher levels of stress. At a stress of about 8 psi the percentage differences began to stabilize. This was a strong indication that the differences in the unit strains between sample sizes were taking place primarily in the realm of stresses where particle reorientation is the predominant mode of deformation. By the time particle deformation became the predominant mode of deformation, no further increase (or decrease) in the difference between the unit strains of the respective samples was observed.

The results of the strain uniformity data are presented in Tables IV and V. In the second column of these tables the average linear

TABLE III

COMPARISON OF UNIT STRAINS BETWEEN THE FOUR AND SIX INCH SAMPLES (REP 2)

Stress[2] (psi)	Unit Strain ϵ_1-4in.	ϵ_1-6in.	% Diff.[1] (%)	Unit Strain ϵ_2-4in.	ϵ_2-6in.	% Diff.[1] (%)	Unit Strain ϵ_3-4in.	ϵ_3-6in.	% Diff.[1] (%)
	(in./in. x 10^2)			(in./in. x 10^2)			(in./in. x 10^2)		
0	0	0	0	0	0	0	0	0	0
1	0.753	0.508	32.5	0.715	0.545	22.5	0.618	0.440	28.8
2	0.868	0.613	29.4	0.820	0.624	23.9	0.553	0.504	8.9
3	0.934	0.664	28.9	0.877	0.675	23.0	0.705	0.523	25.8
5	1.001	0.763	23.8	0.944	0.763	19.2	0.716	0.553	22.8
8	1.278	1.006	21.3	1.211	1.006	16.9	0.911	0.701	23.0
11	1.430	1.144	22.1	1.364	1.144	16.1	1.030	0.790	23.3
14	1.630	1.325	18.7	1.554	1.322	14.9	1.161	0.907	21.9
17	1.754	1.455	17.0	1.688	1.446	14.3	1.258	0.984	21.8
20	1.888	1.556	17.6	1.821	1.554	14.7	1.367	1.061	22.4

[1] $\% \text{ Diff.} = \dfrac{(\epsilon_i\text{-4in.}) - (\epsilon_i\text{-6in.})}{(\epsilon_i\text{-4in.})} \times 100$

[2] Stress equals the hydrostatic compressive stress.

TABLE IV

STRAIN UNIFORMITY DATA FOR THE FOUR INCH SAMPLE UNDER HYDROSTATIC COMPRESSION (REPS 2 AND 3)

Stress[1] (psi)	Avg. Membrane Deformation[2] (in. x 10^2)	Measured Linear Deformation Sta.1 (in. x 10^2)	Sta.2	Sta.3	Sta.4	Sta.5	Avg. Membrane Deformation[3] (in. x 10^2)	Difference Between Deformation[4] (in. x 10^2)
				Rep 2				
0	0	0	0	0	0	0	0	0
1	1.5	1.7	1.0	0.9	1.3	1.5	1.3	-0.2
2	1.7	1.9	1.3	1.7	2.0	1.9	1.8	0.1
3	1.9	2.2	1.7	2.1	2.2	2.2	2.1	0.2
5	2.0	2.6	2.2	2.5	2.3	2.5	2.4	0.4
8	2.6	2.9	2.5	2.9	2.6	3.1	2.8	0.2
11	2.9	3.2	2.7	3.3	3.0	3.5	3.1	0.2
14	3.3	3.5	2.9	3.7	3.3	3.9	3.4	0.1
17	3.5	3.7	3.1	3.9	3.7	4.1	3.7	0.2
20	3.8	4.0	3.3	4.2	3.9	4.4	4.0	0.2
				Rep 3				
0	0	0	0	0	0	0	0	0
1	1.1	0.8	0.9	0.9	1.2	1.1	1.0	-0.1
2	1.1	1.4	1.7	1.5	1.9	1.4	1.6	0.5
3	1.9	1.6	1.8	1.7	2.3	1.9	1.9	0.0
5	2.0	1.8	2.1	2.0	2.5	2.2	2.1	0.1
8	2.5	2.2	2.6	2.6	3.6	2.7	2.5	0.0
11	2.9	2.4	2.9	3.0	3.8	3.0	3.0	0.1
14	3.2	2.6	3.1	3.3	3.9	3.3	3.2	0.0
17	3.5	2.9	3.3	3.5	4.0	3.5	3.4	-0.1
20	3.8	3.1	3.5	3.7	4.1	3.8	3.7	-0.1

[1] Stress equals the hydrostatic compressive stress.
[2] Computed from volumetric deformations
[3] Computed from depth gauge measurements
[4] Difference between avg. deformations

TABLE V

STRAIN UNIFORMITY DATA FOR THE SIX INCH SAMPLE UNDER HYDROSTATIC COMPRESSION (REPS 2 AND 3)

Stress[1] (psi)	Avg. Membrane Deformation[2] (in. x 10^2)	Measured Linear Deformation (in. x 10^2) Sta.1	Sta.2	Sta.3	Sta.4	Sta.5	Avg. Membrane Deformation[3] (in. x 10^2)	Difference Between Deformation[4] (in. x 10^2)
				Rep 2				
0	0	0	0	0	0	0	0	0
1	1.5	1.0	1.2	1.6	1.5	1.4	1.3	-0.2
2	1.8	1.3	1.5	1.9	1.9	1.7	1.7	-0.1
3	2.0	1.5	1.7	2.2	2.1	1.9	1.9	-0.1
5	2.3	1.9	2.2	2.7	2.7	2.3	2.4	-0.1
8	3.0	2.6	2.8	3.3	3.4	2.9	3.0	0.0
11	3.4	3.0	3.3	3.9	3.9	3.3	3.5	-0.1
14	4.0	3.5	3.8	4.4	4.4	3.7	4.0	0.0
17	4.4	3.7	4.4	4.8	4.7	4.1	4.3	-0.1
20	4.7	3.9	4.8	5.1	4.9	4.4	4.6	-0.1
				Rep 3				
0	0	0	0	0	0	0	0	0
1	0.9	0.5	0.7	0.8	0.3	0.3	0.5	-0.4
2	1.9	1.4	1.8	1.7	1.2	1.1	1.5	-0.4
3	2.0	1.6	2.1	2.0	1.5	1.3	1.7	-0.3
5	2.2	2.2	2.8	2.4	2.0	1.6	2.2	0.0
8	2.9	2.9	3.6	3.1	2.7	2.3	2.9	0.0
11	3.4	3.4	4.0	3.6	3.2	2.7	3.4	0.0
14	3.9	3.7	4.3	3.9	3.6	3.1	3.7	-0.2
17	4.3	4.1	4.7	4.3	4.4	3.5	4.2	-0.1
20	4.6	4.3	5.0	4.6	4.7	3.8	4.4	-0.2

[1]Stress equals the hydrostatic compressive stress.
[2]Computed from volumetric deformations
[3]Computed from depth gauge measurements
[4]Difference between avg. deformations

movement of the membrane as computed from the volumetric deformations is tabulated for each stress level. Columns 3 to 7 contain the linear deformations as obtained from the micrometer depth gauges, the location of which are shown in Figure 9. Column 8 is a listing of the average deformation of the membrane as measured by the depth gauges, and column 9 is a tabulation of the difference between the mean average linear deformation computed from the depth gauge measurements and the volumetric deformation measurements.

The membrane deformations were consistent in one sense. At the stations within 1 inch of the membrane edges in the 6 inch stress box and within 1/2 inch of the membrane edges in the 4 inch stress box, there was a slight restriction of the membrane deformation. However, as the measuring stations moved away from the membrane edges, the variation of the deformation became random in both the 4 inch and the 6 inch stress box. Since the uniformity of the membrane deformation was not affected by sample size, it was not a contributing factor in deciding upon an adequate sample size.

The average linear deformations of the membrane as computed by the two methods were in close agreement. Except for a few isolated cases at stresses below 5 psi, the average linear membrane deformations computed by two methods were within 0.002 inches of each other; and in many instances, the difference was 0.000 and 0.001 inch. This close agreement provided confidence in the measuring and data reduction techniques since the two average linear deformations were obtained independently.

Discussion of Size Effect Considerations

From the standpoint of sample uniformity between test runs and the uniformity of membrane deformations, either the 4 or the 6 inch sample would have been equally satisfactory. However, the stress-strain behavior of the samples in the two boxes did indicate variation in response due to size.

It was asserted that smaller unit strains would be expected in the smallest sample if edge effects (wall effects) were responsible for the variation in response due to sample size. The basis for this assertion was that a larger percentage of the material in a given stress plane would be restrained by a wall effect in a smaller sample than in a larger sample. Since the largest unit strains were observed in the smaller stress box, it was concluded that, although wall effects may be present, they were overwhelmed by some other effect which is dependent upon sample size.

Above stresses of 8 psi the stress-strain diagrams for the two sample sizes were similar in shape and slope. The differences in response due to sample size, therefore, were produced during the initial stages of deformation. That is, the differences took place in that portion of deformation during which particle reorientation was the predominant mechanism.

In a finite sample it is hypothesized that particle reorientation will begin at the membrane-particle interface. As the stress is increased, particle reorientation will continue at the interface and begin to occur in planes removed from the membrane. As the stress is further increased, the particle reorientation will proceed towards the center of the sample. However, if the mass of material is large enough, individual particle deformation will begin to occur in particles near the interface before particle reorientation has been completed in the central portion of the sample. Thus, if a sample is large enough, a large strain gradient will be present.

It is concluded that the difference in the stress-strain behavior between the two sample sizes is a result of nonhomogeneous states of strain in the samples. It is also concluded that this strain nonhomogeneity will be more in evidence in the 6 inch box than in the smaller box. This conclusion is supported by the nature of the stress-strain curves.

In the 6 inch stress box particle reorientation has not been completed throughout the entire sample thickness before particle deformation takes place. Since the mass of grain becomes stiffer when particle deformation takes place, it is expected that the unit strains would be lower for the 6 inch box than for a 4 inch box at a given stress level. It was noted earlier that such is the case. At all levels of stress the unit strains in the 6 inch sample were smaller than the corresponding strains in the 4 inch sample.

It has not been concluded that the strains in the 4 inch box were completely homogeneous. The conclusions drawn are that the effects of strain nonhomogeneity are minimized by decreasing sample size, and that the most adequate stress-strain relationship can be obtained with the smaller sample. Since it is impractical physically to consider a sample size smaller than 4 inches, it was decided that the 4 inch stress box be used in all subsequent testing programs.

Gravity, Isotropy, Load Rate, Creep, and Load History Investigations

Purpose of the Investigations

The purpose of these investigations was to define the influence of factors such as gravity, isotropy, load rate, and load history upon the mechanical behavior of wheat en masse. The results of these tests, the objectives of which are outlined below, were used in designing the main experiments.

Test Objectives

Gravity - to determine whether the difference in the stress-strain behavior in the vertical direction with respect to filling was due to particle orientation with respect to gravity or the weight of the sample.

Load Rate - to observe whether a variation in load rate between 3 and 6 psi/minute caused a change in the stress-strain behavior of wheat en masse when subjected to a hydrostatic compressive state of stress or to a deviatoric state of stress.

Creep - to evaluate the characteristic times, τ_i, for wheat en masse under hydrostatic compression. τ_i is defined in the following equation:

$$\frac{\epsilon_i}{\epsilon_{\infty i}} = 1.0 - \left(1.0 - \frac{\epsilon_{oi}}{\epsilon_{\infty i}}\right) e^{-t/\tau_i} \qquad (30)$$

where ϵ_i = strain in ith direction at time, t, in./in.

ϵ_{oi} = instantaneous strain in ith direction, in./in.

$\epsilon_{\infty i}$ = maximum strain in the ith direction, in./in.

t = time from application of load, minutes

τ_i = characteristic time in ith direction, minutes

Isotropy - to determine the degree of elastic symmetry of wheat en masse with respect to principal stresses.

Load History - to determine the dependence of the stress-strain behavior of wheat en masse upon the load history to which it has been subjected. The objectives of these tests were further subdivided as follows:

1. To determine whether or not hysteresis losses decreased with increasing number of full load cycles.
2. To determine if elastic stress-strain behavior is approached with increasing number of load cycles when:
   (a) Complete load-unload cycles are applied.
   (b) Partial load-unload cycles are applied.
3. To determine whether the final strain encountered for a general stress state is affected by the order of applying the hydrostatic and deviatoric component of a general stress state.
4. To determine the effect variation of the stress ratio, $\sigma_1:\sigma_2:\sigma_3$, from 1:1:1 to 4.00:2.50:1 while holding $p = \sigma_1 + \sigma_2 + \sigma_3$ constant, had upon the stress-strain behavior; and to determine whether repeated cyclic variation of the stress ratio resulted in elastic stress-strain behavior.

Test Descriptions

The loading tests conducted are described in Table VI. Except where otherwise indicated, σ_1 and σ_2 refer to horizontal stresses, whereas σ_3 designates the vertical stress.

Test Results

The reduced stress-strain data for these investigations are presented in Appendix D. Representative stress-strain curves are included in the text for all the preliminary tests.

Gravity Effect

Rotation of the wheat sample 90 degrees about a σ_2-axis after filling showed that the strains in the vertical and horizontal directions with respect to filling were not altered by the rotation. Table VII summarizes the strains observed for a rotated and nonrotated sample at a hydrostatic stress, σ_o, of 20 psi. The variations observed in ϵ_i due to sample rotation were small and were attributed to variations in sample voids ratio and experimental error.

It was concluded that the differences in the strain in the vertical and horizontal directions with respect to filling under hydrostatic compression were due to orientation of individual wheat grains with respect to gravity. Gravity orientation takes place because wheat grains are asymmetric; that is, a typical wheat grain approximates an ellipsoid which has a longitudinal axis twice as large as either lateral axis. As a result, the stable orientations of a

TABLE VI

SUMMARY OF PRELIMINARY TESTS

Expt. No.	Effect Studied	Brief Description of Test
1	Gravity	Hydrostatic compression; stress varied from 0 to 20 psi; sample orientation during loading identical to orientation during filling. (Two replications)
2	Gravity	Same as No. 1 except sample rotated 90 degrees so vertical direction with respect to filling became a horizontal direction during loading. (Two replications)
3	Isotropy	Deviatoric stress state with $\sigma_1:\sigma_2:\sigma_3 = 2.33:1.67:1$; p^1 varied from 0 to 45 to 0 psi. (Two replications)
4	Isotropy	Deviatoric stress state with $\sigma_1:\sigma_2:\sigma_3 = 2.33:1.67:1$; p^1 varied from 0 to 45 to 0 psi; σ_1 was the vertical stress and σ_2 and σ_3 were the horizontal stresses. (Two replications)
5	Load Rate	Hydrostatic compression; stress varied from 0 to 40 to 0 psi; load rate equal to 3 psi/minute in top cylinder; load applied in increments of 3 psi.
6	Load Rate	Same as No. 5 except load rate increased to 4.5 psi/minute.
7	Load Rate	Same as No. 5 except load rate increased to 6.0 psi/minute.
8	Load Rate	Deviatoric stress state with $\sigma_1:\sigma_2:\sigma_3 = 2.33:1.67:1$; load varied from 0 to 45 to 0 psi in top cylinder; load rate equal to 3 psi/minute in top cylinder; load applied in increments of 3 psi.
9	Load Rate	Same as No. 8 except load rate increased to 4.5 psi/minute.
10	Load Rate	Same as No. 8 except load rate increased to 6 psi/minute.
11	Creep	Hydrostatic stress, σ_0, of 20 psi applied instantaneously to the sample; strain measured at time intervals up to 1620 minutes from application of the load.
12	Load History	Cyclic hydrostatic compression test; load rate equals 3 psi/minute on top cylinder; load varied

TABLE VI (Continued)

Expt. No.	Effect Studied	Brief Description of Test
		from 0 to 40 to 0 psi on each face three times, then loaded again to 40 psi; partially unloaded, loaded and unloaded in ranges of 40 to 20 psi, 20 to 12 psi, 12 to 6 psi, and 6 to 0 psi.
13	Load History	Cyclic deviatoric stress state with $\sigma_1{:}\sigma_2{:}\sigma_3$ = 2.33:1.67:1; load rate equals 3 psi/minute on top cylinder; load on top cylinder varied from 0 to 45 to 0 psi 3 times; then loaded to 45 psi again and partially loaded and unloaded in ranges of 45 to 30 psi, 30 to 15 psi and 15 to 0 psi.
14	Load History	Same as No. 13 except $\sigma_1{:}\sigma_2{:}\sigma_3$ = 2.67:1.44:1.
15	Load History	Deviatoric stress state ($\sigma_1{:}\sigma_2{:}\sigma_3$ = 2.33:1.67:1) superimposed on hydrostatic compressive stress; hydrostatic compressive stress of 10 psi applied in increments of 3 psi/minute on bottom cylinder; then deviatoric stress superimposed by incrementing top cylinder pressure from 0 to 45 psi in 3 psi increments; deviatoric stresses unloaded; hydrostatic stresses unloaded. Load-unload cycle repeated one time.
16	Load History	Same as No. 15 except deviatoric stress applied first, then hydrostatic compressive stress superimposed.
17	Load History	Radial stress path; top cylinder loaded to 30 psi while located at center of stress plate at 3 psi/minute; load cylinder then moved along radial stress path with θ = 30 degrees from r = 0 to 3 to 0 inches in 1/2 inch increments three times with cylinder still loaded to 30 psi; after 3rd cycle, top cylinder unloaded to 0 psi and reloaded to 30 psi; load cylinder moved along radial stress path from r = 0 to 3 to 0 to 2 to 0 inches in 1/2 inch increments; with load cylinder at R = 0, top cylinder pressure reduced to 0 psi. (See Figure 20.)

[1] $p = \sigma_1 + \sigma_2 + \sigma_3$ = pressure applied to top load cylinder.

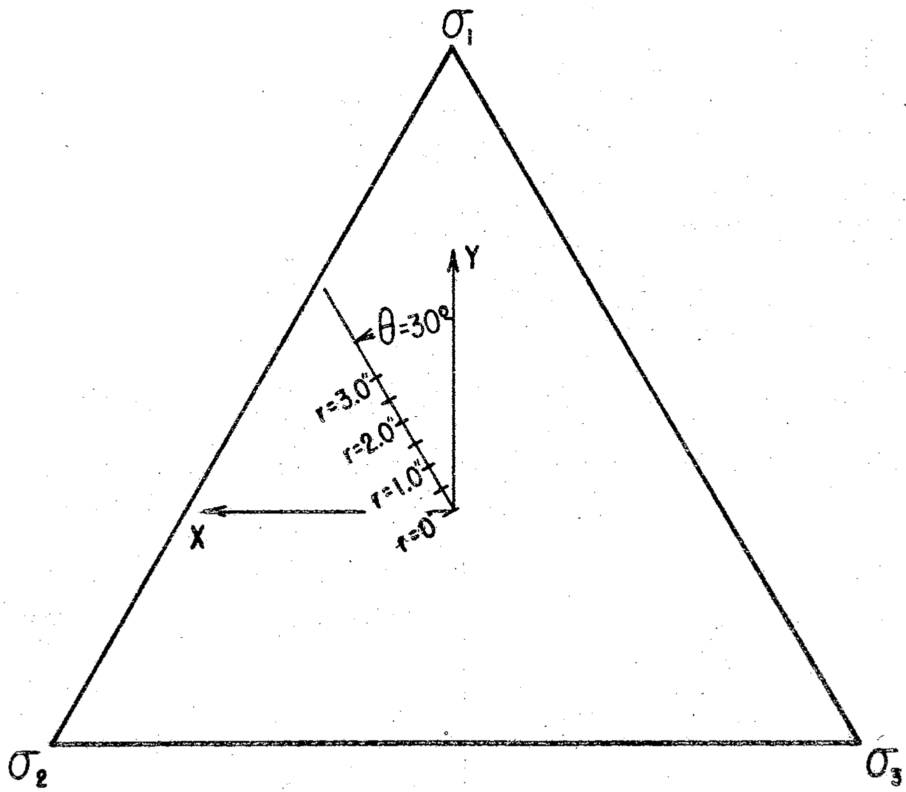

r	$\sigma_1:\sigma_2:\sigma_3$	$\sigma_1+\sigma_2+\sigma_3$ = 30 Psi.		
		σ_1	σ_2	σ_3
0.0	1.00:1.00:1.00	10	10	10
0.5	1.22:1.11:1.00	11	10	9
1.0	1.50:1.25:1.00	12	10	8
1.5	1.86:1.43:1.00	13	10	7
2.0	2.33:1.67:1.00	14	10	6
2.5	3.00:2.00:1.00	15	10	5
3.0	4.00:2.50:1.00	16	10	4

Figure 20. Illustration of a Radial Stress Path in which θ = 30 Degrees and r = 0 to 3 Inches

TABLE VII

GRAVITY EFFECT. COMPARISON OF STRAINS AT 20 PSI FOR ROTATED AND UNROTATED SAMPLES

Test	Voids Ratio	Strains		
		ϵ_1	ϵ_2	ϵ_3
(-)	(-)	(in./in. x 10^2)		
Size Effect (Rep 2)[1]	0.781	1.89	1.82	1.36
Size Effect (Rep 3)[1]	0.765	1.89	1.92	1.23
Gravity Effect (Rep 1)[2]	0.822	2.19	2.08	1.28
Gravity Effect (Rep 2)[2]	0.779	1.91	1.92	1.33

[1]Unrotated sample - ϵ_3 is vertical strain during testing and with respect to filling.

[2]Rotated sample - ϵ_3 direction is horizontal during testing, but vertical with respect to filling.

wheat grain in a gravity field are those in which the longitudinal axis is perpendicular to the gravity field. The orientation of the longitudinal axis within the horizontal plane, however, may be random.

The effect of particle orientation with respect to gravity is that the geometry of an array of particles and the radii of contacting surfaces in the vertical direction vary from those in any horizontal direction. However, due to the random orientation of the longitudinal axis in the horizontal plane, the geometry of the array is identical in any horizontal direction. Thus, the mechanical behavior of wheat en masse is identical in all horizontal planes.

Isotropy

The results of two tests in which $\sigma_1:\sigma_2:\sigma_3 = 2.33:1.67:1$ are plotted in Figures 21 and 22, respectively. In the first test, σ_1 was a horizontal stress, whereas it was a vertical stress in the second test. It must be noted that the vertical direction refers to the vertical direction with respect to filling.

Interchanging the stresses between the two tests had no effect on the characteristic shape of the $\sigma_i - \epsilon_i$ curves. It did, however, tend to alter the magnitude of the strains in each direction. In Table VIII the magnitude of the strains in each direction are listed for a load cylinder pressure of 45 psi.

TABLE VIII

ISOTROPY. STRAINS OBSERVED AT LOAD CYLINDER PRESSURE OF 45 PSI AND $\sigma_1:\sigma_2:\sigma_3 = 2.33:1.67:1$

Test (-)	Voids Ratio (-)	ϵ_1	ϵ_2 (in./in. x 10^2)	ϵ_3
σ_1 - Horizontal	0.772	4.31	1.09	-0.69
σ_1 - Vertical	0.794	3.21	1.89	-0.27

When σ_1 was applied to the vertical direction with respect to filling, the unit strain was nearly 25 percent less than that when σ_1 was applied to a horizontal plane with respect to filling. At the same

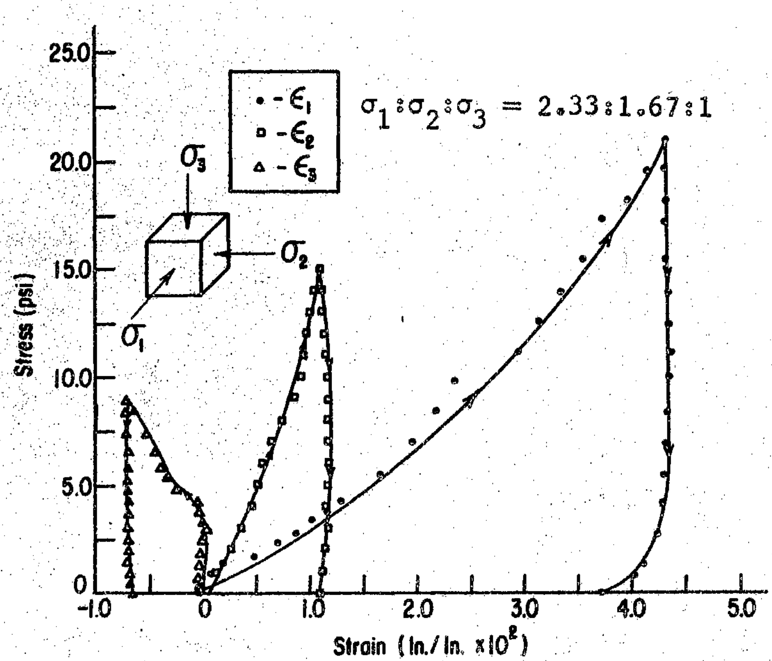

Figure 21. Isotropy Experiment Results. Stress-Strain Curves for Unrotated Stresses.

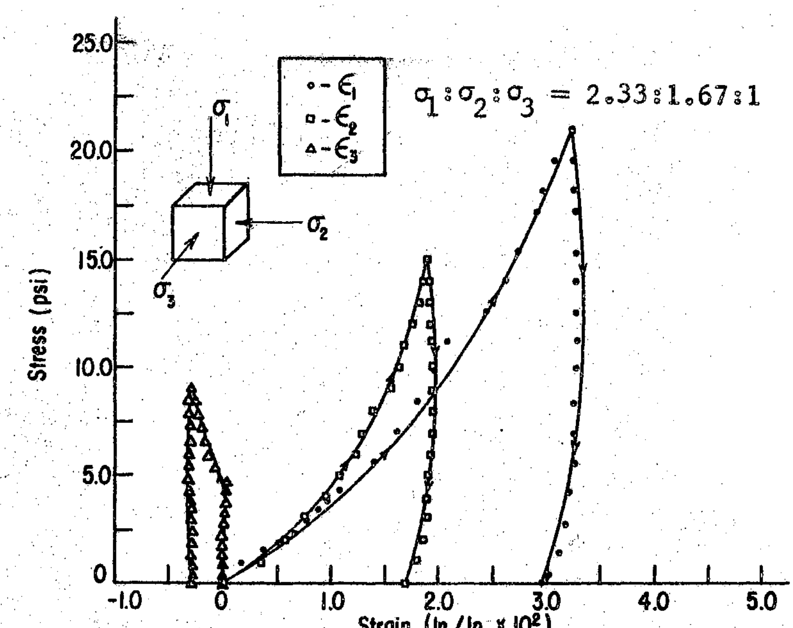

Figure 22. Isotropy Experiment Results. Stress-Strain Curves for Rotated Stresses.

time the strain in the σ_2 direction, which was horizontal in both tests, increased by 80 percent when σ_1 was rotated from a horizontal to a vertical stress. In the σ_3 direction, expansion of the sample was observed by both cases. The magnitude of the expansion was diminished by nearly 57 percent when σ_3 was rotated from a vertical to a horizontal stress with respect to filling.

Recalling that in hydrostatic compression tests the two horizontal strains were equal, whereas the magnitude of the strain in the vertical direction was somewhat smaller, and noting that rotation of a deviatoric stress state significantly altered the magnitude of the unit strains in each direction, it was concluded that the stress-strain behavior of wheat en masse is not completely isotropic. However, the behavior was found to be independent of direction in the horizontal plane. Thus, it was also concluded that wheat en masse is orthotropic with respect to principal stresses in planes perpendicular to the direction of filling.

Load Rate

The hydrostatic compression stress-strain curves for load rates of 3, 4.5 and 6 psi/minute in the load cylinder are shown in Figure 23 for the σ_2 direction. The curves for the σ_1 and σ_3 directions have been omitted since they illustrated similar trends. At a stress level of 40 psi, the strain, ε_2, was 0.0263, 0.0258, and 0.0266 in./in. for load rates of 3, 4.5 and 6 psi/minute, respectively. Since a similar lack of variation of strain with load rate was observed in the other stress directions, it was concluded that load rates within the range of 3 and 6 psi/minute are high enough to minimize long

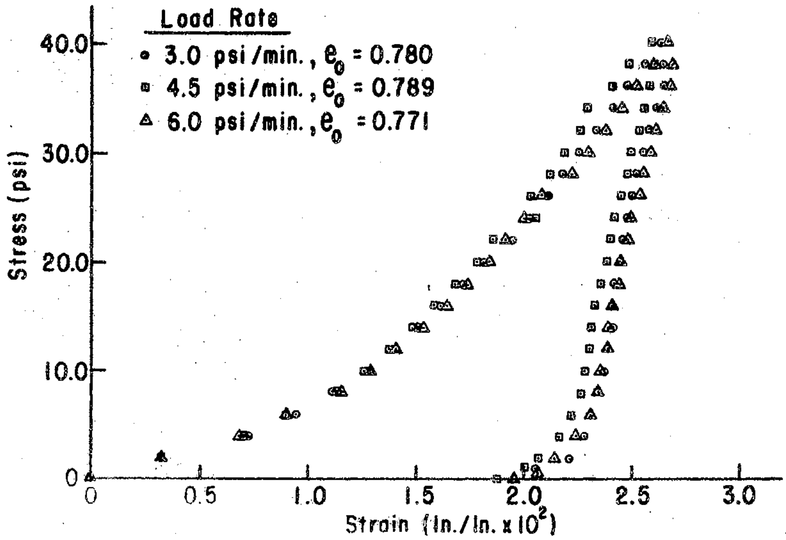

Figure 23. Stress-Strain Curves in the 2-Direction for Hydrostatic Compression Tests Conducted at Various Load Rates

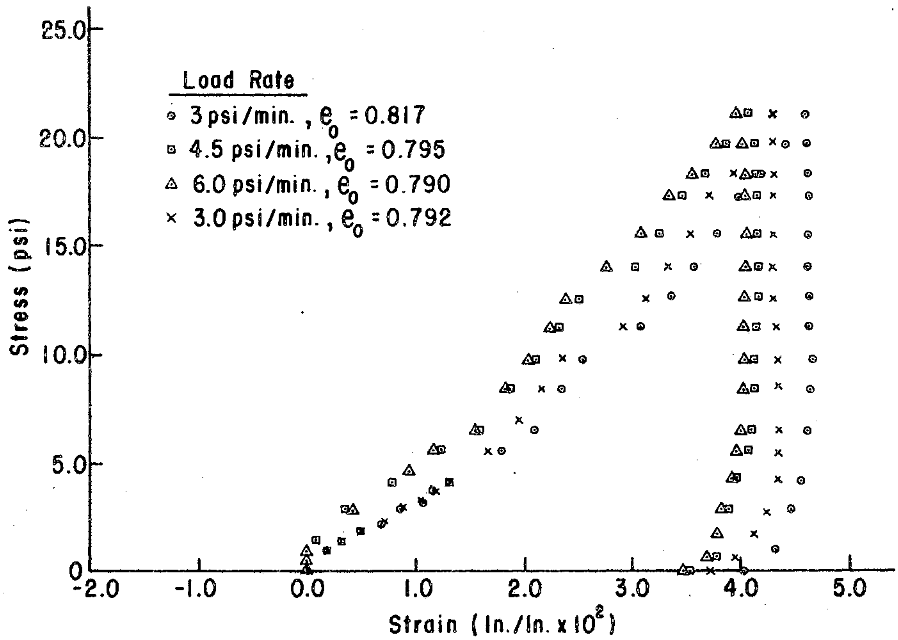

Figure 24. Stress-Strain Curves in the 1-Direction for Deviatoric Stress Tests Conducted at Various Load Rates

term creep effects and low enough to minimize any dynamic, or inertial, behavior. For static testing under hydrostatic compression, load rates in the range of 3 to 6 psi/minute on the load cylinder were deemed satisfactory.

The results of a deviatoric stress test conducted at load rates of 3, 4.5, and 6 psi/minute are illustrated in Figures 24, 25, and 26. The strain in the 1-direction increased with load rate. The strain at a load rate of 3 psi/minute (the test denoted by the circled points) was about 12 percent higher than the strain at the other load rates. However, it was observed that the initial voids ratio for that sample was 0.817, whereas the voids ratio for the other samples was in the range of 0.790 to 0.795. Thus, another test was run at a load rate of 3 psi/minute. In this case, the initial voids ratio was 0.792 and the strain was only about 5 percent higher at a load rate of 3 psi/minute than at the other load rates. (The results of this test are denoted by x's in Figures 24, 25, and 26.) It should be noted that the variation in the strain, ϵ_1, for the two samples loaded at 3 psi/minute was about 0.35×10^{-2} in./in. This is nearly two-thirds of the difference in strain observed between load rates.

The differences in observed strains due to load rate were also small in the 2- and 3-directions. For example, strain differences between the various load rates were only 0.0008 and 0.0010 in./in. in the 2- and 3-directions, respectively. These comparisons ignored the samples which had an initial voids ratio of 0.817.

The variation in strain with load rate was small in all cases; that is, the variation was equal to or less than 8 percent of the observed maximum strain at any stress level. It is asserted that

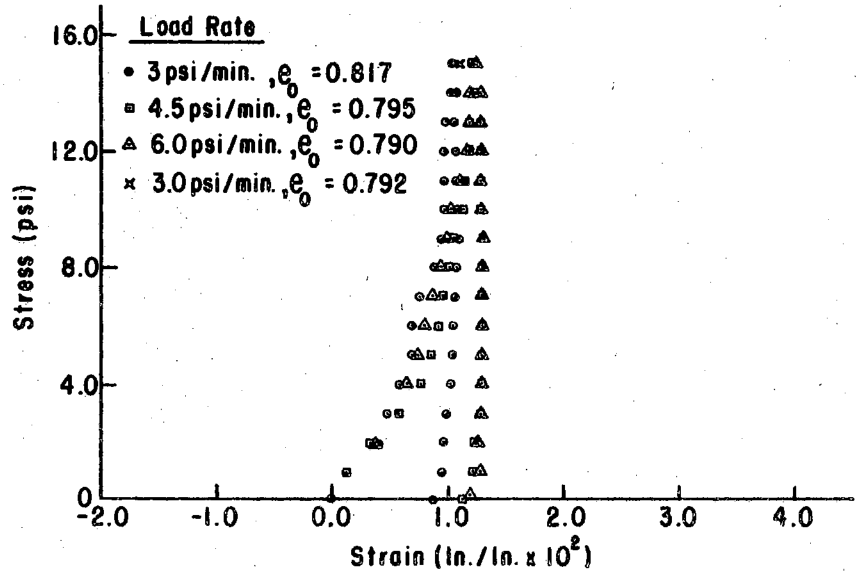

Figure 25. Stress-Strain Curves in the 2-Direction for Deviatoric Stress Tests Conducted at Various Load Rates.

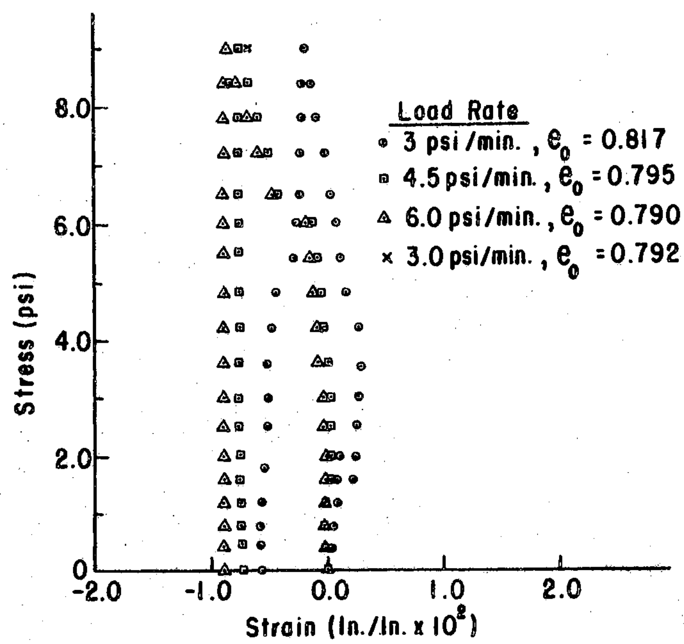

Figure 26. Stress-Strain Curves in the 3-Direction for Deviatoric Stress Tests Conducted at Various Load Rates

differences of such magnitude are attributable to variations in sample preparation, variations in wheat grains between samples, and experimental error.

Since little variation in the magnitude of the strain was observed at load rates of 3, 4.5 and 6 psi/minute in the load cylinder for identical stress paths, it was concluded that valid static stress-strain relationships for wheat en masse can be obtained by employing load rates in the range of 3 to 6 psi/minute in the top load cylinder. Since it was found to be more convenient to conduct the tests at a lower rate, a load rate of 3 psi/minute was used in all subsequent static load deformation studies.

Creep Tests

Strain-time curves for an instantaneously applied stress, σ_0, of 20 psi are plotted in Figure 27. The strain in each stress direction increased rapidly for the first half minute after application of the load. After one-half minute the rate of deformation rapidly decreased; and by the time one minute had elapsed, the rate of deformation was very low. It is noted that the experimental apparatus was designed primarily for gradually applied static loads. Thus, it is not a very accurate apparatus for measuring rapidly varying deformations. It is suspected that part of the time required to approach the nearly horizontal portion of the curves was due to a lag in the deformations. This lag resulted since a finite time is required to convey fluid to the membranes surrounding the sample. Once the instantaneous deformation was achieved; however, the results of the creep tests were valid and resulted in suitable estimates of the characteristic times for

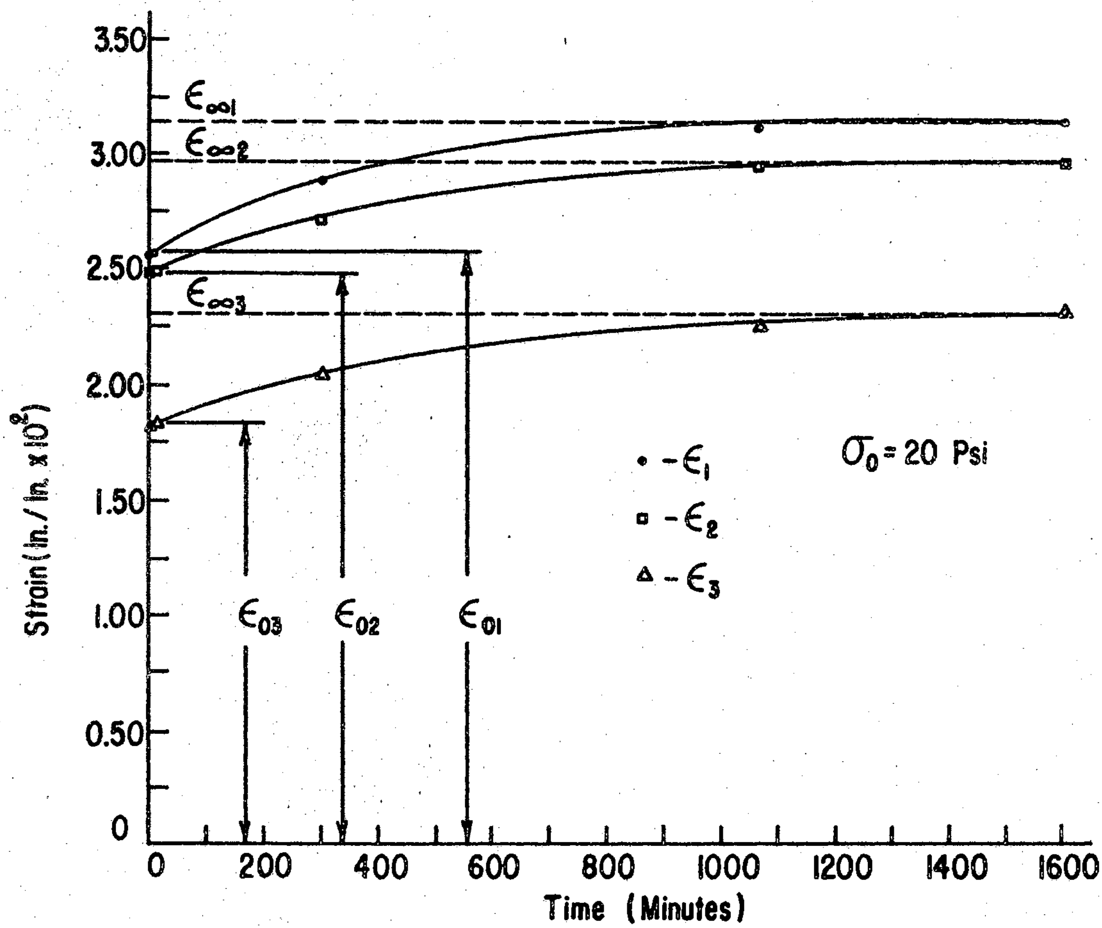

Figure 27. Strain-Time Curves for the Creep Tests in which σ_o = 20 psi

wheat en masse.

The curves in Figure 27 are defined by the general equation

$$\frac{\epsilon_i}{\epsilon_{\infty i}} = 1.0 - (1.0 - \frac{\epsilon_{oi}}{\epsilon_{\infty i}}) e^{-t/\tau_i} \tag{31}$$

The values of $\epsilon_{\infty i}$ and ϵ_{oi} are defined in the figure. The characteristic times were computed by evaluating τ_i at various levels of t. Upon selection of a time level, t, ϵ_i could be obtained from the curve and τ_i was computed by Equation 31. The characteristic times, the instantaneous strains, and the maximum strains are summarized in Table IX for the three stress directions.

TABLE IX

CHARACTERISTIC TIMES FOR WHEAT EN MASSE

Stress Direction (-)	Characteristic Time (minutes)	Instantaneous Strain (in./in x 10^2)	Maximum Strain (in./in. x 10^2)
1	280	2.52	3.16
2	310	2.48	2.98
3	380	1.82	2.30

The characteristic times in the two horizontal directions were 280 and 310 minutes, respectively. In view of the hydrostatic compression tests for the size effect and load rate studies, it is expected that the behavior in the two horizontal directions should be identical. Thus, the difference between the horizontal characteristic times is attributed to random variations. The characteristic time in the vertical direction is 380 minutes, which is 25 to 30 percent larger than the characteristic times in the horizontal directions.

It was observed that over 80 percent of the maximum strain was achieved instantaneously. Furthermore, 3 minutes after application of the load, nearly 85 percent of the maximum strain was achieved.

It is recognized that the stress-strain behavior of wheat en masse is somewhat dependent upon time. However, the change in the strain with time is small as compared to the instantaneous behavior; and the large characteristic times indicate a very low rate of increase in strain with time.

Load History

The stress-strain curves in the horizontal stress direction for a cyclic hydrostatic compression test are plotted in Figure 28. Again ϵ_2 was nearly identical to ϵ_1. The strain in the vertical direction was about 40 to 45 percent lower than that in the two horizontal directions.

In all three stress planes the hysteresis loss[1] decreased with increasing number of loading cycles. For example, in the 1-direction the hysteresis losses were 69 and 48 percent in the first and second cycles, respectively. Hysteresis losses decreased as the number of load cycles increased, because less particle reorientation took place

---

[1]Hysteresis loss refers to the energy absorbed by the material during a load-unload cycle.

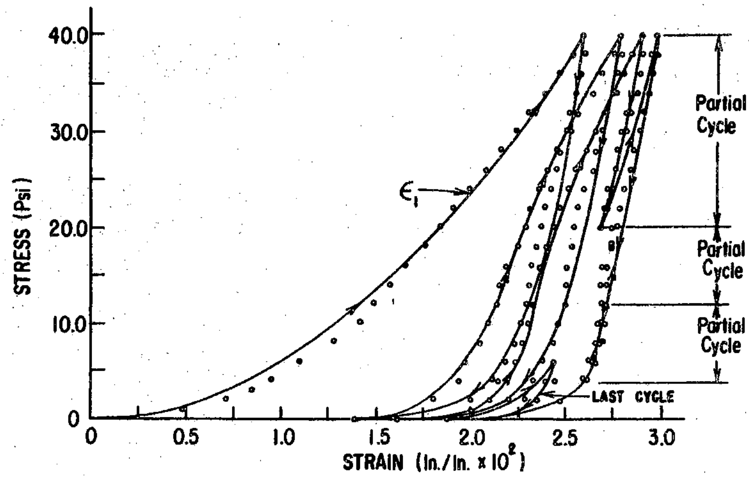

Figure 28. Stress-Strain Curves in the 1-Direction for a Cyclic Hydrostatic Compression Test

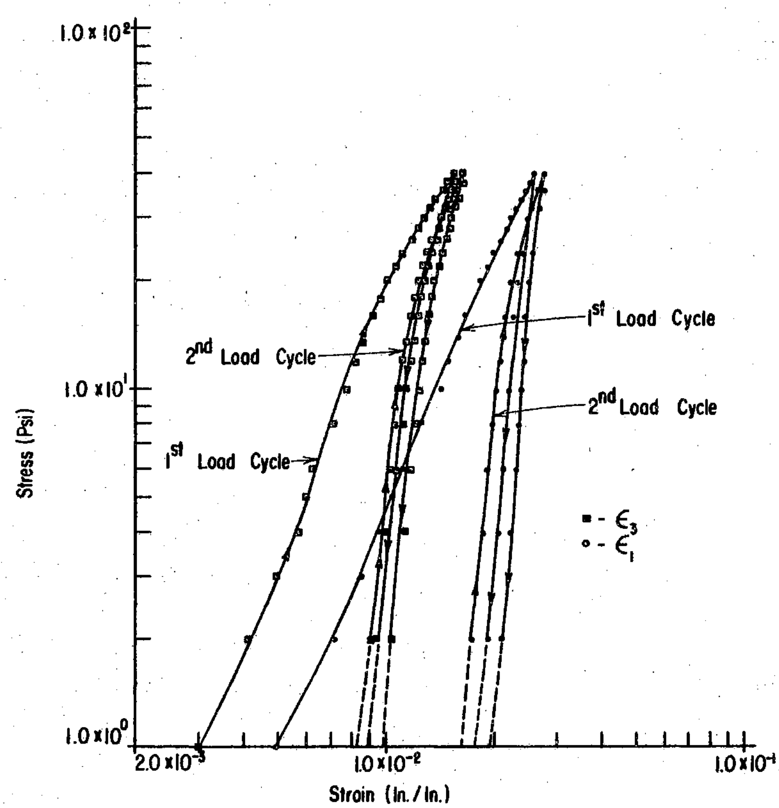

Figure 29. Log Stress-Log Strain Curves for a Cyclic Hydrostatic Compression Test

in each subsequent load cycle. That hysteresis losses were present after three full load cycles indicated, however, that some particle reorientation occurred even after several loading cycles, or that individual particle deformation also exhibited hysteresis losses.

The results of the partial load cycles indicated that most of the particle reorientation occurred at stress levels between 0 and 4 psi. Partial load cycles during the third full load cycle resulted in nearly elastic stress-strain behavior between stresses of 4 and 40 psi. However, at stress levels between 0 and 4 psi hysteresis losses were present even for the partial load cycles.

A log-log plot of the stress-strain curves are shown in Figure 29. In the σ_1 direction, the log-stress log-strain relationship was nearly linear for the first two cycles of both loading and unloading. This indicated that deformation during hydrostatic compression in the σ_1 and σ_2 directions is approximated by the general form $\epsilon_i = A\,\sigma_i^{\,n}$. In the σ_3 direction the log-stress log-strain relationship was also approximately linear, but it did have some curvature at stresses above 20 psi.

Similar to the behavior under hydrostatic compression, the hysteresis losses decreased with repeated load-unload cycles of deviatoric stress. In Figure 30, the $\sigma_1 - \epsilon_1$ curves are presented for a cyclic deviatoric stress test in which $\sigma_1:\sigma_2:\sigma_3 = 2.33:1.67:1$. Whereas the hysteresis loss in the first cycle was 95 percent, the loss in the second cycle was only 83 percent. Due to continuing re-orientation of particles within the sample during full load cycles, the deformation did not approach elastic behavior with increased number of load cycles. In the σ_1 and σ_2 directions the strains became

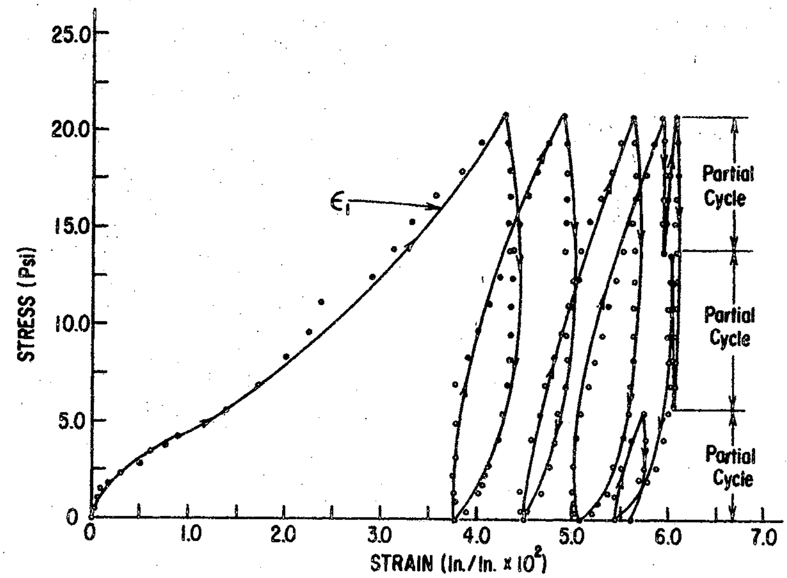

Figure 30. Stress-Strain Curve in the 1-Direction for a Cyclic Deviatoric Stress State.

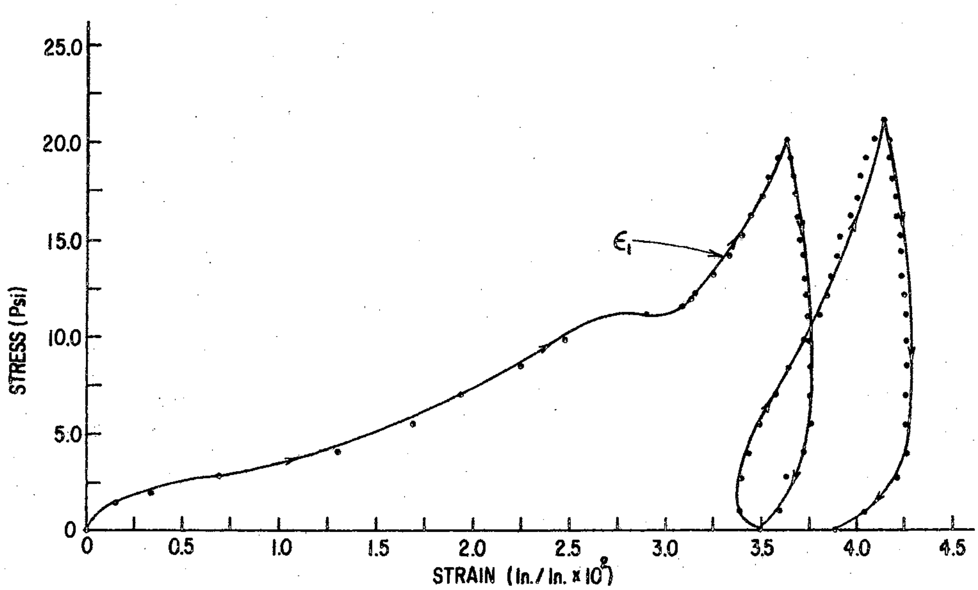

Figure 31. Stress-Strain Curves in the 1-Direction for a Hydrostatic Compression Stress State Superimposed upon a Deviatoric Stress State $\sigma_1:\sigma_2:\sigma_3 = 2.33:1.67:1.00$

increasingly larger in the positive direction with each successive load cycle, whereas the strain in the σ_3 direction became increasingly negative (expansion) with successive load cycles.

Partial load cycles during the fourth full load cycle revealed that: ϵ_1 was not elastic even for partial load cycles; ϵ_2 was elastic for partial load cycles above a stress level of 5 psi; and ϵ_3 was not elastic for partial load cycles.

Another cyclic deviatoric stress state with $\sigma_1:\sigma_2:\sigma_3 = 2.63:1.44:1$ ($\theta = 15$ degrees and $r = 2.5$ inches on the stress plate in Figure 20.) resulted in trends similar to those for the stress state described in Figure 30. The only difference in the results of the two deviatoric stress states was the relative magnitude of the strains in each direction. In Table X the magnitude of the strains in each stress direction are listed at a load cylinder pressure of 30 psi during the first load cycle for each deviatoric stress state.

TABLE X

STRAINS OBSERVED AT p = 30 PSI DURING FIRST LOAD CYCLE WHEN $\sigma_1:\sigma_2:\sigma_3 = 2.33:1.67:1$ AND WHEN $\sigma_1:\sigma_2:\sigma_3 = 2.63:1.44:1$

Stress State ($\sigma_1:\sigma_2:\sigma_3$)	Voids Ratio (-)	ϵ_1 (in./in. x 10^2)	ϵ_2	ϵ_3
2.33:1.67:1	0.687	3.15	0.97	-0.52
2.63:1.44:1	0.704	4.26	0.03	-0.41

The result of superimposing a hydrostatic stress state upon a deviatoric stress state is illustrated in Figure 31. The result of reversing the order of application of identical stress states is plotted in Figure 32. (Only $\sigma_1 - \epsilon_1$ curves are shown in Figures 31 and 32.) Comparison of these figures led to the conclusion that the sample deformation is greatly affected by the order of application of the stress components. It is further evidence that the deformations encountered in wheat en masse are highly dependent upon load history.

In Table XI the magnitude of the strains at the end of each load and unload portion of the curves are compared. At the end of each load or unload cycle, differences in the strains observed for the two tests were in excess of 70 percent of the maximum strain observed in Figure 31. The incremental nature of the stress-strain behavior precludes the separation of general stress states into hydrostatic and deviatoric components when dealing with wheat en masse. That is, the principle of superposition cannot be applied to the strain behavior of wheat en masse.

The $\sigma_1 - \epsilon_1$ curves for a radial stress path test in which the stress ratio $\sigma_1:\sigma_2:\sigma_3$ was varied while holding $\sigma_1 + \sigma_2 + \sigma_3$ constant are presented in Figure 33. The stress path has been described in Figure 20.

The variation of ϵ_2 with stress ratio was essentially 0. (See Appendix D-XII.) This is expected since the stress, σ_2, remained constant as the load cylinder moved from r = 0 to r = 3 inches.

In the σ_1 direction the stress increased from 10 to 16 psi as the load cylinder moved from r = 0 to r = 3 inches. The corresponding strain, ϵ_1, increased along a curved path as the stress increased.

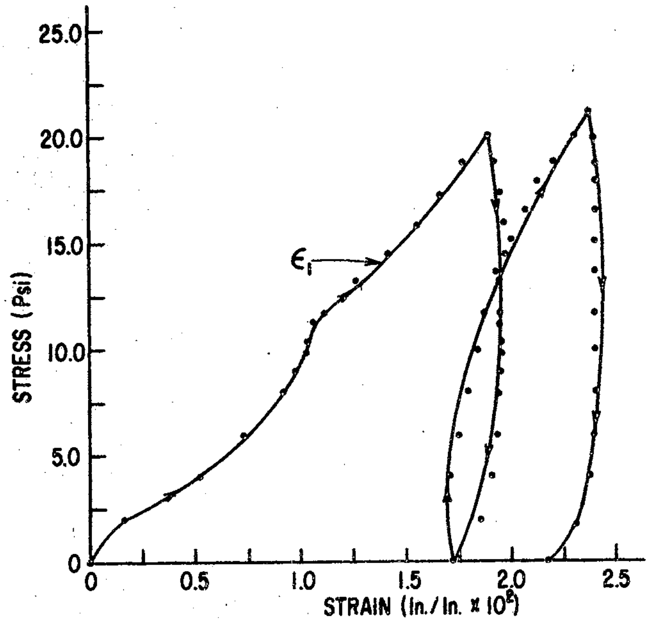

Figure 32. Stress-Strain Curves in the 1-Direction for a Deviatoric Stress State $\sigma_1 : \sigma_2 : \sigma_3 = 2.33:1.67:1.00$ Superimposed upon a Hydrostatic Compression Stress State

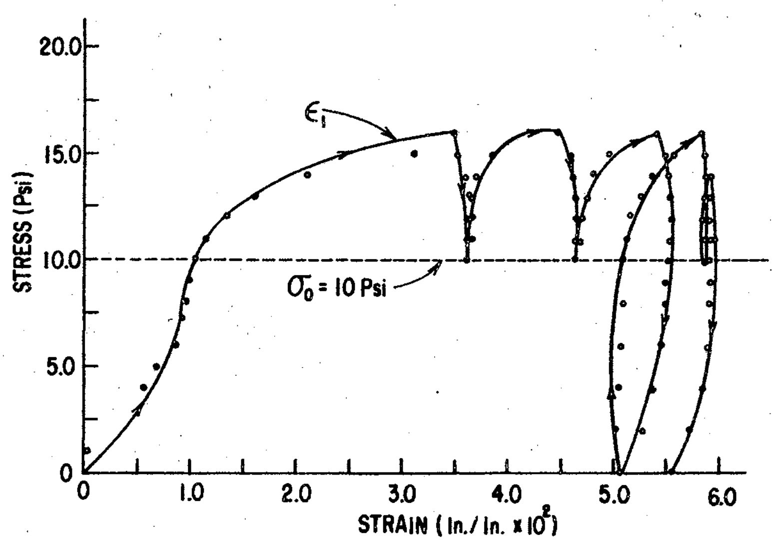

Figure 33. Stress-Strain Curve in the 1-Direction for a Radial Stress Path with $\theta = 30$ Degrees and r Varying from 0 to 3 Inches on the Stress Plate

TABLE XI

STRAINS OBSERVED AT END OF THE LOAD CYCLES FOR PRELIMINARY TESTS 15 AND 16

	Hydrostatic Over Deviatoric			Deviatoric Over Hydrostatic		
	ϵ_1	ϵ_2	ϵ_3	ϵ_1	ϵ_2	ϵ_3
	(in./in. x 10^2)			(in./in. x 10^2)		
End of 1st Load Cycle	3.65	0.95	-0.16	1.88	1.47	0.76
End of 1st Unload Cycle	3.50	0.73	-0.18	1.72	1.17	0.64
End of 2nd Load Cycle	4.15	1.05	-0.22	2.37	1.70	0.67
End of 2nd Unload Cycle	3.89	0.85	-0.22	2.17	1.44	0.60

At r = 2.5 and 3 inches the strain increased very rapidly with increasing stress. It is asserted that the rapid increase is due to plastic shear and particle reorientation. The sample was observed to change shape since the rapid increase in ϵ_1 was accompanied by a rapid expansive increase in ϵ_3. When the stress ratio was altered towards 1:1:1 as r varied from 3 to 0 inches, very little strain was recovered in the ϵ_1 direction. As r is varied from 0 to 3 to 0 inches in subsequent cycles, the increase in ϵ_1 decreased with the number of cycles. However, there was still little or no strain recovery when σ_1 decreased as a consequence of returning the load cylinder to the plate centroid. During the last cycle, r was varied only from 0 to 2 to 0 inches. This procedure avoided the very large deformations experienced for $r > 2$ inches. Consequently, irrecoverable strains during this cycle were much smaller than in the previous cycles.

It must be concluded that wheat en masse responds nonlinearly and nonelastically to changing states of deviatoric stress. Repeated cycling of the deviatoric stress states resulted in a decrease in the irrecoverable strains associated with each cycle, but the rate of decrease was relatively small after the second cycle. Many more than four cyclings of the stress ratios are required before the behavior approaches elastic behavior.

Discussion of Load History Results

The stress-strain behavior of wheat en masse was found to be highly dependent upon load history. All the test results indicated large hysteresis losses and irrecoverable deformations during repeated loading and unloading cycles. The hysteresis losses did, however, decrease slowly with repeated cycles of loading. The irreversible nature of the stress-strain behavior was attributed generally to continuing plastic deformations in which the voids ratio is constantly being reduced, to continuing particle reorientation, and to plastic deformations of individual particles.

Due to the dependence of the stress-strain relationship upon stress path, it was apparent that a general stress state for wheat en masse cannot be separated into its deviatoric and hydrostatic components for testing purposes. Instead, any desired stress state will have to be applied to the sample intact.

The load history results lead to the conclusion that wheat en masse behaves as an elasto-plastic material which undergoes strain hardening. Unloading of the wheat mass results in pseudo-elastic recovery of deformation.

CHAPTER VII

THE EXPERIMENTAL DESIGN

The three dimensional stress-strain behavior of wheat en masse is visualized as a necessary component in a rational solution for the pressure distributions in storage systems for wheat. The complicated nature of the deformation mechanism for wheat en masse precluded an analytical evaluation of the stress-strain behavior. An experimental approach based on the theory of similitude was adopted to evaluate the stress-strain behavior of wheat en masse during monotonically increasing stresses. For unloading, an alternate experimental procedure based on the findings of the preliminary studies was adopted. In the following chapters the term, loading function, refers to the strain prediction function for loading. Similarly, the unloading function refers to the strain prediction function for unloading.

Functional Relationship for Loading

Similitude and the Buckingham Pi Theorem

The number of required experiments can be significantly reduced by application of the Pi Theorem developed by Buckingham (8). Buckingham noted that if a phenomenon is describable in equation form, then that function can be expressed as a function of dimensionless combinations of the pertinent physical quantities. The theorem is written in general equation form as:

$$f\ (\pi_1,\ \pi_2,\ \ldots\ \pi_n) = 0 \tag{32}$$

where f = an arbitrary function

π_i = any dimensionless group

The only restriction imposed upon the dimensionless groups is that they be independent. The number of dimensionless groups required to adequately define a physical phenomenon is equal to the number of physical quantities required to define the system minus the rank of the dimensional matrix.

Definition of the System

The physical system sketched in Figure 34 represents a cubical element of wheat grains en masse. The pertinent quantities for evaluation of the three dimensional static stress-strain behavior during loading of the system are listed in Table XII.

The dependent quantity in the group is ϵ_i. The variable subscript is used to demonstrate that there are three dependent quantities, each of which is dependent upon the remaining 18 quantities.

The three stress levels, σ_i, are pertinent because the three dimensional stress-strain behavior of wheat is desired. It is assumed that a Poisson effect exists; that is, a stress in the jth or kth direction influences the strain in the ith direction.

The quantity σ_c is pertinent because of the incremental nature of the deformation of wheat en masse. To make the strain function unique it is required that the stress levels imposed be referred to a non-zero datum. In the case of plastic deformation of solids, σ_c would be

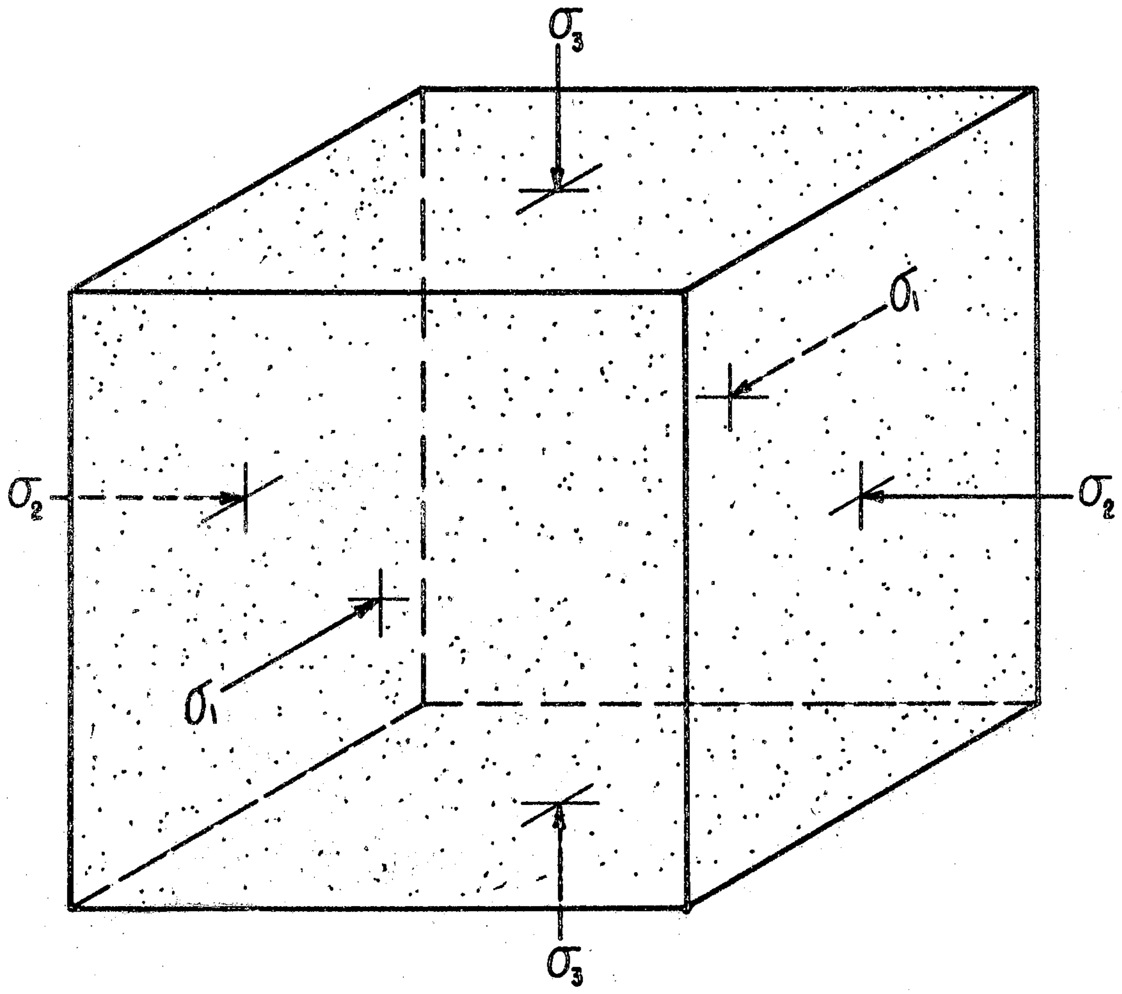

Figure 34. A Sketch of a Cubical Element of Wheat En Masse

TABLE XII

LIST OF PERTINENT QUANTITIES FOR STRESS-STRAIN BEHAVIOR OF WHEAT EN MASSE

No.	Symbol	Quantity	Units
1	ϵ_i	Principal strain in the ith direction	in./in.
2	σ_1	Principal stress in the 1-direction	$lb._f$/sq.in.
3	σ_2	Principal stress in the 2-direction	$lb._f$/sq.in.
4	σ_3	Principal stress in the 3-direction	$lb._f$/sq.in.
5	σ_c	Characteristic stress level	$lb._f$/sq.in.
6	n	Number of load cycles	--
7	e_o	Initial voids ratio	--
8	Δm	Change in grain moisture content	--
9	ΔT	Change in grain temperature	^oF
10	α	Temperature coefficient of expansion	in./^oF
11	ϕ	Angle of internal friction	degrees
12	S.G.	Specific gravity of kernels	--
13	a	Length of major axis of kernel	in.
14	b	Length of intermediate axis of kernel	in.
15	c	Length of minor axis of kernel	in.
16	E	Modulus of elasticity of kernels	$lb._f$/sq.in.
17	μ	Effective Poisson's ratio of kernels	--
18	τ_i	Characteristic time in the ith direction	seconds
19	r_ℓ	Load rate	$lb._f$/sq.in.-sec.

the stress level at which yielding occurs under an axial state of stress. For granular noncohesive materials, the Mohr failure theory predicts yielding at $\sigma_i = 0$ psi for an axial stress state. Further, Mohr's failure theory predicts a unique failure stress for each level of σ_1/σ_2 in a triaxial stress state $(\sigma_1 > \sigma_2 = \sigma_3)$. At this time a three dimensional failure surface has not been defined for wheat en masse. Thus, it does not seem feasible to define σ_c in terms of failure stresses. In the absence of a characteristic failure stress level the maximum stress level expected in a storage system was used for σ_c.

The preliminary studies on load history dependence illustrated the influence of the number of loading cycles upon the stress-strain behavior. The quantity, n, reflects the load history dependence of the strain.

Initial voids ratio dependence of the stress-strain behavior was also illustrated in the preliminary studies. It was observed that the larger the initial voids ratio, the larger was the associated strain for a given stress state.

Items 8 through 18 in the list are material properties of the wheat grains which influence the deformation behavior of wheat en masse. Changes in both the moisture and temperature levels affect the stress-strain behavior. The level of moisture content was observed by Brubaker and Pos (7) to influence the static coefficient of friction of wheat on various surfaces, while Lorenzen (32) observed that moisture changes altered the angle of internal friction of wheat.

The angle of internal friction is of importance since it plays a role in the sliding of one particle over another during particle reorientation. The value of the coefficient varies with granular medium and with the temperature, moisture content, and maturity of the granular medium.

The quantities, a, b and c, define the size and shape of the granular particles. The geometry of the particulates is of importance in defining the packing arrays encountered in a mass of particles, and in evaluating the magnitude of contact stresses and deformations experienced by individual particles.

The contribution of deformation of individual particles under load is reflected by the modulus of elasticity and Poisson's ratio of the particles. Particle deformation is one of the two primary modes of deformation in a particulate mass.

The influence of time upon the load deformation behavior is included in the quantities τ_i and r_λ. The quantity, τ_i, is the same characteristic time defined in the section entitled "Creep Tests" in Chapter VI. The subscript i denotes the directional dependence of the characteristic time.

Pi Terms

The rank of the dimensional matrix is 4. Thus, 15 dimensionless groups are required to define the system. One set of independent dimensionless quantities is listed below.

$\pi_1 = \epsilon_i$ - (dependent) $\qquad \pi_5 = e_o$

$\pi_2 = \sigma_1/\sigma_3 \qquad \pi_6 = n$

$\pi_3 = \sigma_2/\sigma_3 \qquad \pi_7 = \Delta m$

$\pi_4 = \sigma_1/\sigma_c \qquad \pi_8 = \alpha(\Delta T)/a$

$\pi_9 = \phi$

$\pi_{10} = S.G.$

$\pi_{11} = a/b$

$\pi_{12} = b/c$

$\pi_{13} = \sigma_c/E$

$\pi_{14} = \mu$

$\pi_{15} = \sigma_c/r_\ell \tau_i$

In the introductory chapter the scope of the study was limited to the definition of the stress-strain behavior of one variety of grain at one temperature and moisture content. In so doing, wheat at a given level of moisture content and temperature is likened to an alloy of steel. The engineering properties of each alloy of steel must be evaluated experimentally. Similarly, it was proposed that the mechanical behavior be evaluated for one "alloy" of wheat in this study. Generalization of the functional behavior of wheat for varying physical properties may be attempted if and when it is demonstrated that the methods employed in this study are adequate.

Thus, the influence of many of the pi terms was neglected. Specifically, π_7, π_8, π_9, π_{10}, π_{11}, π_{12}, π_{13}, and π_{14} are all dependent upon the physical properties of the granular medium and their influence upon the functional behavior will not be considered.

The pi term reflecting the influence of load rate, π_{15}, was also excluded from the functional relationship for ϵ_i. It was noted in the preliminary investigations that the stress-strain behavior of wheat en masse was not highly time dependent and that static behavior is achieved if the load rate is incremented at rates between 3 and 6 psi/minute. The influence of π_{15} was held constant by applying all loads at the rate of 3 psi/minute at the load cylinder.

π_1, the dependent π-term, is the principal strain in the ith direction. This π-term will be measured in each of the principal directions. To distinguish this term from a similar term for the unloading portion of the stress-strain relationship, it has been given the subscript L; i.e., $\pi_1)_L = \epsilon_i)_L$.

π_2 and π_3 are both ratios of principal stresses. The range of these ratios have been established by the ranges expected in storage structures containing wheat en masse. Based on published materials concerning the ratio of lateral to vertical pressures in storage structures for granular media and on the friction experienced between wheat and the confining wall, it is expected that π_2 and π_3 would vary within the range 0.375 to 1. The lower limit is the lowest published value for the ratio of lateral to vertical stress in a storage structure;[1] whereas the upper limit corresponds to the hydrostatic state of stress. In the experimental design, π_2 and π_3 were varied from 0.326 to 2.590. The range was extended in order that the stress-strain behavior could be defined on both sides of the hydrostatic stress state.

π_4 is an index of the ratio of the stress level in the 1-direction to the characteristic stress level. Based on Janssen's equation for lateral pressures, the maximum stress level expected in a 30 x 100 feet grain silo containing wheat is 12.8 psi. Allowing for stress increases of two to three times those predicted by Janssen's equation, σ_c has been arbitrarily set at 40 psi. Using σ_c = 40 psi, π_4 was varied from 0 to 1.0.

π_5, the initial voids ratio, was held constant in this study. Initial voids ratio has a marked effect upon the stress-strain

---

[1]Mohsenin (36) has summarized the published physical properties of small grains in the Appendices of his text.

behavior, but in the present study its effect will not be evaluated. π_5 will be held constant within the approximate range of 0.750 and 0.780. Any variation in e_o was assumed to be random.

A granular medium, such as wheat en masse, behaves as a nonlinear elasto-plastic substance. Therefore, stress-strain behavior is dependent upon load history. Load history is characterized by $\pi_5 = n$ in the list of π-terms. This, however, is an oversimplication of the elasto-plastic behavior. Consider, as an example, the stress path illustrated in the stress-strain diagram of Figure 35.

The stress-strain curve is nonsingular whenever any stress path is considered other than a monotonically increasing stress. If unloading occurs during the loading history, the stress-strain function is dependent not only upon the load cycle encountered, but also upon the maximum stress to which the material has been loaded in the nth cycle and all previous n-1 cycles.

As an example, if a stress path $\overline{OAB}$ in Figure 35 is followed during the first load cycle, then when n = 2 the stress-strain curve will follow the path $\overline{BGH}$. However, if the first load cycle terminates at point C and is unloaded, then the path followed during the second load cycle is $\overline{DEF}$.

At this point the problem would become too wide in scope to consider the general nature of the stress-strain function for all variations with n greater than 1. Therefore, it has been decided that a thorough study of the first cycle of loading and unloading is the most logical course to follow. Thus $\pi_7 = n = 1$ throughout the study. This decision is justified because the behavior of the first cycle must be established before subsequent cycles may be defined.

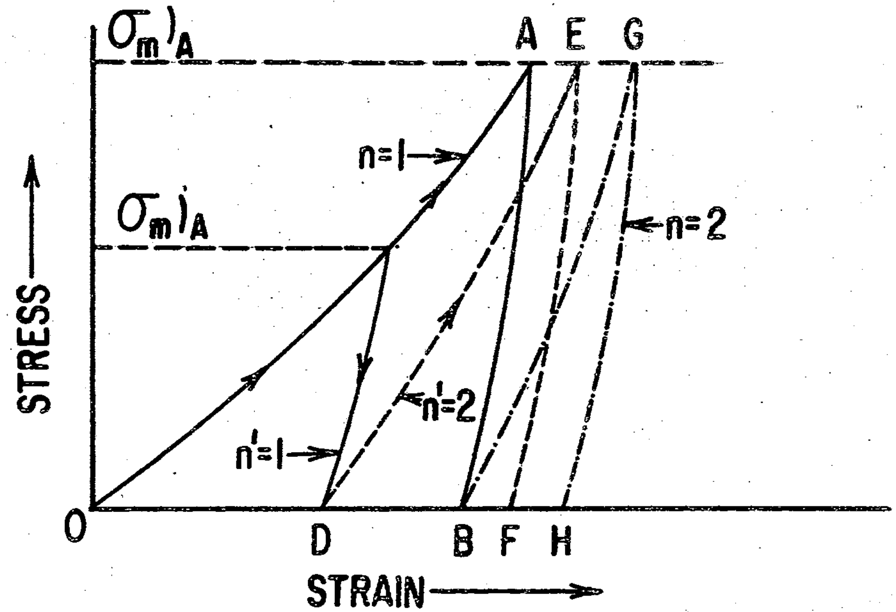

Figure 35. Stress-Strain Diagram for Two Load-Unload Cycles of an Elasto-Plastic Medium

Prediction Equations

The functional relationships for predicting strains are reduced considerably by the aforementioned limitations. For loading the prediction equations reduced to:

$$\epsilon_1)_L = f_1(\pi_2, \pi_3, \pi_4) \tag{33}$$

$$\epsilon_2)_L = f_2(\pi_2, \pi_3, \pi_4) \tag{34}$$

$$\epsilon_3)_L = f_3(\pi_2, \pi_3, \pi_4) \tag{35}$$

The method of component equations discussed by Murphy (37) was employed to obtain the arbitrary functions f_1, f_2, and f_3. That is, three experimental series were conducted. In each series the three principal strains were measured, one pi term was varied, and two pi terms were held constant at a specified value. The generalized experimental design for obtaining the prediction equation for strain during loading is summarized in Table XIII. It was assumed that there was no interaction between the pi terms in this design.

TABLE XIII

GENERALIZED EXPERIMENTAL DESIGN
FOR THE LOADING FUNCTION

Experiment Series	$\pi_1 = \epsilon_i$	$\pi_2 = \sigma_1/\sigma_3$	$\pi_2 = \sigma_2/\sigma_3$	$\pi_4 = \sigma_1/\sigma_c$
1	Measure	Vary	Constant	Constant
2	Measure	Constant	Vary	Constant
3	Measure	Constant	Constant	Vary

From each experiment series three component equations were obtained; one for each principal stress direction. Equations 36, 37, and 38 are representations of the three component equations for $\epsilon_1)_L$. Similar equations were obtained for $\epsilon_2)_L$ and $\epsilon_3)_L$. A bar over a pi term indicated that it was held constant.

$$\pi_1 = \epsilon_1)_L = f_4(\pi_2, \bar{\pi}_3, \bar{\pi}_4) \tag{36}$$

$$\pi_1 = \epsilon_1)_L = f_5(\bar{\pi}_2, \pi_3, \bar{\pi}_4) \tag{37}$$

$$\pi_1 = \epsilon_1)_L = f_6(\bar{\pi}_2, \bar{\pi}_3, \pi_4) \tag{38}$$

Upon combination of the component equations in each of the three orthogonal directions, the desired stress-strain functions were derived.

The complete experimental design for the loading function along with the specified pi term levels is outlined in Table XIV. Three replications of each experiment were run, and experiments were conducted in random order so that the experimental errors would be randomly distributed.

Validation

The accuracy of the experimental results was checked by two separate procedures. The accuracy of the combination procedures for developing the prediction equations was evaluated by plotting the predicted strains versus the observed strains used to develop the prediction equations.

Two validation experiments were conducted on a four inch cubical sample with the stress control device. A stress ratio, $\sigma_1 : \sigma_2 : \sigma_3$, of

TABLE XIV

EXPERIMENTAL DESIGN FOR THE LOADING FUNCTION

Expt. Series	Expt. No.	$\frac{\pi_1}{\epsilon_1)_L\ \epsilon_2)_L\ \epsilon_3)_L}$	$\pi_2 = \frac{\sigma_1}{\sigma_3}$	$\pi_3 = \frac{\sigma_2}{\sigma_3}$	$\pi_4 = \frac{\sigma_1}{\sigma_c}$	σ_1 (psi)	σ_2 (psi)	σ_3 (psi)	σ_c (psi)	r (in.)	θ (deg.)	p (psi)
	1		0.326				24.40	24.40		-2.5		56.8
	16		0.436				18.40	18.40		-2.0		44.8
	2		0.557				14.40	14.40		-1.5		36.8
	17		0.688				11.60	11.60		-1.0		31.2
I	3	Measure	0.835	1.000	0.200	8.00	9.60	9.60	40.00	-0.5	0	27.2
	4		1.000				8.00	8.00		0.0		24.0
	18		1.184				6.75	6.75		0.5		21.5
	5		1.392				5.75	5.75		1.0		19.5
	6		1.901				4.21	4.21		1.5		16.4
	7		2.590				3.09	3.09		2.0		14.2
	8			0.326			2.61			-2.5		18.6
	19			0.436			3.50			-2.0		19.5
	9			0.557			4.46			-1.5		20.5
	20			0.688			5.50			-1.0		21.5
II	10	Measure	1.00	0.835	0.200	8.00	6.70	8.00	40.00	-0.5	120	22.7
	11			1.000			8.00			0.0		24.0
	21			1.184			9.46			0.5		25.5
	12			1.392			11.10			1.0		27.1
	13			1.901			15.20			1.5		31.2
	14			2.590			20.70			2.0		36.7
					0.00	0.00	0.00	0.00				0.0
					0.05	2.00	2.00	2.00				6.0
					0.10	4.00	4.00	4.00				12.0
					0.20	8.00	8.00	8.00				24.0
					0.30	12.00	12.00	12.00				36.0
III	15	Measure	1.00	1.00	0.40	16.00	16.00	16.00	40.00	0.0	0	48.0
					0.50	20.00	20.00	20.00				60.0
					0.60	24.00	24.00	24.00				72.0
					0.70	28.00	28.00	28.00				84.0
					0.80	32.00	32.00	32.00				96.0
					0.90	36.00	36.00	36.00				108.0
					1.00	40.00	40.00	40.00				120.0

0.91:0.82:1.00 was randomly selected from those ratios within the range of the pi terms. The load cylinder pressure was varied from 0 to 60 psi. The observed strains were plotted against the strains predicted by Equations 33, 34, and 35. The standard deviation from a straight line of 45 degrees and the correlation coefficient were used as measures of the degree of agreement between the observed and predicted strains.

Functional Relationship for Unloading

Hypothesis

The preliminary studies revealed that the unloading behavior is exponential for selected loading paths. This behavior was observed for both hydrostatic and deviatoric stress states. It was therefore hypothesized that the unloading path of wheat en masse is linear in log stress-log strain space.

Preliminary studies also indicated that unloading from any point on a given loading curve proceeded along parallel paths. That is, the unloading path $\overline{CD}$ in Figure 35 is parallel to, and thus has the same characteristic shape as, unloading path $\overline{AB}$. The two paths are merely shifted by an amount $\overline{DB}$.

It is therefore hypothesized that unloading paths at a particular stress ratio $\sigma_1:\sigma_2:\sigma_3$ are parallel for various levels of σ_m. σ_m, the stress level at which unloading commences, is defined graphically in Figure 35. It is not known whether the unloading paths between stress ratios are parallel.

The Experimental Approach

If the hypothesis is valid, then the unloading path at any stress state can be defined by the generalized form

$$\epsilon_i)_U = \epsilon_{im}(\sigma_i/\sigma_{im})^{n_i} \tag{39}$$

where $\epsilon_i)_U$ = strain in the ith direction, in./in.

ϵ_{im} = strain in the ith direction at which unloading commenced, in./in.

σ_i = stress level in the ith direction, psi.

σ_{im} = stress level in the ith direction at which unloading commenced, psi.

n_i = slope of the unloading path in log-log space in the ith direction.

In Equation 39, ϵ_{im} can either be the observed value of strain or the value of strain predicted from either Equation 33, 34, or 35. The stress level, σ_{im}, is a known quantity as is σ_i. Since $\epsilon_i)_U$ is the quantity to be predicted, only n_i is unknown.

According to the hypothesis, the shape of the unloading path, and therefore n_i, is independent of the level of stress at which unloading commences for a given stress ratio. However, the variation of n_i with stress ratio is not known. If the variation of n_i with stress ratio is evaluated, then the general form of the unloading path will have been determined.

The experiments used for obtaining the loading path were also used for defining the variation of n_i. The slope of the unloading curves in log-log space was evaluated by the least squares linear regression procedure for each experiment included in Table XIV. The variation of n_i with stress ratio was obtained by plotting n_i versus σ_1/σ_3 and n_i versus σ_2/σ_3. If n_i varied with stress ratio, then the component equations for n_i would be combined and substituted into Equation 39. If, on the other hand, n_i did not vary with $\sigma_1:\sigma_2:\sigma_3$, then the unloading path is defined by Equation 39.

It is noted that all the limitations imposed upon the loading function also apply to the unloading function.

Validation

Procedures similar to those described for the loading function were employed. Only one variation was incorporated. In Equation 39 the quantity, ϵ_{im}, could be either an observed or a predicted quantity. The observed and predicted strains were plotted both when ϵ_{im} was an observed quantity and when it was predicted by $\epsilon_i)_L$.

CHAPTER VIII

PRESENTATION OF DATA AND RESULTS

The Loading Functions

Component Equations

Early in the experimental program it was observed that flow conditions existed in the stress box at π_2 and π_3 levels above 1.392 and below 0.557. That is, the deformation did not stabilize with time. Instead, the deformation continued to vary with time until either the capacity of the stress cylinders, L, was exceeded or the water supply was depleted behind the membranes in one of the stress directions. The initiation of the flow condition was always associated with a reversal of the strains in one of the principal directions. The strain changed sign during flow so that expansive deformations were observed during a compressive type loading condition.

Since wheat is a noncohesive substance, flow conditions are expected at critical stress ratios. For example, when the stress ratio, σ_1/σ_3, approaches 0 while holding σ_2/σ_3 constant at any finite non-zero level, flow conditions are established in the direction of σ_1. Since σ_1 must equal 0 for σ_1/σ_3 to be 0 in this case, ϵ_1 would be expansive and increase without limit. At the other extreme, as σ_1/σ_3 increases without limit while σ_2/σ_3 is held constant, it is implied that $\sigma_1 \gg \sigma_3$. Expansion would be experienced in the σ_3

direction, and the expansion in that direction would increase without bounds as σ_1/σ_3 increased without limit. Similar arguments may be developed for the case of σ_2/σ_3.

Since flow conditions commenced at π_2 and π_3 levels above and below 1.392 and 0.557, respectively, these levels were considered to be the limits bounding static stress-strain behavior of wheat en masse. The data for the static stress-strain behavior of wheat en masse within these limits are presented in Tables XV, XVI, and XVII.

The component equations for $\epsilon_i)_L$ versus π_2 and $\epsilon_i)_L$ versus π_3 were linear in arithmetic space and did not include the origin, whereas the component equations for $\epsilon_i)_L$ versus π_4 were linear in log-log space. The nine component equations, three for each principal direction, are plotted in Figures 36 through 44.

The observed values of strain are plotted in each figure. The straight line plotted in each figure is the linear regression line obtained by the method of least squares which is discussed in detail in the text by Natrella (39). The equation of the regression lines is included in each figure as is the correlation coefficient, R, and the standard deviation from regression, S. A summary of the component equations is presented in Table XVIII. The lowest correlation coefficient was 0.967, and the highest standard deviation from regression was 0.0013×10^{-2} in./in. in Equation 43. Thus, the largest observed standard deviation from regression was only 7.4 percent of the observed range of variation of strain.

TABLE XV

UNIT STRAIN AS A FUNCTION OF THE STRESS RATIO, σ_1/σ_3, WITH π_3 AND π_4 HELD CONSTANT

Run No.	Unit Strain $\epsilon_1)_L$	$\epsilon_2)_L$ (in./in. x 10^2)	$\epsilon_3)_L$	π_2 σ_1/σ_3 (-)	Initial Voids Ratio e_o (-)
2A	-0.11	2.46	1.62	0.557	0.751
2B	0.07	2.44	1.34	0.557	0.755
2C	0.13	2.46	1.41	0.557	0.780
17A	0.30	2.18	1.41	0.688	0.764
17B	0.62	2.11	1.22	0.688	0.801
17C	0.47	2.09	1.22	0.688	0.769
3A	0.92	1.60	0.95	0.835	0.779
3B	0.98	1.57	0.94	0.835	0.784
3C	0.92	1.66	0.95	0.835	0.772
4A	1.30	1.31	0.65	1.000	0.791
4B	1.23	1.25	0.63	1.000	0.773
4C	1.33	1.35	0.63	1.000	0.770
18A	1.73	0.88	0.53	1.184	0.768
18B	1.80	1.06	0.54	1.184	0.789
18C	1.59	0.91	0.51	1.184	0.756
5A	2.16	0.82	0.19	1.392	0.774
5B	2.23	0.69	0.28	1.392	0.778
5C	2.02	0.70	0.36	1.392	0.771

TABLE XVI

UNIT STRAIN AS A FUNCTION OF THE STRESS RATIO, σ_2/σ_3, WITH π_2 AND π_4 HELD CONSTANT

Run No.	Unit Strain $\epsilon_1)_L$	$\epsilon_2)_L$ (in./in. x 10^2)	$\epsilon_3)_L$	π_3 σ_2/σ_3 (-)	Initial Voids Ratio e_o (-)
9A	1.81	0.26	1.20	0.557	0.788
9B	1.81	0.22	1.11	0.557	0.766
9C	1.64	0.21	0.95	0.557	0.759
20A	1.66	0.45	1.04	0.688	0.782
20B	1.66	0.40	0.97	0.688	0.760
20C	1.55	0.48	0.90	0.688	0.761
10A	1.37	0.97	0.80	0.835	0.776
10B	1.47	0.82	0.80	0.835	0.773
10C	1.42	0.91	0.83	0.835	0.770
11A	1.29	1.31	0.63	1.000	0.775
11B	1.35	1.33	0.68	1.000	0.785
11C	1.29	1.26	0.52	1.000	0.765
21A	1.00	1.92	0.58	1.184	0.783
21B	0.96	1.87	0.57	1.184	0.775
21C	0.95	1.93	0.54	1.184	0.768
12A	0.78	2.39	0.31	1.392	0.766
12B	0.90	2.53	0.33	1.392	0.788
12C	0.80	2.39	0.34	1.392	0.752

TABLE XVII

UNIT STRAIN AS A FUNCTION OF THE STRESS RATIO, σ_1/σ_c, WITH π_2 AND π_3 HELD CONSTANT

Unit Strain									π_4
Expt. No. 15A[1]			Expt. No. 15B[2]			Expt. No. 15C[3]			
ϵ_1	ϵ_2	ϵ_3	ϵ_1	ϵ_2	ϵ_3	ϵ_1	ϵ_2	ϵ_3	σ_1/σ_c
(in./in. x 10^2)			(in./in. x 10^2)			(in./in. x 10^2)			(-)
0.00	0.00	0.00	0.00	0.00	0.00	0.00	0.00	0.00	0.00
0.77	0.77	0.30	0.68	0.67	0.29	0.69	0.69	0.33	0.05
0.97	0.98	0.45	0.98	0.97	0.41	0.94	0.95	0.46	0.10
1.11	1.11	0.54	1.14	1.15	0.49	1.13	1.14	0.56	0.15
1.28	1.29	0.64	1.29	1.32	0.55	1.26	1.30	0.65	0.20
1.38	1.39	0.72	1.42	1.45	0.60	1.37	1.41	0.71	0.25
1.45	1.47	0.78	1.53	1.57	0.65	1.46	1.50	0.76	0.30
1.55	1.59	0.85	1.61	1.64	0.68	1.50	1.58	0.81	0.35
1.66	1.68	0.92	1.69	1.73	0.72	1.61	1.67	0.86	0.40
1.75	1.77	0.99	1.79	1.84	0.77	1.71	1.76	0.92	0.45
1.81	1.85	1.04	1.87	1.93	0.82	1.78	1.84	0.97	0.50
1.90	1.93	1.10	1.95	2.02	0.87	1.87	1.93	1.04	0.55
2.00	2.03	1.18	2.05	2.11	0.92	1.95	2.01	1.08	0.60
2.07	2.12	1.23	2.13	2.20	0.97	2.03	2.10	1.14	0.65
2.15	2.20	1.29	2.22	2.29	1.01	2.10	2.19	1.21	0.70
2.24	2.28	1.36	2.29	2.38	1.06	2.18	2.26	1.26	0.75
2.31	2.36	1.43	2.38	2.46	1.12	2.26	2.33	1.32	0.80
2.48	2.43	1.49	2.46	2.53	1.18	2.33	2.41	1.38	0.85
2.46	2.50	1.53	2.54	2.60	1.23	2.39	2.48	1.45	0.90
2.53	2.56	1.58	2.60	2.69	1.28	2.46	2.54	1.50	0.95
2.59	2.62	1.64	2.65	2.73	1.32	2.51	2.61	1.54	1.00

[1] e_o = 0.783   [2] e_o = 0.782   [3] e_o = 0.780

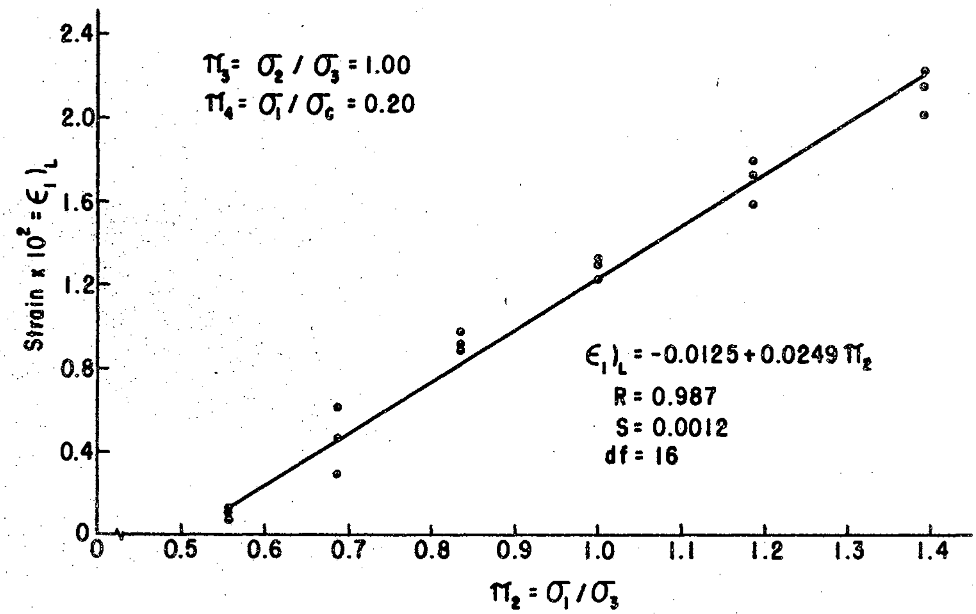

Figure 36. Component Equation. Strain in the 1-Direction vs. Stress Ratio, σ_1/σ_3, During Loading

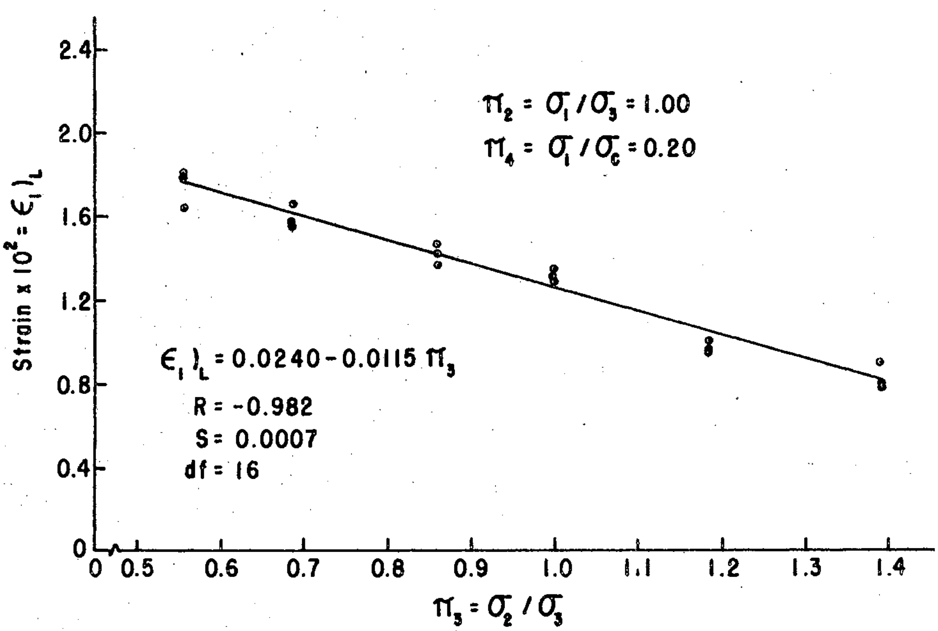

Figure 37. Component Equation. Strain in the 1-Direction vs. Stress Ratio, σ_2/σ_3, During Loading

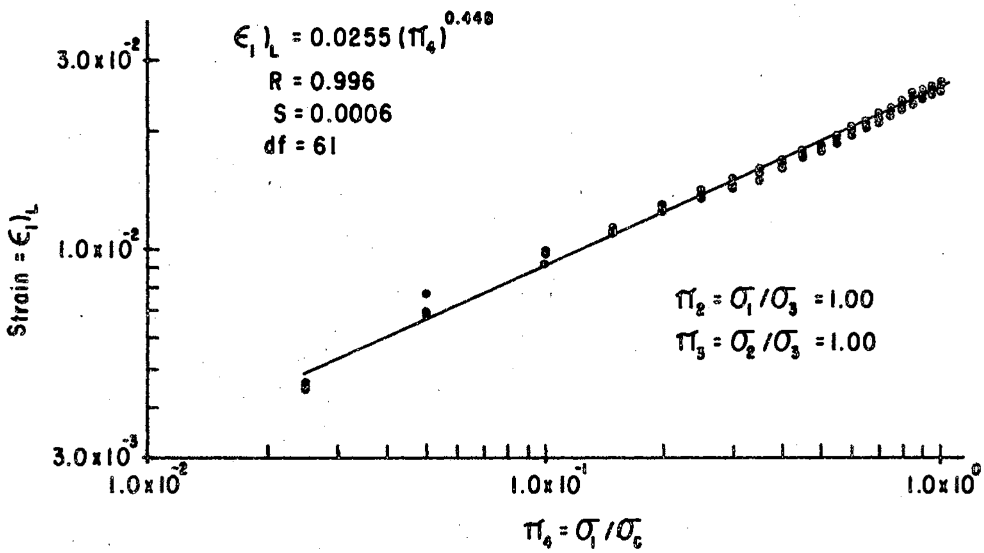

Figure 38. Component Equation. Log Strain in the 1-Direction vs. Log Stress Ratio, σ_1/σ_c, During Loading

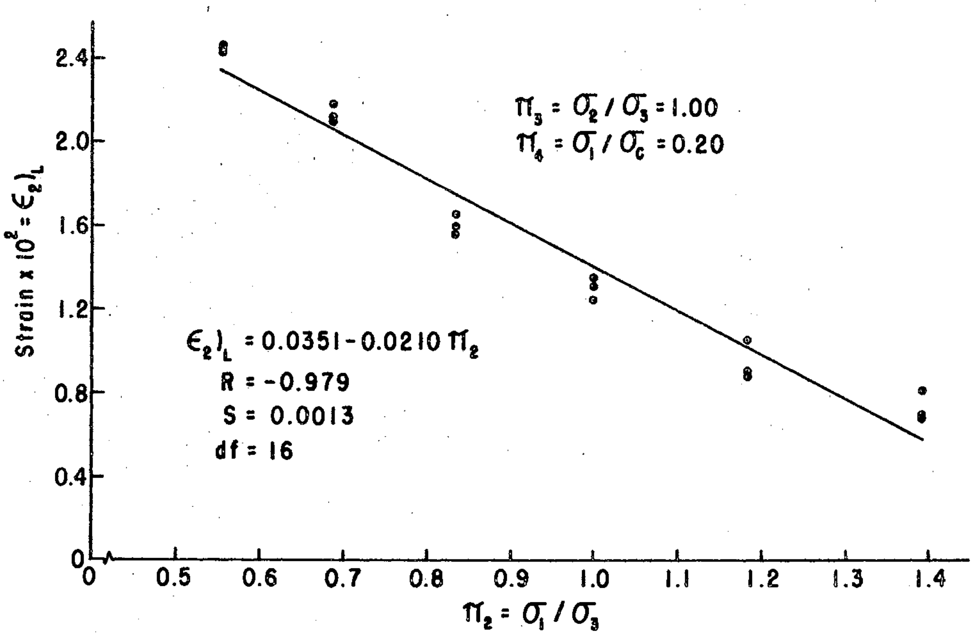

Figure 39. Component Equation. Strain in the 2-Direction vs. Stress Ratio, σ_1/σ_3, During Loading

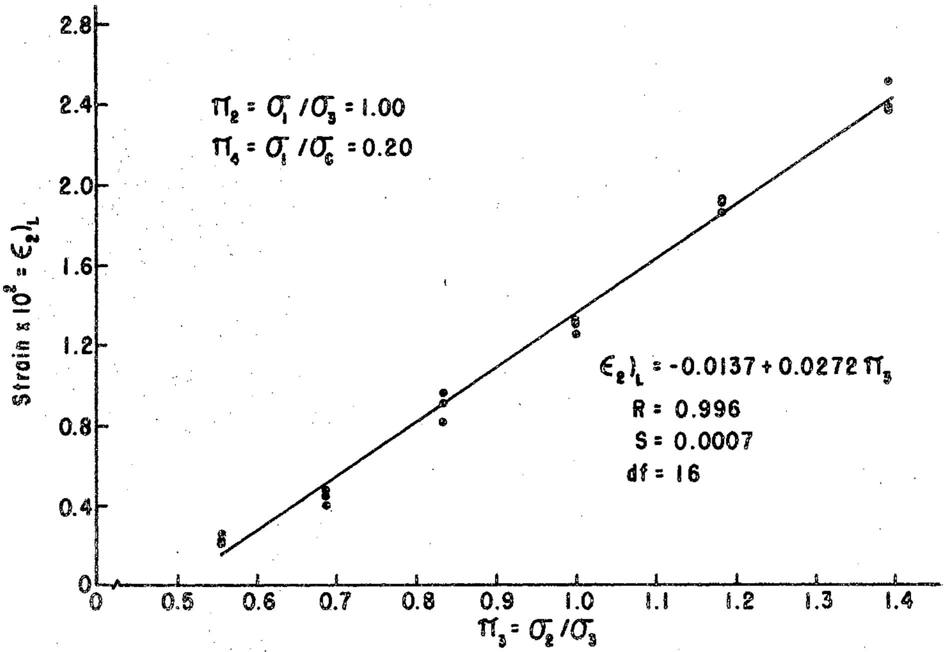

Figure 40. Component Equation. Strain in the 2-Direction vs. Stress Ratio, σ_2/σ_3, During Loading

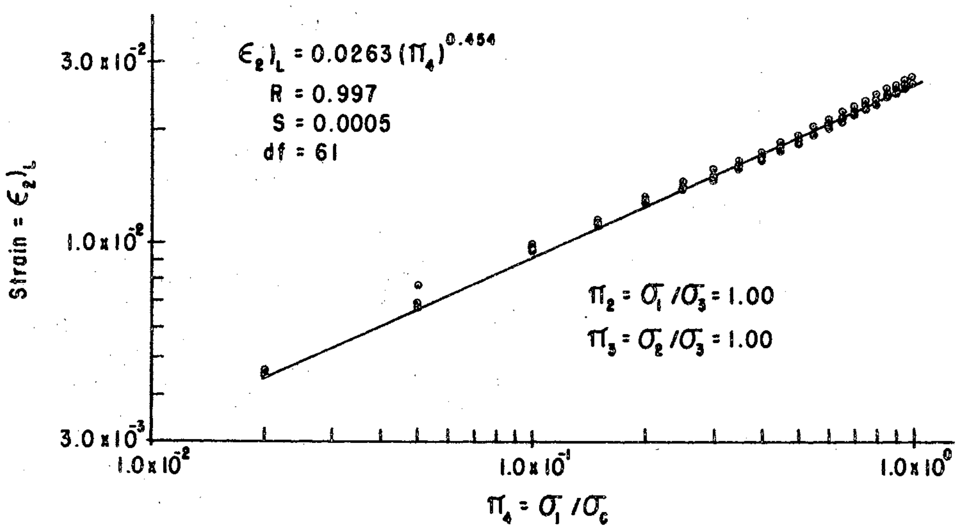

Figure 41. Component Equation. Log Strain in the 2-Direction vs. Log Stress Ratio, σ_1/σ_c, During Loading

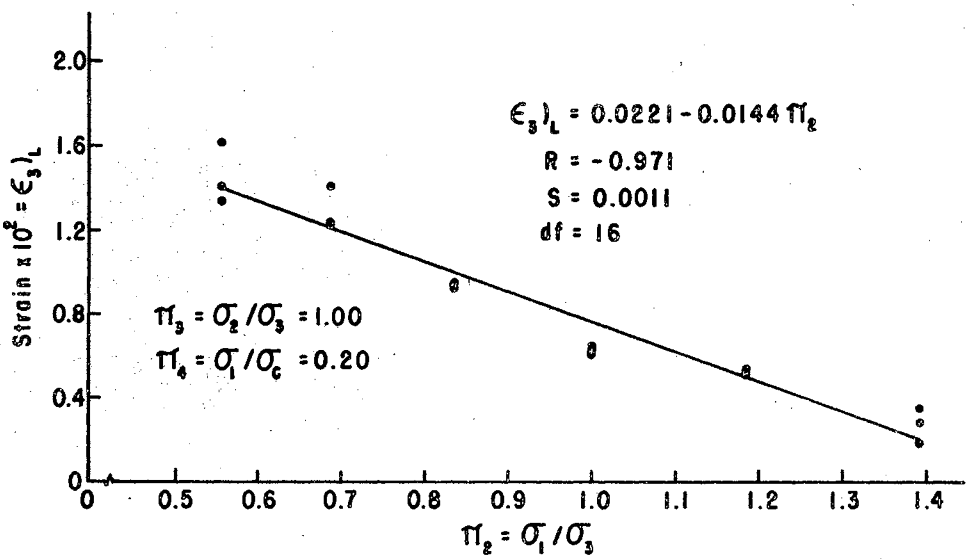

Figure 42. Component Equation. Strain in the 3-Direction vs. Stress Ratio, σ_1/σ_3, During Loading

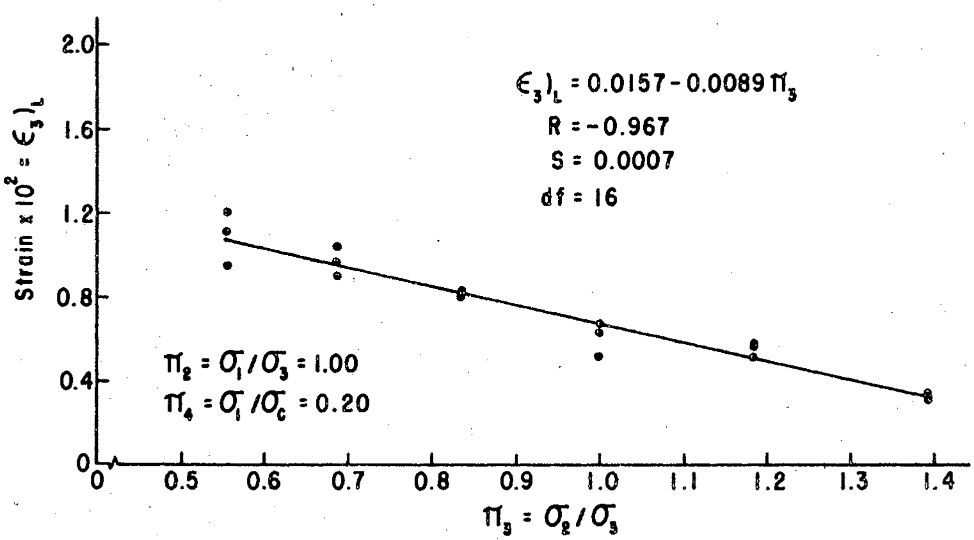

Figure 43. Component Equation. Strain in the 3-Direction vs. Stress Ratio, σ_2/σ_3, During Loading

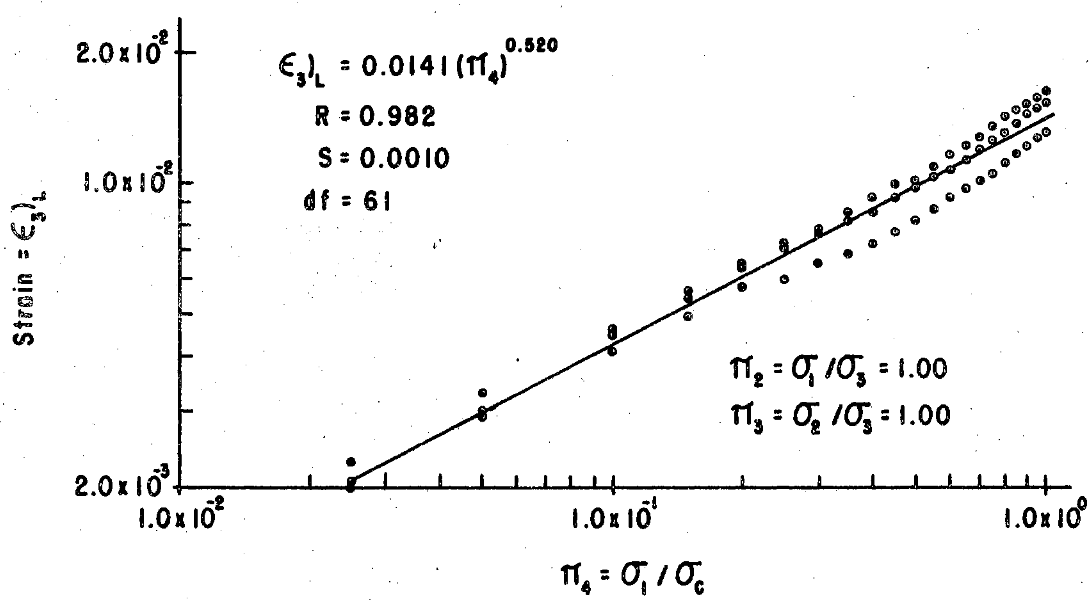

Figure 44. Component Equation. Log Strain in the 3-Direction vs. Log Stress Ratio, σ_1/σ_c, During Loading

TABLE XVIII

SUMMARY OF THE COMPONENT EQUATIONS

Component Equation	Correlation Coefficient (-)	Standard Deviation (in/in x 10^2)	Equation No.
$\epsilon_1)_L = -0.0125 + 0.0249\ \pi_2$	0.987	0.0012	(40)
$\epsilon_1)_L = 0.0240 - 0.0115\ \pi_3$	-0.982	0.0007	(41)
$\epsilon_1)_L = 0.0255\ \pi_4^{0.448}$	0.996	0.0006	(42)
$\epsilon_2)_L = 0.0351 - 0.0210\ \pi_2$	-0.979	0.0013	(43)
$\epsilon_2)_L = -0.0137 + 0.0272\ \pi_3$	0.996	0.0007	(44)
$\epsilon_2)_L = 0.0263\ \pi_4^{0.454}$	0.997	0.0005	(45)
$\epsilon_3)_L = 0.0221 - 0.0144\ \pi_2$	0.971	0.0011	(46)
$\epsilon_3)_L = 0.0157 - 0.0089\ \pi_3$	0.967	0.0007	(47)
$\epsilon_3)_L = 0.0141\ \pi_4^{0.520}$	0.982	0.0010	(48)

Prediction Equations

Murphy (37) noted that, if the component equations were linear in log-log space, the component equations could be combined by multiplication into the general form.

$$\pi_1 = \phi \pi_2^{\ a} \pi_3^{\ b} \ \pi_4^{\ c} \tag{49}$$

where ϕ = a dimensionless coefficient

a, b, c = dimensionless exponents

Since the component equations for $\epsilon_1)_L$ consisted of two linear equations in arithmetic space and one linear equation in log-log space, the equations had to be transformed as shown in Equation 50 before they could be combined.

Component Equations 40 and 41 were transformed to linear functions in log-log space in the following manner. First, the observed strains were plotted against those predicted by Equation 40 and the observed strains were plotted against those predicted by Equation 41. The resulting lines were linear with a slope of 45 degrees and an intercept of 0.0 and were described in equation form as

$$\pi_1 = \epsilon_1)_L = (-0.0125 + 0.0249 \ \pi_2)^1 = (\pi_2')_1^1 \tag{50}$$

and

$$\pi_1 = \epsilon_1)_L = (0.0240 - 0.0115 \ \pi_3)^1 = (\pi_3')_1^1 \tag{51}$$

Equations 50 and 51 have the basic form $y = Ax^B$, which is a linear function in log-log space. Substituting π_2' and π_3' into the Equation 49 yielded the basic prediction equation for strain in the 1-direction.

$$\epsilon_1)_L = \phi_1 \; (\pi_2')_1^1 \; (\pi_3')_1^1 \; (\pi_4)^{0.448} \tag{52}$$

Similarly, the general prediction equations in the other principal directions were

$$\epsilon_2)_L = \phi_2 \; (\pi_2')_2^1 \; (\pi_3')_2^1 \; (\pi_4)^{0.454} \tag{53}$$

$$\epsilon_3)_L = \phi_3 \; (\pi_2')_3^1 \; (\pi_3')_3^1 \; (\pi_4)^{0.520} \tag{54}$$

The prediction equation for strain in the ith direction was complete upon evaluation of ϕ_i.

Generally, the coefficient in each of Equations 52, 53, and 54 were defined by Equation 55.

$$\phi_i = \frac{\epsilon_i)_L\text{-observed}}{(\pi_2')_i (\pi_3')_i (\pi_4)^{a_i}} \tag{55}$$

Utilizing Equation 55, a value of ϕ_i was evaluated for each data point used to develop the prediction equation. The mean values of the dimensionless coefficient were found to be:

$$\bar{\phi}_1 = 164.4 \tag{56}$$

$$\bar{\phi}_2 = 145.1 \tag{57}$$

$$\bar{\phi}_3 = 290.6 \tag{58}$$

The standard deviation of the means were 1.4, 2.0, and 5.0, respectively.

Substitution of the values for ϕ_i, $(\pi_2')_i$, and $(\pi_3')_i$ into Equations 52, 53, and 54 yielded the final form of the prediction equations.

$$\epsilon_1)_L = (-4.92 + 9.81\ \pi_2 + 2.36\ \pi_3 - 4.71\ \pi_2\ \pi_3)(10^{-2})(\pi_4)^{0.448} \tag{59}$$

$$\epsilon_2)_L = (-6.97 + 4.18\ \pi_2 + 13.85\ \pi_3 - 8.23\ \pi_2\ \pi_3)(10^{-2})(\pi_4)^{0.454} \tag{60}$$

$$\epsilon_3)_L = (10.00 - 6.55\ \pi_2 - 5.71\ \pi_3 + 3.71\ \pi_2\ \pi_3)(10^{-2})(\pi_4)^{0.520} \tag{61}$$

Owing to the orthotropic nature of the stress-strain behavior of wheat en masse, Equations 59 and 60 may be written in an alternate form by interchanging subscripts on the π-terms and by substituting σ_2/σ_c for π_4.

$$\epsilon_2)_L = (-4.92 + 2.36\ \pi_2 + 9.81\ \pi_3 - 4.71\ \pi_2\ \pi_3)(10^{-2})(\sigma_2/\sigma_c)^{0.454} \tag{62}$$

and

$$\epsilon_1)_L = (-6.97 + 13.85\ \pi_2 + 4.18\ \pi_1 - 8.23\ \pi_1\ \pi_2)(10^{-2})(\sigma_2/\sigma_c)^{0.454} \tag{63}$$

Observed versus predicted strains have been plotted for each of the principal stress directions in Figures 45 through 48. The observed strains were those used to develop the prediction equations. Thus, these plots served only to indicate how well the component equations were combined. In Figures 45, 46, and 48 the standard prediction equations were used to evaluate the predicted strains, whereas the predicted strains in Figure 47 were evaluated by the alternate form of the prediction equation for $\epsilon_2)_L$. The magnitude of the slope, intercept, and standard deviation of the regression line are given in each figure.

The largest observed intercept of the regression lines was 0.0002 and the lowest slope of the regression lines was 0.928. The nearness of these statistics to the slope and intercept of a 45 degree line indicated that the component equations were satisfactorily combined. The high correlation coefficients (the lowest was 0.953) coupled with standard deviations from regression less than 8 percent of the range of $\epsilon_i)_L$ in all cases also indicated that the component equations were satisfactorily combined.

By using the alternate form for predicting $\epsilon_2)_L$ (See Equation 63), the observed and predicted values of $\epsilon_2)_L$ agreed more closely than when the original prediction equation, Equation 60, was used to predict $\epsilon_2)_L$. More favorable agreement was reflected in the intercept, slope, and standard deviation from regression of the $\epsilon_2)_L$-observed versus $\epsilon_2)_L$-predicted regression lines. Since isotropy was established

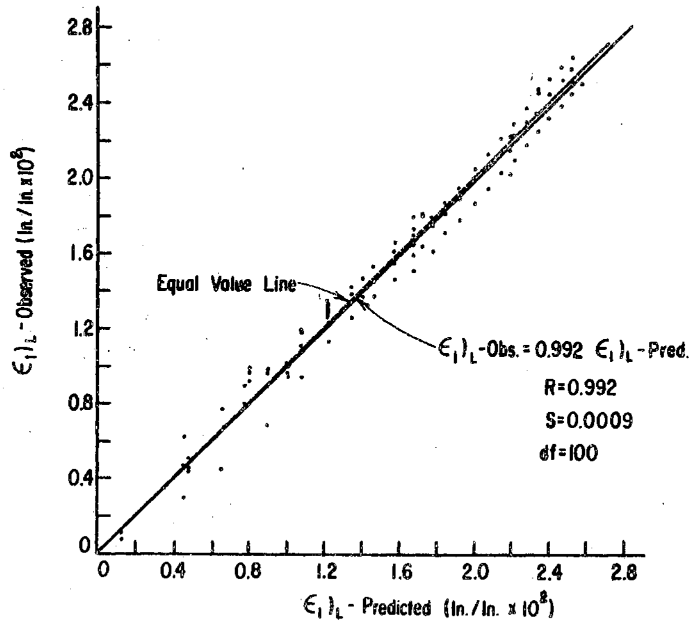

Figure 45. Observed vs. Predicted Strain in the 1-Direction During Loading

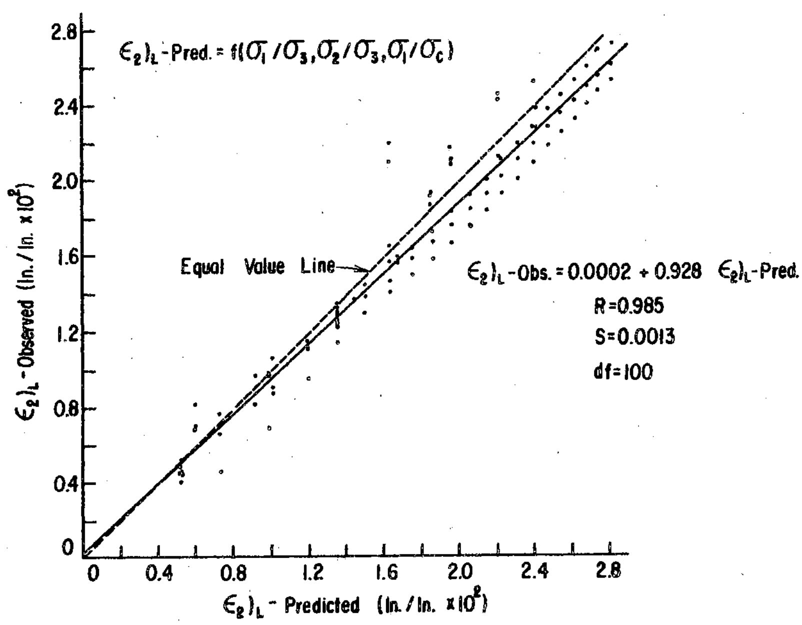

Figure 46. Observed vs. Predicted Strain in the 2-Direction During Loading

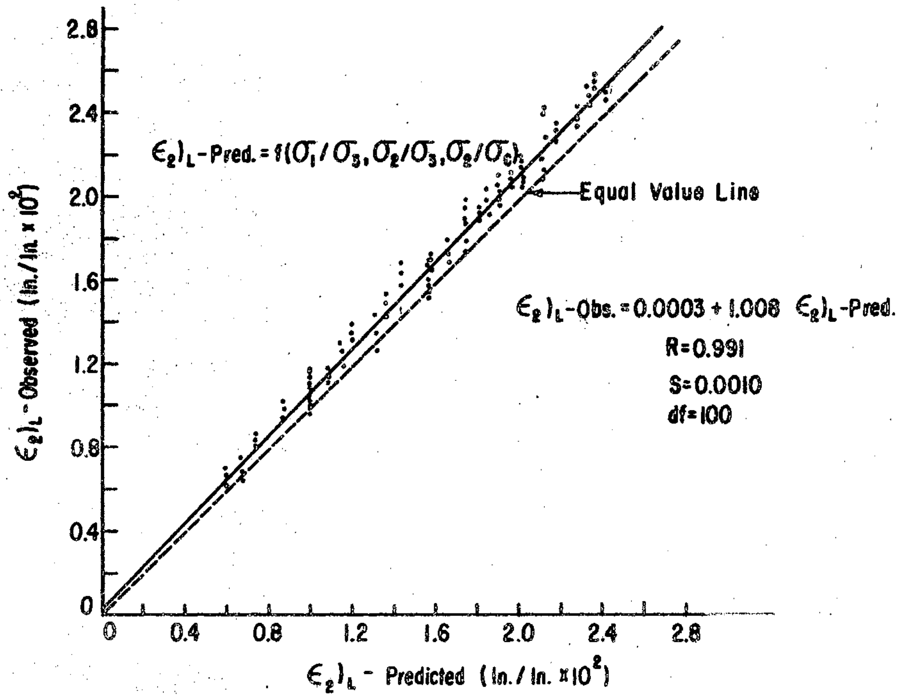

Figure 47. Observed vs. Predicted Strain in the 2-Direction During Loading.

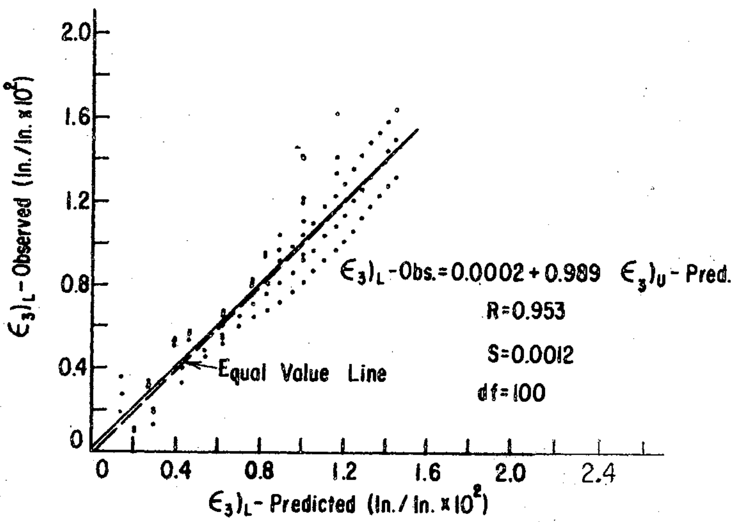

Figure 48. Observed vs. Predicted Strain in the 3-Direction During Loading

independent of the experimental design, and since strains in the 2-direction computed by the alternate prediction equation for $\epsilon_2)_L$ were in closer agreement with observed strains than were those predicted by Equation 60, it was concluded that Equation 63 should be used to predict $\epsilon_2)_L$.

The Unloading Functions

Slope of the Unloading Curves

The slopes of the unloading curves in log-log space for each experiment in series I and II were obtained by the least squares linear regression method. The results of these regressions are presented in Tables XIX and XX. The data for experiments 2A, 2B, and 2C in the 1-direction were lost and are not included in the results.

All n_i versus σ_1/σ_3 and n_i versus σ_2/σ_3 curves plotted as horizontal lines in arithmetic space. Any variation in n_i with stress ratio was, therefore, assumed to be random and attributable to experimental errors.

Studentized "t-tests" at the 0.05 level revealed that the mean slopes, $\bar{n}_1$, $\bar{n}_2$, and $\bar{n}_3$, did not vary between the experiments where σ_1/σ_3 was varied and the experiments where σ_2/σ_3 was varied. This equality determined, the means for $\bar{n}_1$, $\bar{n}_2$, and $\bar{n}_3$ were pooled across the two experiment series, and another studentized "t-test" was conducted at the 0.05 level to determine whether the slopes varied between principal stress directions.

The results of these tests were that: (1) The slopes of the unloading curves in log-log space were equal in the two horizontal stress directions and (2) The slope of the unloading curves in log-log space

TABLE XIX

SLOPE OF THE UNLOADING CURVES IN LOG-LOG SPACE WITH σ_2/σ_3 CONSTANT

Expt. No. (-)	σ_1/σ_2 (-)	Slope[1] n_1 (-)	n_2	n_3
2A	0.557	--	0.0437	0.0604
2B	0.557	--	0.0507	0.0851
2C	0.557	--	0.0447	0.0588
17A	0.688	0.0385	0.0416	0.0667
17B	0.688	0.0246	0.0460	0.0890
17C	0.688	0.0399	0.0431	0.0718
3A	0.835	0.0306	0.0465	0.0756
3B	0.835	0.0342	0.0512	0.0886
3C	0.835	0.0399	0.0408	0.0724
4A	1.000	0.0928	0.0994	0.2305
4B	1.000	0.0850	0.0886	0.2039
4C	1.000	0.0634	0.1019	0.2505
18A	1.184	0.0171	0.0183	0.0633
18B	1.184	0.0368	0.0289	0.0905
18C	1.184	0.0312	0.0452	0.0659
5A	1.392	0.0362	0.0526	0.3518
5B	1.392	0.0360	0.0541	0.1035
5C	1.392	0.0322	0.0487	0.0904
Mean ($\bar{n}_i$)		0.0426	0.0525	0.1177

[1]Subscripts refer to the principal stress direction.

TABLE XX

SLOPE OF THE UNLOADING CURVES
IN LOG-LOG SPACE WITH
σ_1/σ_3 CONSTANT

Expt. No. (-)	σ_2/σ_3 (-)	Slope[1] (-) n_1	n_2	n_3
9A	0.557	0.0435	0.0694	0.0724
9B	0.557	0.0369	0.0581	0.1457
9C	0.557	0.0249	0.0096	0.0426
20A	0.688	0.0447	0.0519	0.0643
20B	0.688	0.0430	0.0432	0.0706
20C	0.688	0.0324	0.0388	0.1392
10A	0.835	0.0448	0.0224	0.0749
10B	0.835	0.0359	0.0424	0.0847
10C	0.835	0.0291	0.0197	0.0697
11A	1.000	0.1118	0.1109	0.2046
11B	1.000	0.0995	0.1001	0.2495
11C	1.000	0.1095	0.1166	0.2396
21A	1.184	0.0459	0.0279	0.0618
21B	1.184	0.0369	0.0379	0.0795
21C	1.184	0.0422	0.0428	0.1242
12A	1.392	0.0455	0.0385	0.0635
12B	1.392	0.0507	0.0236	0.2756
12C	1.392	0.0299	0.0235	0.0651
Mean ($\bar{n}_i$)		0.0504	0.0487	0.1182

[1]Subscripts refer to the principal stress direction.

in the vertical direction differed from the slopes in the horizontal directions. Thus,

$$\bar{n}_1 = \bar{n}_2 \neq \bar{n}_3 \tag{64}$$

The mean slopes encountered and the associated 95 percent confidence intervals were

$$\bar{n}_1 = \bar{n}_2 = \bar{n}_h = 0.0486 \pm 0.0067 \tag{65}$$

$$\bar{n}_3 = \bar{n}_v = 0.1180 \pm 0.0264 \tag{66}$$

The Prediction Equations

The generalized unloading function, Equation 39, was presented in Chapter VII. Substitution of the values for $\bar{n}_i$ into the generalized equation yielded the prediction equations for unloading.

$$\epsilon_1)_U = \epsilon_{1m}(\sigma_1/\sigma_{1m})^{0.0486} \tag{67}$$

$$\epsilon_2)_U = \epsilon_{2m}(\sigma_2/\sigma_{2m})^{0.0486} \tag{68}$$

$$\epsilon_3)_U = \epsilon_{3m}(\sigma_3/\sigma_{3m})^{0.1180} \tag{69}$$

The values of ϵ_{im} were either the predicted strains or the observed strains at which unloading commenced. In the event that predicted strains were desired for a complete loading cycle, then the ϵ_{im} value had to be predicted from the appropriate loading function.

The observed versus predicted unloading strains are plotted in

Figures 49, 50, and 51. In these figures the predicted strains were computed using observed values for ϵ_{im}. The data plotted were the same data used to obtain the average slopes of the unloading curves.

The results plotted in Figures 49 through 51 indicated that the techniques employed to derive prediction Equations 67, 68, and 69 were satisfactory. In this series of curves the lowest correlation coefficient was 0.990, the largest standard deviation from regression was only 3.1 percent of the range of observed strains, the slopes of the regression curves were essentially 1.0, and the intercept of the regression lines were all within 0.03 x 10^{-2} in./in. of the origin.

The data plotted in Figures 52 through 54 differ from those in Figures 49 through 51 in that the strain levels, ϵ_{im}, were predicted from the prediction equation for $\epsilon_{i})_L$. The standard deviation from regression was less than 8 percent of the range of observed strains in all cases, and the correlation coefficient ranged from 0.954 to 0.980. The slope and intercept of the regression lines for the two horizontal stress directions were essentially equal to unity and zero, respectively.

In the vertical stress direction, the intercept of the regression line was zero, but the slope of the regression line was equal to 1.236. Noting that the slope of the regression line in Figure 51, in which ϵ_{3m} was an observed value, was only 1.064 and close to the equal value line, the divergence of the regression line in Figure 54 must be due to an accumulative type of error. That is, differences between the observed and predicted strains in Figure 54 are the sum of differences in the observed and predicted values for ϵ_{im} and the error introduced by the prediction equation for strain during unloading.

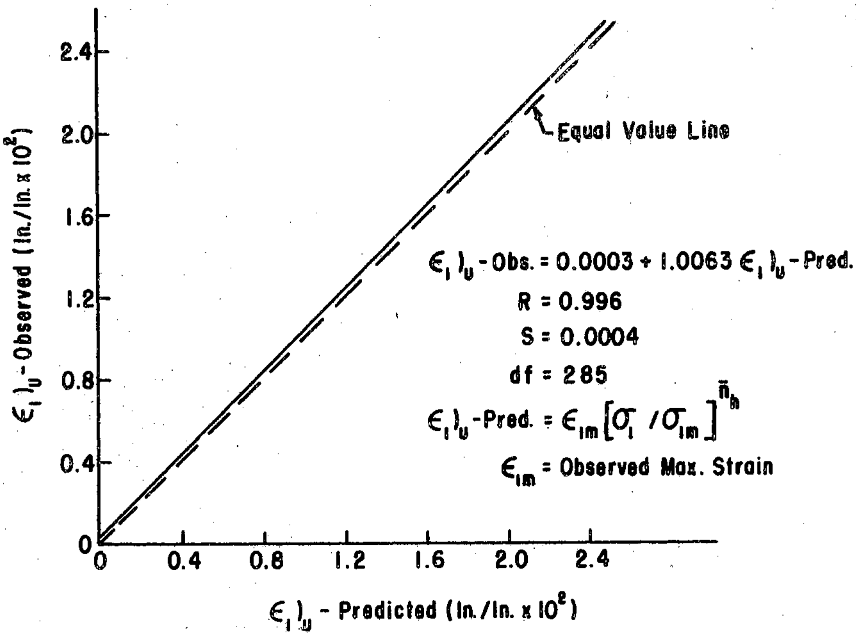

Figure 49. Observed vs. Predicted Strain in the 1-Direction During Loading

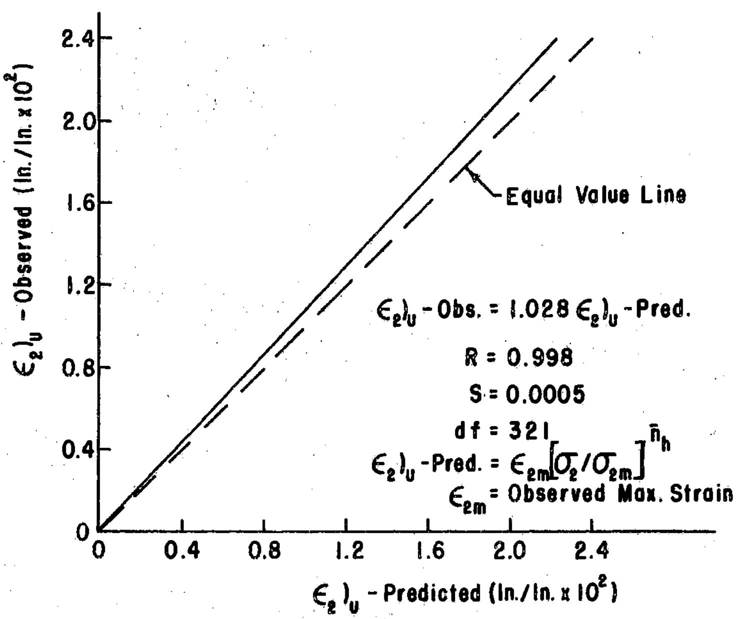

Figure 50. Observed vs. Predicted Strain in the 2-Direction During Unloading

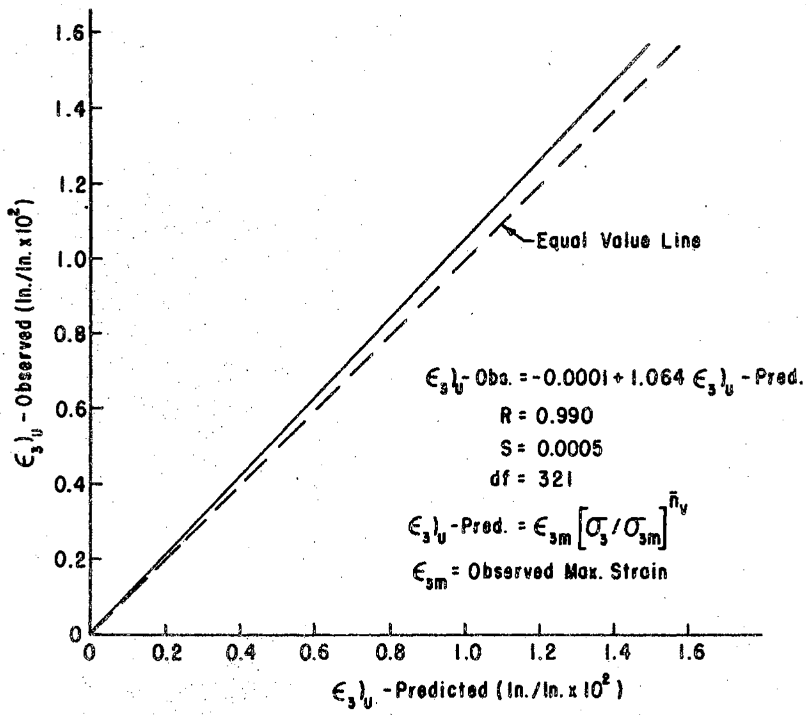

Figure 51. Observed vs. Predicted Strain in the 3-Direction During Unloading

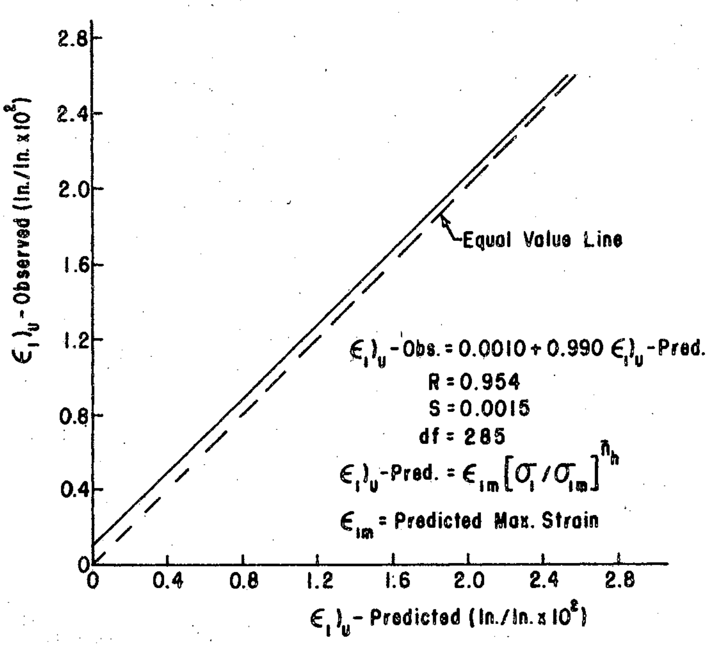

Figure 52. Observed vs. Predicted Strain in the 1-Direction During Unloading

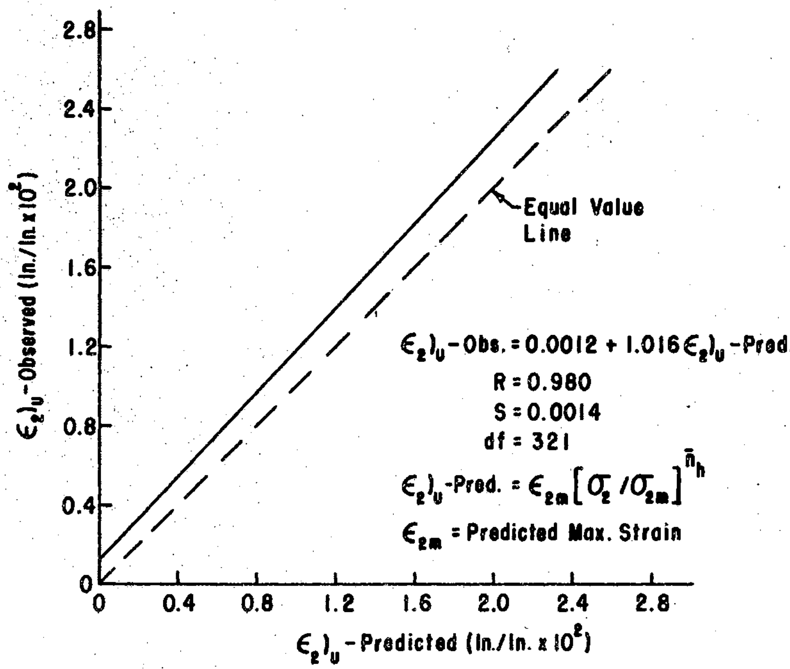

Figure 53. Observed vs. Predicted Strain in the 2-Direction During Unloading

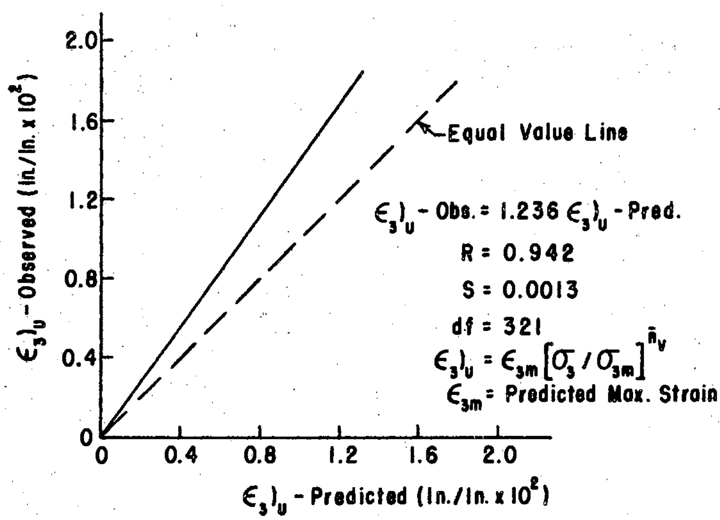

Figure 54. Observed vs. Predicted Strain in the 3-Direction During Unloading

Validation Results

The results of the validation tests, in which $\sigma_1 : \sigma_2 : \sigma_3 =$ 0.91:0.82:1.00, are presented in Figures 55 through 63. A stress-strain curve, a plot of the observed versus predicted strains during loading, and a plot of the observed versus predicted strains during unloading are presented for each principal direction.

In the 1-direction the observed and predicted strains during loading were in close agreement. At the maximum stress level encountered in the 1-direction, the difference between the observed and predicted strains was 6.3 percent. The observed versus predicted strains plotted in Figures 56 and 57 for loading and unloading, respectively, both approximate a 45 degree line with intercept 0.0. The divergence of the intercept and slope of the regression line in Figure 56 is due primarily to differences in the observed and predicted strains at stresses below 4 psi. These differences were due to errors in strain measurement at small stress levels.

The results in the 2-direction are plotted in Figures 58, 59, and 60. The stress-strain curve indicated very good agreement between observed and predicted strains as the maximum difference between observed and predicted strain was 0.001 in./in. The slope and intercept of the observed versus predicted regression line for loading were -0.0010 in./in. and 1.078, respectively; whereas for the unloading function an intercept and slope of 0.0 in./in. and 1.022, respectively, were observed. Again the strains experienced at stress levels below 4 psi diverged considerably from the regression lines. Exclusion of those points below 4 psi would result in even better agreement between the observed and predicted strains during loading.

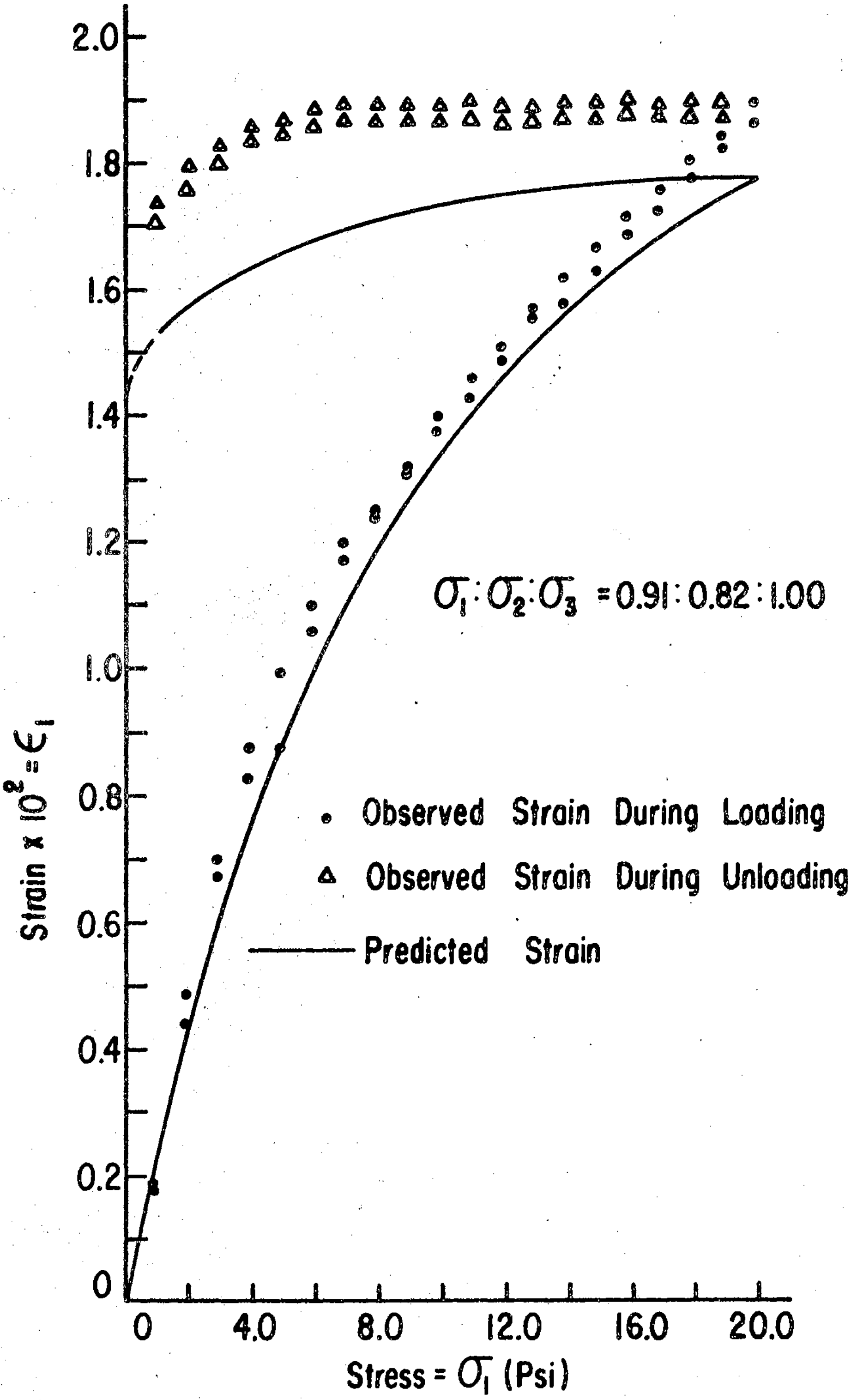

Figure 55. Strain-Stress Curve in the 1-Direction for the Validation Test

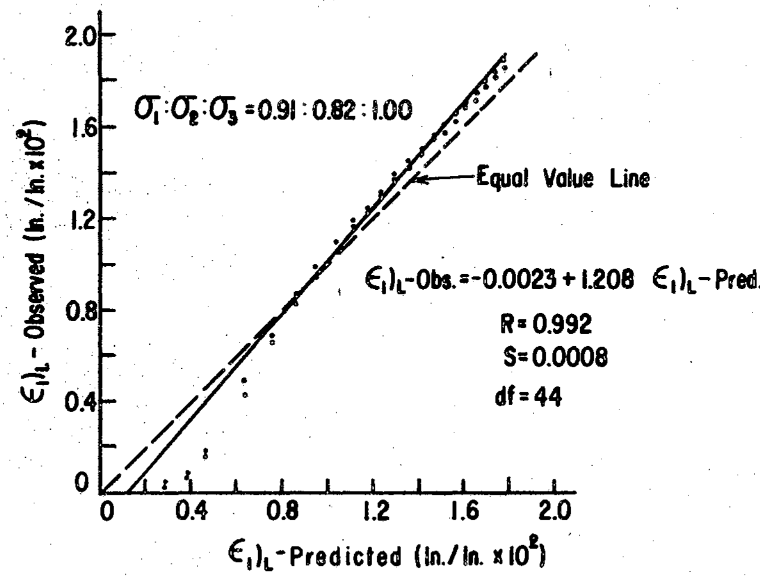

Figure 56. Observed vs. Predicted Strain in the 1-Direction During Loading for the Validation Tests

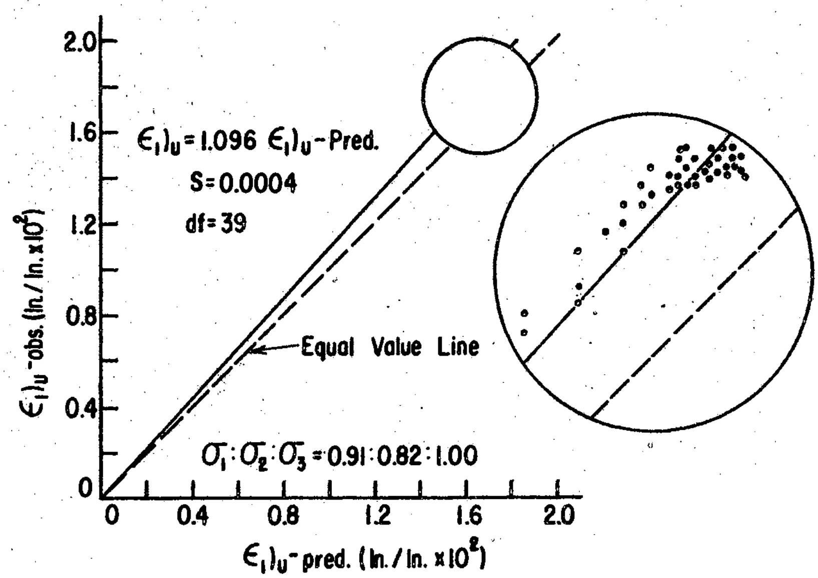

Figure 57. Observed vs. Predicted Strain in the 1-Direction During Unloading for the Validation Tests

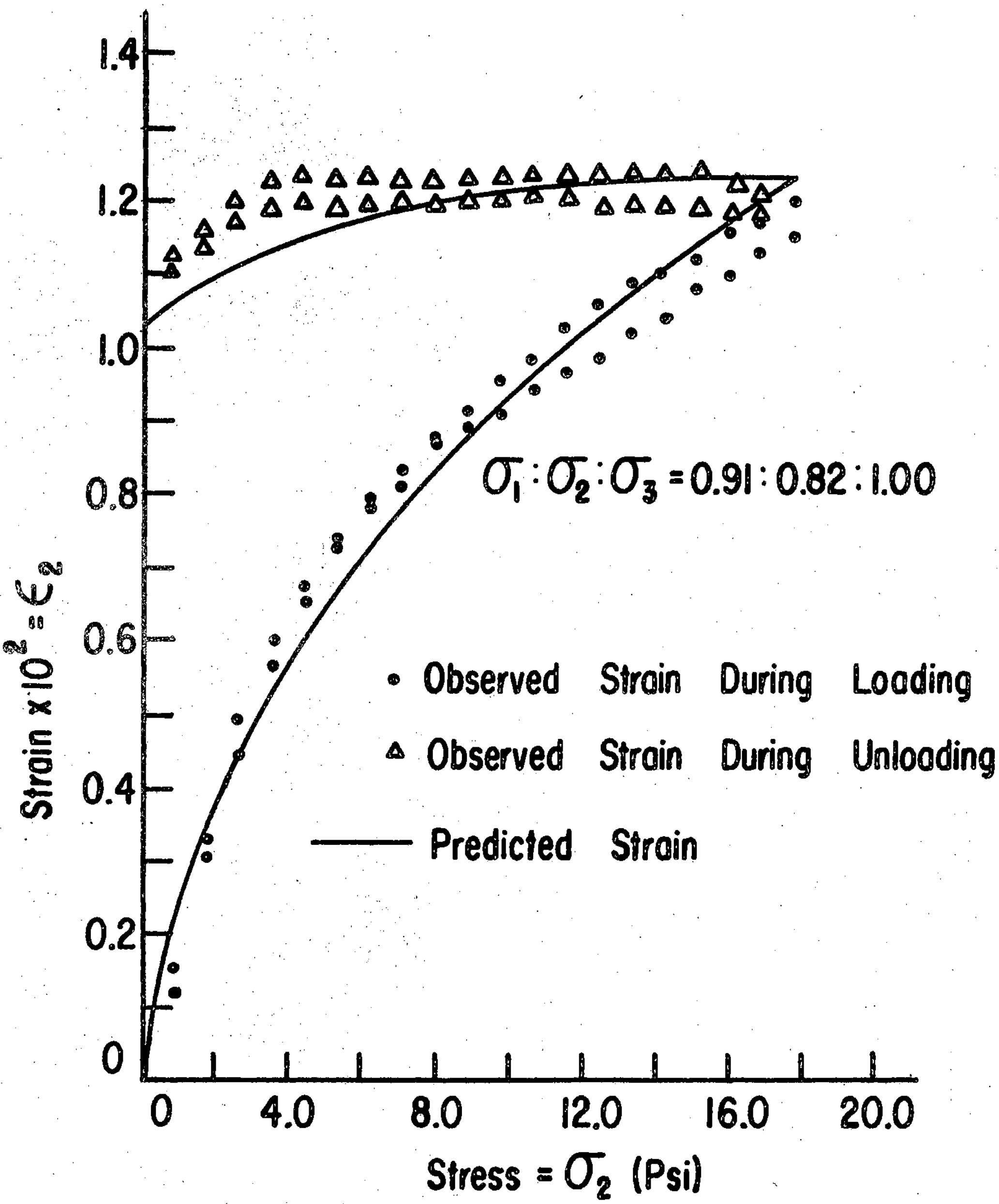

Figure 58. Strain-Stress Curve in the 2-Direction for the Validation Tests

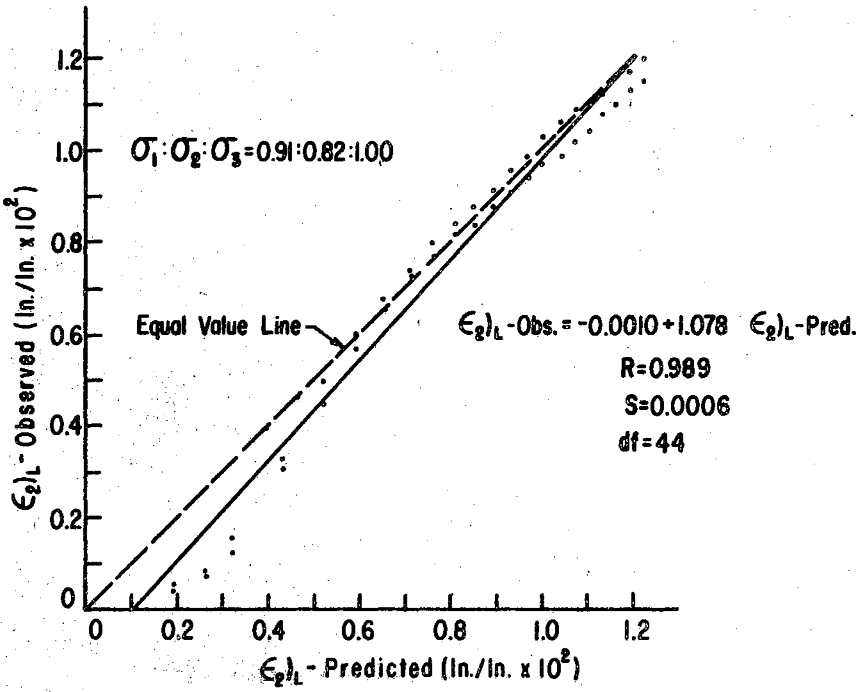

Figure 59. Observed vs. Predicted Strain in the 2-Direction During Loading for the Validation Tests

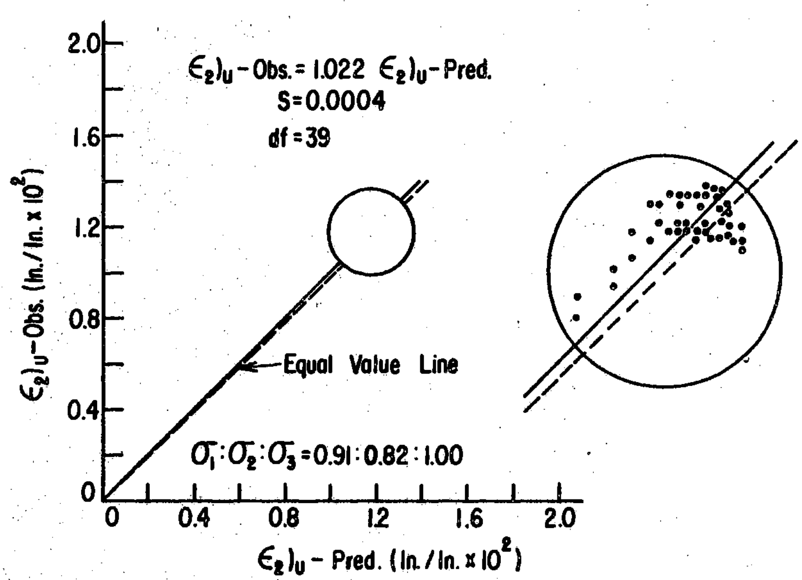

Figure 60. Observed vs. Predicted Strain in the 2-Direction During Unloading for the Validation Tests

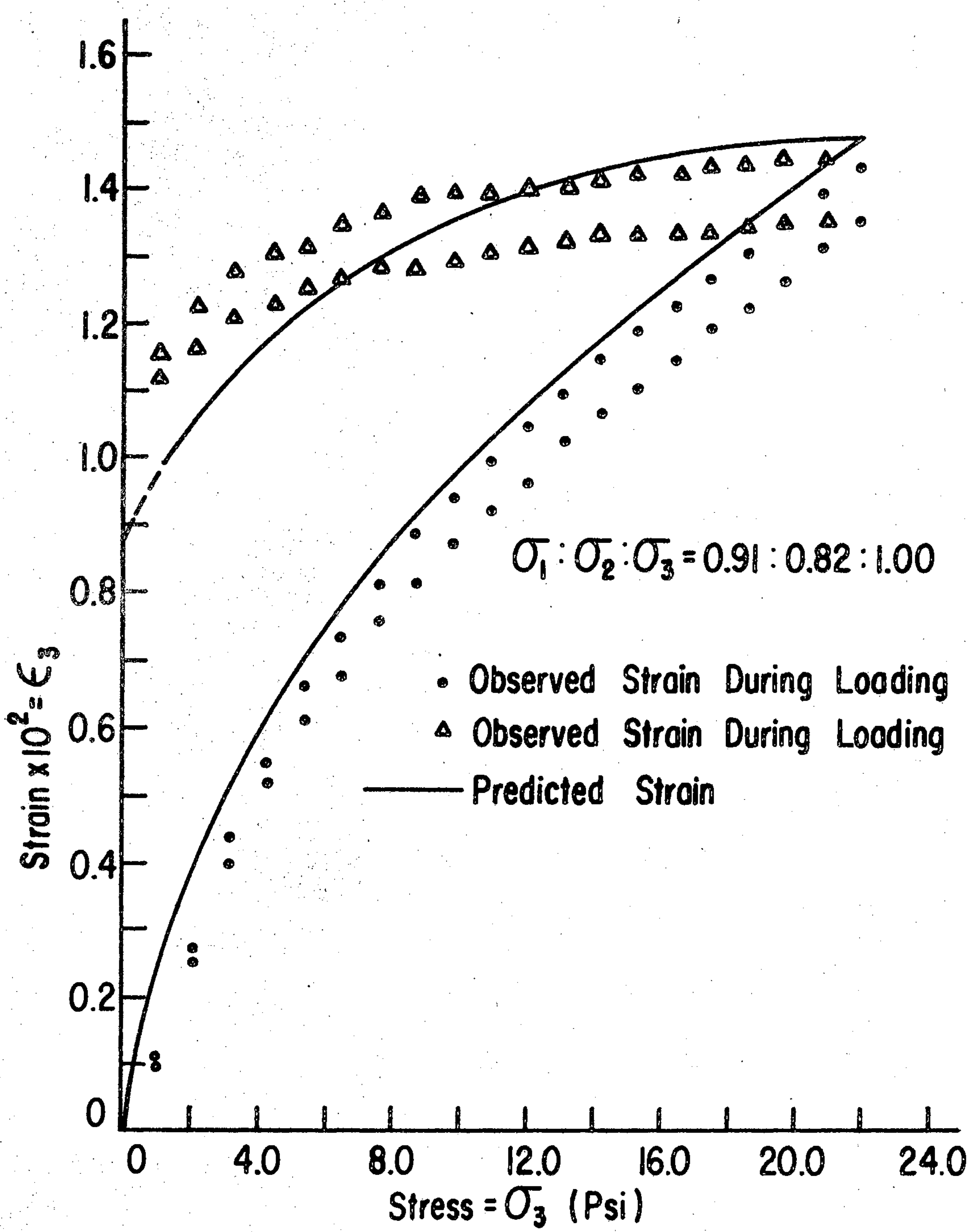

Figure 61. Strain-Stress Curve in the 3-Direction for the Validation Tests

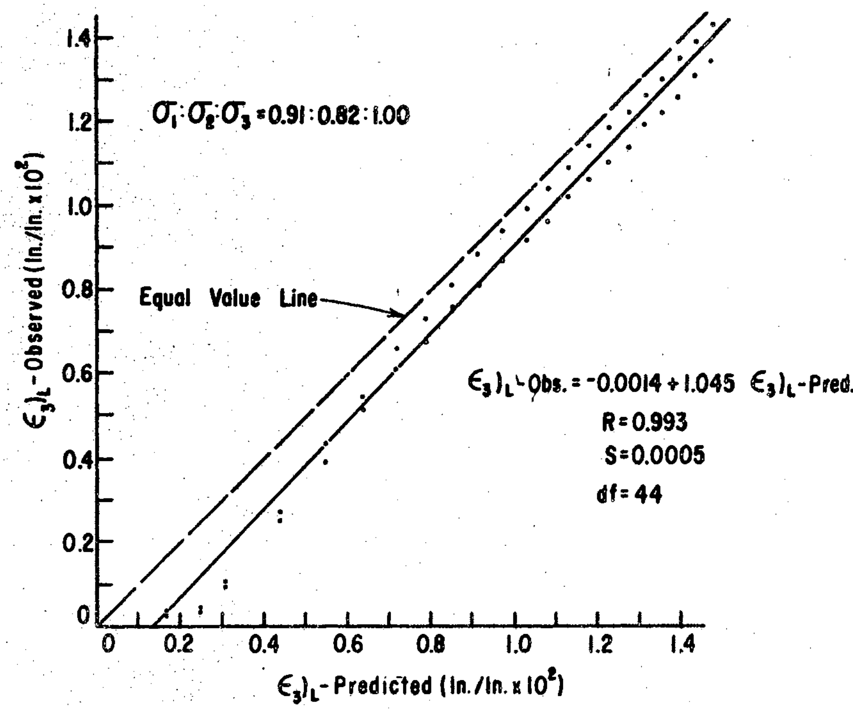

Figure 62. Observed vs. Predicted Strain in the 3-Direction During Loading for the Validation Tests

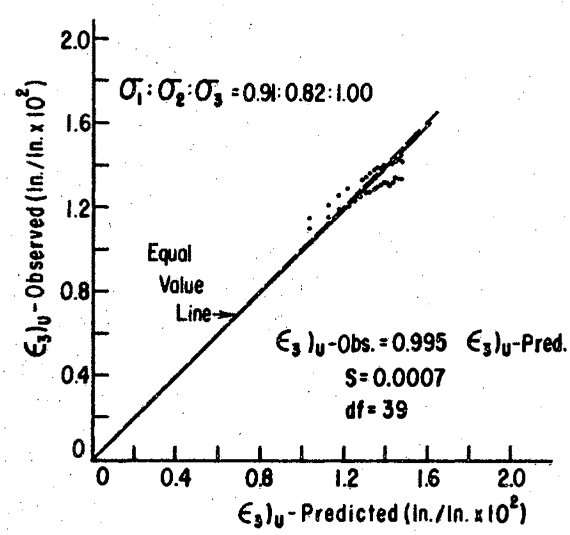

Figure 63. Observed vs. Predicted Strain in the 3-Direction During Unloading for the Validation Tests

The observed strains in the 3-direction during loading are consistently 0.1 x 10^{-2} in./in. lower than the predicted strains at any given stress level. At stress levels above 8 psi, the difference between observed and predicted strain was less than 10 percent. The linear regression line in Figure 62 for observed versus predicted strains during loading had a slope of 1.045 and an intercept of -0.0014 in./in. These statistics approximated those of a 45 degree line with an intercept of -0.0014. The observed versus predicted strains during unloading are plotted in Figure 63. The least squares regression line forced through the origin had a slope of 0.995.

Except for a few instances at stress levels between 0 and 4 psi, the observed and predicted strains differed by less than 10 percent. Furthermore, the 95 percent confidence interval for the regression lines included the equal value line in every instance. Thus, it was concluded that within the limitations imposed by the experimental design, prediction Equations 59, 61, 62, 67, 68, and 69 were valid and could be used to predict the strains in wheat en masse subjected to three dimensional states of stress.

CHAPTER IX

DISCUSSION OF THE RESULTS

Theoretical Considerations

Total Strain

In an attempt to substantiate the results of the previous chapter, the upper and lower bounds of the strain in the vertical direction during loading, $\epsilon_3)_L$, were evaluated analytically for the case of hydrostatic compression. The lower limit of the strain was obtained by consideration of Hertzian contact deformations, whereas the upper bound was obtained by superimposing the strains due to particle reorientation upon the Hertzian deformations. In general, the strain in the vertical direction during loading was written as

$$\epsilon_3)_T = \epsilon_3)_H + \epsilon_3)_R \tag{70}$$

where $\epsilon_3)_T$ = total strain in the vertical direction, in./in.

$\epsilon_3)_H$ = strain due to Hertzian contact stresses, in./in.

$\epsilon_3)_R$ = strain due to particle reorientation, in./in.

Contact Strain

Contact strains may be computed by the Hertz theory of contact stresses. The Hertz solution assumes that: (1) The contacting bodies are homogeneous; (2) The loads are static; (3) Hooke's Law holds; (4) The radii of curvature of the contacting bodies are larger than the radius of the surface of contact; and (5) The particles are smooth such that tangential forces are negligible.

According to Hertz (19), the centers of two bodies in contact approach each other by an amount D along the line of action of the load

$$D = \frac{k}{2}\left[\frac{9P^2A^2}{\pi^2}\left(\frac{1}{R_1} + \frac{1}{R_1'} + \frac{1}{R_2} + \frac{1}{R_2'}\right)\right]^{1/3} \tag{71}$$

where D = deformation of the centers of two contacting bodies, in.

P = contact load, lbs_f.

$$A = \frac{1 - \mu_1^2}{E_1} + \frac{1 - \mu_2^2}{E_2}$$

$k = f(\cos T)$

μ_1 = Poisson's ratio for body 1

μ_2 = Poisson's ratio for body 2

E_1 = modulus of elasticity for body 1, psi

E_2 = modulus of elasticity for body 2, psi

R_1, R_1' = principal radii of body 1, in.

R_2, R_2' = principal radii of body 2, in.

$$\cos T = \frac{\left[\left(\frac{1}{R_1} - \frac{1}{R_1'}\right)^2 + \left(\frac{1}{R_2} - \frac{1}{R_2'}\right)^2 + 2\left(\frac{1}{R_1} - \frac{1}{R_1'}\right)\left(\frac{1}{R_2} - \frac{1}{R_2'}\right)\cos 2\eta\right]^{1/2}}{\left(\frac{1}{R_1} + \frac{1}{R_1'} + \frac{1}{R_2} + \frac{1}{R_2'}\right)} \tag{72}$$

The value of k has been tabulated by Kosma and Cunningham (29) for all levels of cos T. The angle η is the angle between the normal planes containing the principal curvatures of the contacting bodies.

A typical wheat grain is illustrated in Figure 64. It has been observed by Shelef and Mohsenin (47), and it was demonstrated in Chapter V that the longitudinal axis of a kernel of wheat is approximately twice as long as the height. That is,

$$L = 2H \tag{73}$$

In Chapter V, it was shown that the length and height of the wheat grains used in this study were 0.196 and 0.098 inches, respectively.

Arnold and Roberts (2, 3) have observed the following relationships between the axial dimensions of wheat grains and their principal radii of curvature.

$$R_1 = H/2 \tag{74}$$

$$R_1' = \frac{H^2 + L^2/4}{2H} = H \tag{75}$$

$$R_2 = R_1/2 = H/4 \tag{76}$$

$$R_2' = 2R_1' = 2H \tag{77}$$

It has been asserted in Chapter VI that the wheat grains will orient themselves with their longitudinal axes perpendicular to the gravity field. However, the orientation of the longitudinal axis in

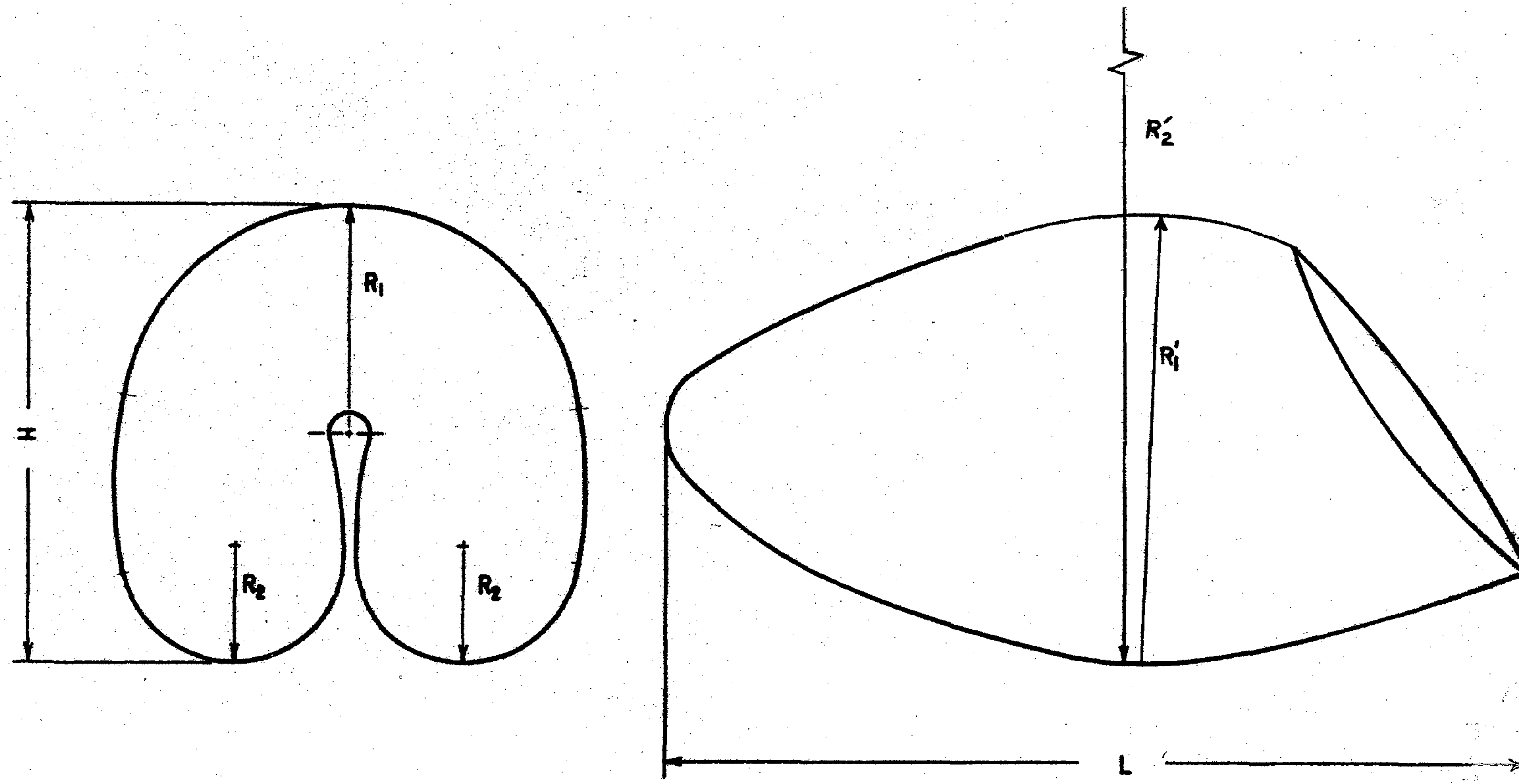

Figure 64. Sketch of a Typical Wheat Grain

the horizontal plane is random.

Because of the random orientation of the longitudinal axis in the horizontal plane, many combinations of contacting surface radii are possible within an array of wheat grains. For example, in the vertical direction of an array of wheat grains contacts could be visualized in which the following combinations of principal radii would be involved: (1) A surface with principal radii of R_1 and R_1' in contact with a surface with principal radii of R_1 and R_1'; (2) A surface with principal radii of R_1 and R_1' in contact with a surface with principal radii of R_2 and R_2'; or (3) A surface with principal radii of R_2 and R_2' in contact with a surface with principal radii of R_2 and R_2'. (Note that the radii referred to are those illustrated in Figure 64.) Furthermore, the angle between the planes of principal radii, η, of two contacting bodies may vary.

Since any of these combinations of contacting can, and probably do, occur and since the limiting bounds of contact deformation were sought, the approach of two wheat kernels under load was evaluated for all the combinations of principal radii and angle, η.

Hertzian strains were evaluated for two particulate packing arrays: A simple rectangular array as shown in Figure 65, and an ortho-parallelepipedal array as shown in Figure 66. The arrays sketched assume that the wheat grains approximate circular ellipsoids with major and minor axes of L and H, respectively. The first of these arrays represented the loosest possible packing arrangement of uniform ellipsoids, whereas the second array is the densest array of ellipsoids which one would expect to find in nature. Orr (40) noted that the orthorhombic arrangement of uniform spherical particles was the most

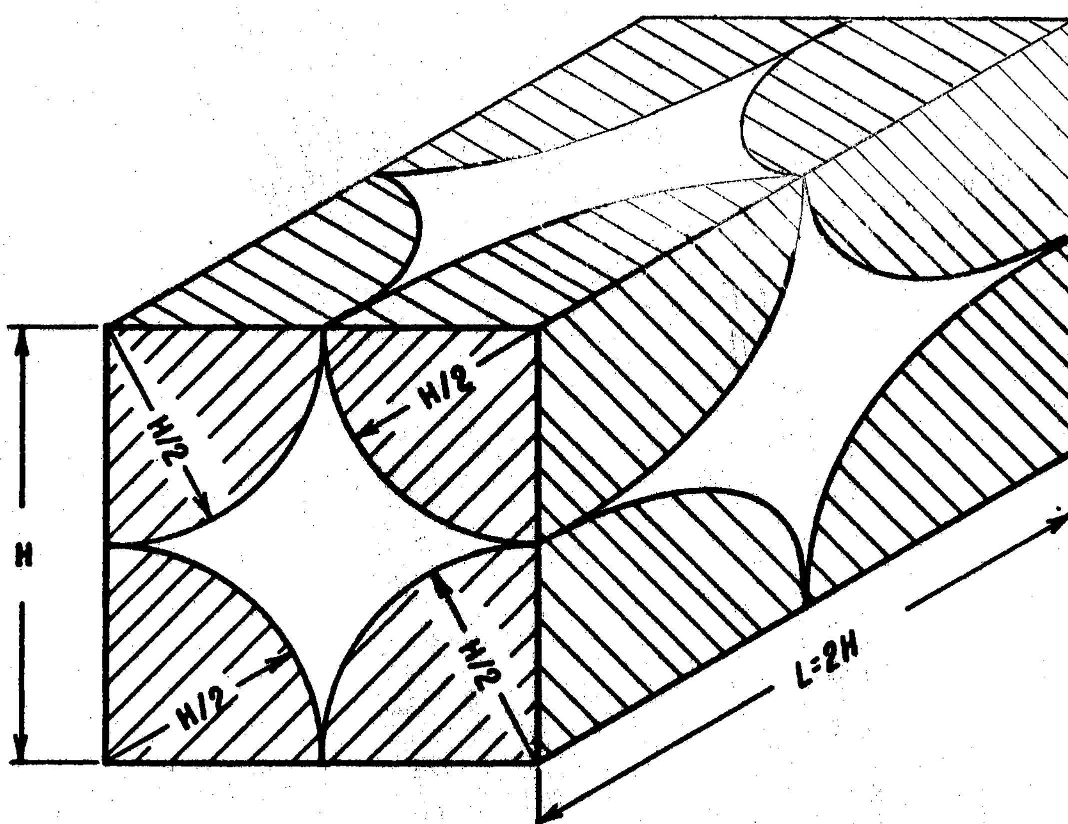

Figure 65. An Element of a Simple Rectangular Arrangement of Wheat Grains

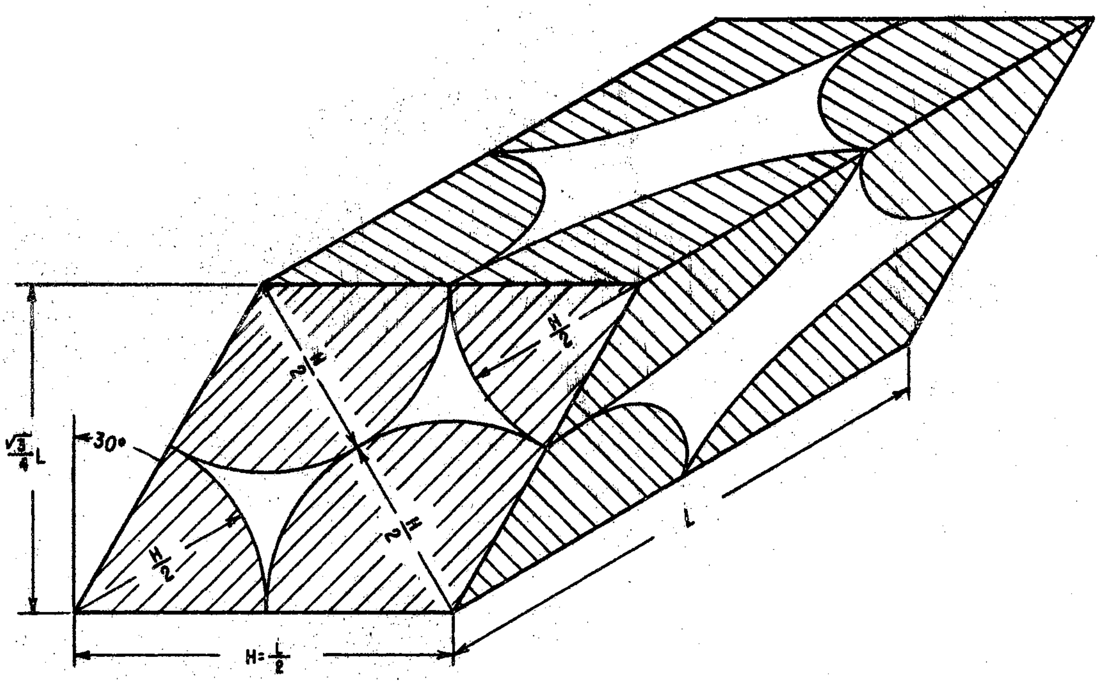

Figure 66. An Element of an Ortho-parallelepipedal Arrangement of Wheat Grains

dense array found in practice. This observation was extended to the case of ellipsoidal particulate arrays.

In the case of the simple rectangular array (SRA), the unit vertical contact strain was computed by Equation 78.

$$\epsilon_3)_H = \frac{D}{H} \tag{78}$$

In the case of the ortho-parallelepipedal array (OPA), the unit vertical contact strain was evaluated by Equation 79.

$$\epsilon_3)_H = \frac{4D}{\sqrt{3}\ H} \tag{79}$$

Hertzian strains were evaluated for all the combinations by assuming that $E_1 = E_2 = 4.12 \times 10^5$ psi [Shelef and Mohsenin (47)] and by assuming that $\mu_1 = \mu_2 = 0.30$ [Arnold and Roberts (3)]. Of all the combinations, the maximum vertical Hertzian strain was obtained for a simple rectangular arrangement of particles. The principal radii of the contact points for body 1 were $R_1 = 0.148$ inch and $R_1' = 0.074$ inch, whereas the principal radii of the contact points for body 2 were $R_2 = 0.296$ inch and $R_2' = 0.037$ inch. The angle, η , associated with the maximum Hertzian strain was 0 degrees.

The minimum contact strain was evaluated for an ortho-parallelepipedal arrangement of particles. The principal radii of contact for body 1 were $R_1 = 0.148$ inch and $R_1' = 0.074$ inch, whereas the principal radii of the second contacting grain were $R_2 = 0.296$ inch and 0.037 inch. The angle, η , was equal to 0 degrees. The computed upper and lower bounds for Hertzian strains in the vertical direction are plotted in Figure 67.

Particle Reorientation

The voids ratio for the simple rectangular array of particles was 0.910, whereas the voids ratio of the ortho-parallelepipedal array of particles was 0.655. The unit strain encountered, assuming the initial distance between particle centers to be H and assuming no particle deformation when transforming the particles from an SR to an OP arrangement, was 0.134 in./in. That is,

$$\epsilon_R)_{max} = 0.134 \text{ in./in.} \tag{80}$$

However, the observed initial voids ratios of the wheat samples, e_o, had an average value of 0.750. If a linear relationship is assumed between the difference in voids ratio and the unit strains due to rearrangement, then the unit strain expected due to rearrangement from a voids ratio of 0.750 to the OP array with e = 0.655 is

$$\epsilon_3)_R = \frac{e_o - 0.655}{0.910 - 0.655} (\epsilon_R)_{max} = 5.0 \times 10^{-2} \text{ in./in.} \tag{81}$$

The preliminary results of Chapter VI indicated that particle reorientation was the predominant mode of deformation in a hydrostatic compression test up to a stress level of 8 psi. Above stresses of 8 psi individual particle deformation was observed to be the predominant deformation mechanism. Assuming that all the particle reorientation strain, $\epsilon_3)_R$, has been achieved at a stress level of 8 psi, the maximum total strain at 8 psi is obtained by adding $\epsilon_3)_R$ from Equation 81 to

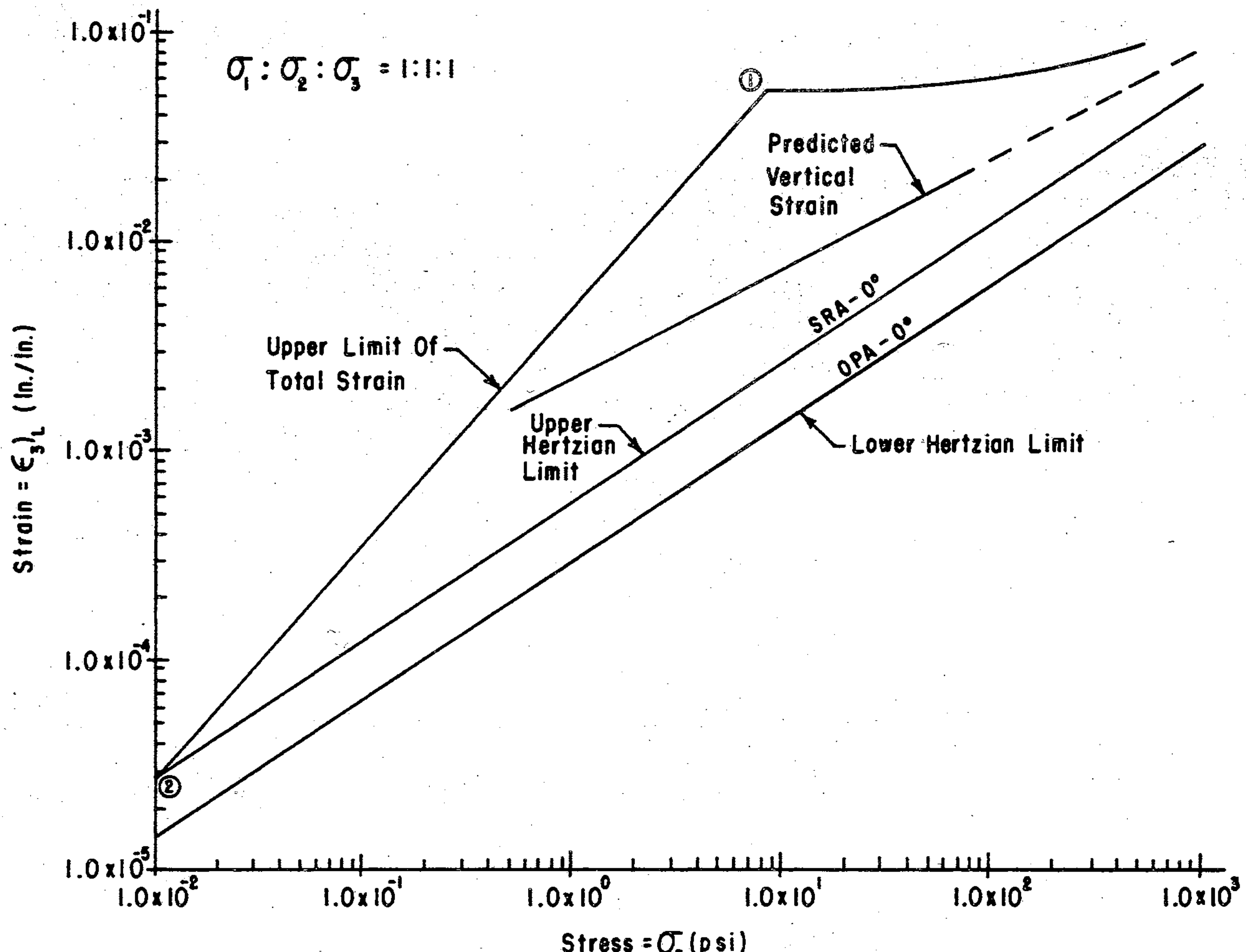

Figure 67. Diagram of the Bounding Theoretical Strains in the Vertical Stress Direction for an Element Subjected to Hydrostatic Compressive Stresses

the maximum contact strain at 8 psi. Thus, the location of point 1 in Figure 67 is established.

Now, if it is assumed that at some value of stress near 0 psi, say 0.01 psi, the maximum contact strain and the total strain are essentially equal, the location of point 2 on the upper limit of total strain curve is defined. Narayan and Bilanski (38) noted that the total vertical deformation of wheat en masse under axial load varied logarithmically with stress when particle reorientation was the predominant mode of deformation. Thus, an approximation of the upper bound of total strain between stress levels of 0.01 and 8 psi is a straight line in log-log space joining points 1 and 2 in Figure 67. Above a stress level of 8 psi, the upper bound of total strain is plotted by simply adding a constant strain of 5.0×10^{-2} in./in. to the maximum contact strain.

Comparison of Experimental and Analytical Results

The upper and lower bounds for strain were developed independently of any experimental results except that the experimentally observed initial voids ratio was used in the development of $\epsilon_3')_R$ and a stress level of 8 psi was experimentally observed as the stress level at which particle reorientation ceased to be the major mechanism of deformation.

The predicted vertical strains, which are computed by Equation 61 in Chapter VIII and are plotted in Figure 67 for the case of hydrostatic compressive stresses, fell within the upper and lower bounds of strain for stress levels between 0.3 and 1000 psi. The slope of the predicted stress-strain function was 0.520, whereas the slope of the

Hertzian stress-strain function was 0.667. Thus, as the stress level increased, the predicted and Hertzian strains converged.

The accuracy of the strains measured by the methods proposed in this study is not proved conclusively by this independent analytical approach. However, the results of this study can be used with a greater degree of confidence with the knowledge that the predicted strains do fall within the limiting bounds. Conclusive proof of the accuracy of the method will be obtained only when the stress-strain functions are successfully applied to the solution of the pressure distribution in a physical system.

Nature of the Stress-Strain Behavior

Probably the most outstanding feature of the stress-strain behavior of wheat en masse was the directional dependence of the strains. In hydrostatic compression tests the strain in the vertical direction with respect to gravity filling was always observed to be nearly 50 percent smaller than the strains encountered in the horizontal direction. Similarly, in deviatoric stress tests, anisotropic behavior was also observed. For example, the strain in the 1-direction under a stress state of $\sigma_1:\sigma_2:\sigma_3 = \lambda:m:m$ was always observed to be greater than the strains experienced in the 3-direction under a stress state in which $\sigma_1:\sigma_2:\sigma_3$ equaled $m:m:\lambda$. Whereas the vertical and horizontal strains differed in hydrostatic compression tests, the strains in the horizontal planes were identical.

The anisotropic behavior of wheat en masse has been discussed in Chapter VI in the sections on "Isotropy" and "Gravity Effects." In summary, the anisotropy was attributed to the asymmetric configuration of wheat grains. Because of their asymmetric shape, a horizontal orientation of their longitudinal axis is the only stable one in a gravity field. However, the orientation of the longitudinal axis within the horizontal plane is random. Thus, due to differences in geometry between the vertical and horizontal directions, the strains in these directions differ under identical stress states; and due to the macroscopic similarity of the particulate packing arrangement in any horizontal direction, the strains in all horizontal planes are identical when subjected to identical stress states.

Another characteristic of the mechanical behavior of wheat en masse is the presence of large residual strains upon removal of the loads. The typical stress-strain diagram for wheat en masse in Figure 68 illustrates the residual strains. The total strain at the beginning of unloading is denoted by $\epsilon_i)_T$ and may be separated into two components: (1) The elastic component, $\epsilon_i)_e$, and (2) The plastic component, $\epsilon_i)_p$. The elastic strain is that portion of the total strain which is recoverable. Previously, it has been noted that the recoverable strain encountered in wheat en masse is associated with recoverable individual particle deformations. The plastic strain is the irrecoverable portion of the total strain and has been attributed primarily to irreversible friction losses and irrecoverable work accomplished in the reorientation of individual particles from one packing arrangement to another. A minor portion of the plastic strain is a result of irrecoverable strains encountered during loading and unloading of individual grains. Arnold and Roberts (3), Zoerb (55), and Shelef and Mohsenin (47) also observed irrecoverable deformations when individual grains were loaded and unloaded; while Narayan and

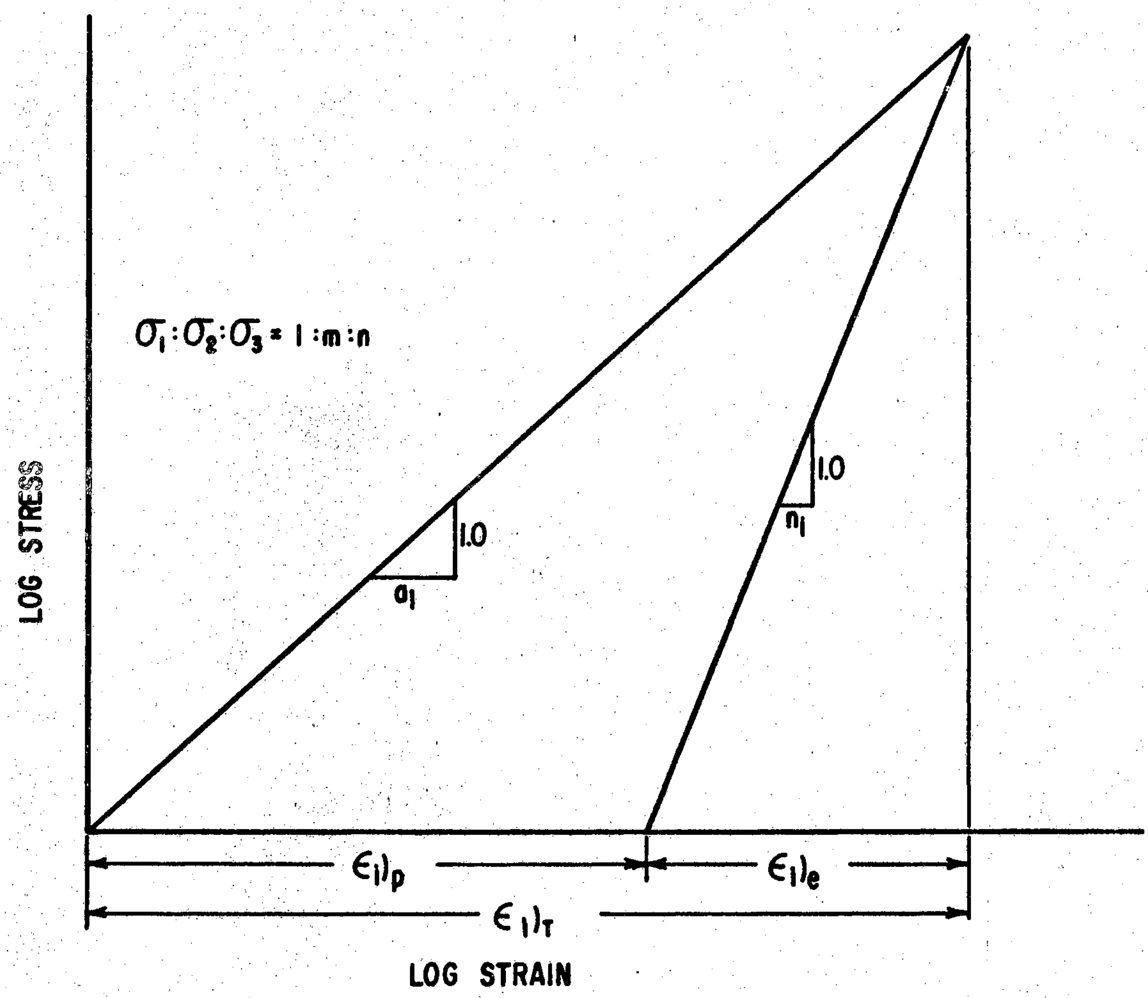

Figure 68. Idealized Static Stress-Strain Diagram for Wheat En Masse

Bilanski (38) observed large irrecoverable strains in wheat en masse loaded and unloaded axially in a confining cylinder.

A larger portion of the total strain is recovered in the vertical stress direction than in the horizontal stress directions. For example, in the validation experiments in which $\sigma_1:\sigma_2:\sigma_3 = 0.91:0.82:1$, the strain recovered in the vertical direction was 41 percent of the total strain, whereas only 17 and 20 percent of the total strain was recovered in the two horizontal directions. The anisotropic nature of wheat en masse due to particle orientation with respect to gravity was responsible for this effect.

The mechanical behavior of wheat en masse has been found to be very complex. It is classified as an anisotropic elastic-plastic material. The preliminary tests indicated that wheat en masse exhibits strain hardening tendencies with repeated loading cycles.

Loading Function

The prediction equations for the static strain during the first cycle of loading for cases where $\sigma_1:\sigma_2:\sigma_3$ does not vary during loading were presented in Equations 59, 61, and 62 in Chapter VIII. These equations have been verified by the results of the validation experiments and the analytical results of this chapter. All three prediction equations for strain were of the form

$$\epsilon_i)_L = A_i(\pi_2, \pi_3)\,\pi_4^{a_i} \tag{82}$$

where $A_i(\pi_2, \pi_3)$ = dimensionless function of π_2 and π_3

a_i = a dimensionless exponent

If $\epsilon_i)_L$ were plotted versus π_2 and π_3 in arithmetic space with π_4 as a parameter, a family of parallel planes would be described. The spacing between the planes would decrease logarithmically as π_4 increased.

The anisotropic nature of the deformational behavior is manifested in the prediction equations. For example, a_1 and a_2 were both equal to 0.454, but a_3 was equal to 0.520. The coefficients, A_i, also demonstrated the directional dependence of the strains. A_1 (π_2, π_3) and A_2 (π_2, π_3) differed only in that the coefficients of π_2 and π_3 terms were interchanged. However, the coefficient, A_3 (π_2, π_3), was completely different from A_2 and A_3. For example, for the case of hydrostatic compressive stresses, the magnitudes of A_1 and A_2 were identical, whereas the magnitude of A_3 was approximately one-half as great as A_1 or A_2.

Unloading Function

Unloading strains in the ith direction are predicted by Equations 67, 68, and 69 in Chapter VIII. The hypothesis that these equations were of the form

$$\epsilon_i)_U = \epsilon_{im} (\sigma_i/\sigma_{im})^{n_i} \tag{83}$$

has been verified.

Unloading behavior is of the exponential form. The coefficient in Equation 83 must be predicted from the loading function, $\epsilon_i)_L$, at the stress level at which unloading commenced. The slope parameter was shown to be dependent only upon the direction, i, of the principal strain. Further, elastic symmetry and observed results dictated that n_i was equal to 0.0486 in both horizontal directions. In the vertical direction the slope, $n_3 = 0.1180$, was approximately twice as large as both n_1 and n_2. Thus, a larger percentage of the strain in the vertical direction was recovered during unloading than in either of the horizontal directions. Because of the independence of n_i upon both stress ratio and the value of ϵ_{im}, all the log-log unloading curves in the ith direction were parallel straight lines with slope n_i.

CHAPTER X

SUMMARY AND CONCLUSIONS

Summary

The primary objective of this study was to functionally define the static stress-strain behavior of wheat en masse. Use was made of the hydraulic-mechanical analog stress control device and the cubical stress box developed by Ko and Scott (25) for the study of the stress-strain behavior of granular soils.

Preliminary studies were conducted with wheat en masse to evaluate the effect of sample size, gravity, time, and load history upon its mechanical behavior and to determine its degree of mechanical isotropy. It was found that a four inch cubical sample was adequate for studying the stress-strain behavior of wheat en masse. Gravity affected the behavior in that the wheat grains oriented themselves with respect to gravity during sample preparation. Wheat en masse was found to be anisotropic since strains were observed to be greater in any horizontal stress direction than in the vertical stress direction during hydrostatic compression tests. (Horizontal is defined as being perpendicular to the gravity filling axis.) In the first minute after application of a sustained load, the deformation of wheat en masse was observed to be highly dependent upon time. However, nearly 80 percent of the final strain, $\epsilon_{\infty i}$, was attained during the first minute of loading. After one minute the rate of increase in strain was extremely low. Variation of load rate from 3 to 6 psi per minute did not cause any variation in the observed strains in either hydrostatic or deviatoric tests. The stress-strain behavior was observed to be very dependent upon load history, thus indicating that the stress-strain behavior was incremental in nature and, therefore, closely bound to the stress path followed.

An experimental design based upon the theory of similitude and the preliminary findings was developed to define the functional nature of the static stress-strain behavior of wheat en masse. The following limitations were imposed by the design.

1. The physical properties of the wheat were held constant.
2. The loading rate was held constant at 3 psi/minute.
3. Only one cycle of loading and unloading was studied.
4. The stress ratio, $\sigma_1:\sigma_2:\sigma_3$, was held constant throughout a test while $\sigma_1 + \sigma_2 + \sigma_3$ was varied.
5. Stress ratios expected in grain storage structures were spanned.
6. All loads were below failure loads.

The six prediction equations for strain, excluding those terms held constant, for loading and unloading were of the form

$$\epsilon_1)_L = f_1 \ (\sigma_1/\sigma_3, \ \sigma_2/\sigma_3, \ \sigma_1/\sigma_c) \tag{84}$$

$$\epsilon_2)_L = f_2 \ (\sigma_1/\sigma_3, \ \sigma_2/\sigma_3, \ \sigma_2/\sigma_c) \tag{85}$$

$$\epsilon_3)_L = f_3 \ (\sigma_1/\sigma_3, \ \sigma_2/\sigma_3, \ \sigma_1/\sigma_c) \tag{86}$$

$$\epsilon_i)_U = \epsilon_{im} \ (\sigma_i/\sigma_{im})^{n_i}, \ i = 1, 2, 3 \tag{87}$$

The ranges of the variables considered were

$$0.557 \leq \sigma_1/\sigma_3 \leq 1.392$$

$$0.557 \leq \sigma_2/\sigma_3 \leq 1.392$$

$$0.000 \leq \sigma_1/\sigma_c \leq 1.000$$

$$0.000 \leq \sigma_2/\sigma_c \leq 1.000$$

$$0.000 \leq \sigma_i/\sigma_{im} \leq 1.000$$

Component equations were developed, transformed to linear functions, and combined by analysis of the functions to obtain the following prediction equations for strain.

$$\epsilon_1)_L = (-4.92 + 9.81\,\pi_2 + 2.36\,\pi_3 - 4.71\,\pi_2\,\pi_3)(10^{-2})(\sigma_1/\sigma_c)^{0.454} \qquad (88)$$

$$\epsilon_2)_L = (-4.92 + 2.36\,\pi_2 + 9.81\,\pi_3 - 4.71\,\pi_2\,\pi_3)(10^{-2})(\sigma_2/\sigma_c)^{0.454} \qquad (89)$$

$$\epsilon_3)_L = (10.00 - 6.55\,\pi_2 - 5.71\,\pi_3 + 3.71\,\pi_2\,\pi_3)(10^{-2})(\sigma_1/\sigma_c)^{0.520} \qquad (90)$$

$$\epsilon_1)_U = \epsilon_{1m}\,(\sigma_1/\sigma_{1m})^{0.0486} \qquad (91)$$

$$\epsilon_2)_U = \epsilon_{2m}\,(\sigma_2/\sigma_{2m})^{0.0486} \qquad (92)$$

$$\epsilon_3)_U = \epsilon_{3m}\,(\sigma_3/\sigma_{3m})^{0.1180} \qquad (93)$$

At any stress ratio, $\sigma_1:\sigma_2:\sigma_3$, large irrecoverable strains are predicted upon unloading the grain since the exponents in the expressions for $\epsilon_i)_U$ are much less than those for $\epsilon_i)_L$. Based upon the results of the preliminary studies and the form of the prediction equations for strain, wheat en masse has been classified as an anisotropic elastic-plastic material.

Two tests, in which $\sigma_1:\sigma_2:\sigma_3 = 0.91:0.82:1.00$, were conducted in order to validate the prediction equations. The predicted and observed strains were in agreement. Also, an analytical solution of the upper and lower bounds of the vertical strain of wheat en masse during hydrostatic compression indicated that the predicted strains fell within the limiting bounds.

Conclusions

The following conclusions were drawn from the experimental results.

1. The strains in a four inch stress box are more homogeneous than those in a six inch stress box. The smaller the sample size, the more homogeneous are the observed strains.
2. Wheat en masse is not isotropic with respect to principal strains. Mechanical symmetry exists in all horizontal planes with respect to gravity, but is absent with respect to vertical normal strains. The lack of complete symmetry is a result of particle orientation with respect to gravity.
3. The stress-strain behavior of wheat en masse is time dependent. However, 85 percent of the maximum strain is attained during the first minute after application of loads. Approximately 24 hours were required to attain the maximum strain level in hydrostatic compression tests.
4. The stress-strain behavior of wheat en masse is incremental.
5. The component equations for $\varepsilon_i)_L$ versus σ_1/σ_3 and $\varepsilon_i)_L$ versus σ_2/σ_3 during the first loading cycle were linear in arithmetic space.
6. The component equations for $\varepsilon_i)_L$ versus σ_1/σ_c were linear in

log-log space. This is in agreement with the experimental results of other investigations for individual particles of wheat.

7. The equations which predict the normal strains for wheat en masse during the first cycle of loading are:

$$\epsilon_1)_L = (-4.92 + 9.81\ \sigma_1/\sigma_3 + 2.36\ \sigma_2/\sigma_3 - 4.71\ \sigma_1\sigma_2/\sigma_3^2)(10^{-2})(\sigma_1/\sigma_c)^{0.454} \tag{94}$$

$$\epsilon_2)_L = (-4.92 + 2.36\ \sigma_1/\sigma_3 + 9.81\ \sigma_2/\sigma_3 - 4.71\ \sigma_1\sigma_2/\sigma_3^2)(10^{-2})(\sigma_2/\sigma_c)^{0.454} \tag{95}$$

$$\epsilon_3)_L = (10.00 - 6.55\ \sigma_1/\sigma_3 - 5.71\ \sigma_2/\sigma_3 + 3.71\ \sigma_1\sigma_2/\sigma_3^2)(10^{-2})(\sigma_1/\sigma_c)^{0.520} \tag{96}$$

8. In the ith direction the stress-strain behavior of wheat en masse during unloading proceeds along straight line paths in log-log space. The prediction equations for strain during the first unload cycle are

$$\epsilon_1)_U = \epsilon_{1m}\ (\sigma_1/\sigma_{1m})^{0.0486} \tag{97}$$

$$\epsilon_2)_U = \epsilon_{2m}\ (\sigma_2/\sigma_{2m})^{0.0486} \tag{98}$$

$$\epsilon_3)_U = \epsilon_{3m}\ (\sigma_3/\sigma_{3m})^{0.1180} \tag{99}$$

The exponents do not vary with stress ratio or with ϵ_{im}.

9. At stress ratios of σ_1/σ_3 and σ_2/σ_3 above 1.392 and below 0.557 in wheat en masse, static behavior ceases and flow conditions commence. Thus, the prediction equations should not be extrapolated beyond the limits imposed in the study.

10. The magnitude of the strains measured by the methods and apparatus described herein fall within the limiting theoretical bounds for strain.

11. Wheat en masse behaves as an anisotropic elastic-plastic material.

12. The methods and procedures described in this report are adequate for defining the static stress-strain behavior of particulate materials en masse found in agricultural enterprises.

SELECTED BIBLIOGRAPHY

(1) Airy, W. The pressure of grain. Minutes of Proceedings of the Institution of Civil Engineers. 131:347-358. 1898.

(2) Arnold, P. C. and A. W. Roberts. Mechanical and rheological properties of Australian wheats. Part 1. Effect of variety on load-deformation characteristics. Wollongong University Colloquium Bulletin 12. 1967.

(3) Arnold, P. C. and A. W. Roberts. Fundamental aspects of load-deformation behavior of wheat grains. Transactions of ASAE. 12:1:104-108. 1969.

(4) Bell, J. M. Stress-strain characteristics of cohesionless granular materials subjected to statically applied homogeneous loads in an open system. Ph.D. thesis. California Institute of Technology. 1965.

(5) Biot, M. A. Theory of deformation of a porous visco-elastic anisotropic solid. Journal of Applied Physics 27. 1956.

(6) Brown, E. H. A theory for the mechanical behavior of sand. Proceedings of the 11th International Congress of Applied Mechanics. 1964.

(7) Brubaker, J. E. and J. Pos. Determination of static coefficients of friction of some grains on various structural surfaces. Paper No. 63-828. American Society of Agricultural Engineers. St. Joseph, Michigan. 1963.

(8) Buckingham, E. On physically similar systems: Illustrations of the use of dimensionless equations. Physical Review. 4:10:345. 1914.

(9) Collins, R. V. Determination of pressures in cylindrical storage structures. Transactions of ASAE. 6:2:98-101, 103. 1963.

(10) Cox, A. D., G. Eason and H. D. Hopkins. Axially symmetric plastic deformation in soils. Philosophical Transactions of the Royal Society. A 254:1-45. 1961.

(11) Dabrowski, R. Shell analysis of intermediate silo bins. Journal of the American Concrete Institute. 7:795-803. 1965.

(12) Dale, A. C. and R. N. Robinson. Pressures in deep grain storage structures. Agricultural Engineering. 35:8:570-573. 1954.

(13) Drucker, D. C., R. E. Gibson and D. J. Henkel. Soil mechanics and work hardening theories of plasticity. Transactions of ASCE. 122. 1957.

(14) Duffy, J. and R. D. Mindlin. Stress-strain relations and vibrations of a granular medium. Journal of Applied Mechanics, ASME. 24:585. 1957.

(15) Duffy, J. A differential stress-strain relation for the hexagonal close-packed array of elastic spheres. Journal of Applied Mechanics, ASME. 26:3:88-94. 1959.

(16) Hamilton, H. E. An analysis of lateral strain in cylindrical grain bin walls subjected to active and passive pressures. Unpublished M.S. thesis. Oklahoma State University. 1964.

(17) Hardin, B. O. and F. E. Richart. Elastic wave velocities in granular soils. Journal of the Soil Mechanics and Foundations Division, ASCE. 89:SM1:33-65. 1963.

(18) Hardin, B. O. and W. L. Black. Sand stiffness under various triaxial stresses. Journal of the Soil Mechanics and Foundations Division, ASCE. 92:SM2:27-42. 1966.

(19) Hertz, H. Miscellaneous Papers. MacMillan and Company: New York. 1896.

(20) Isaacson, J. D. and J. S. Boyd. Mathematical analysis of lateral pressures in flat-bottomed deep grain bins. Transactions of ASAE. 8:3. 1965.

(21) Jaky, J. Pressure in silos. Proceedings 2nd Int. Conference Soil Mchs. and Found. Engr. 1:103-107. Rotterdam. June, 1948.

(22) Janssen, H. A. Versuche uber Getreidedrucke in Silozellen. Zeitschrift des Vereines Deutscher Ingenieure. 39:1045-1049. 1895.

(23) Jenike, A. W. and J. R. Johanson. Bin loads. Proceedings of ASCE. 94:ST4:1011-1041. 1968.

(24) Kjellman, W. Report on an apparatus for consummate investigation of the mechanical properties of soils. Proceedings of International Conference on Soil Mechanics. 2:16. 1936.

(25) Ko, H. Y. and R. F. Scott. A new soil testing apparatus. Geotechnique. 17:1:40-56. 1967.

(26) Ko, H. Y. and R. F. Scott. Deformation of sand in shear. Journal of the Soil Mechanics and Foundations Division, ASCE. 93:SM5:283-310. 1967.

(27) Ko, H. Y. and R. F. Scott. Deformation of sand in hydrostatic compression. Journal of the Soil Mechanics and Foundations Division, ASCE. 93:SM3:137-156. 1967.

(28) Ko, H. Y. and R. F. Scott. Deformation of sand at failure. Journal of the Soil Mechanics and Foundations Division, ASCE. 94:SM4:883-898. 1968.

(29) Kosma, A. and H. Cunningham. Tables for calculating the compressive surface stresses and deflections in the contact of two solid elastic bodies whose principle planes of curvature do not coincide. Journal of Industrial Mathematics. 12:1:31-40.

(30) __________, Natural latex dipping process. Latex Technical Bulletin. General Latex and Chemical Corporation. Ashland, Ohio.

(31) Lambe, T. W. Soil Testing for Engineers. John Wiley and Sons, Inc.: New York. 1967.

(32) Lorenzen, R. T. Moisture effect on friction coefficients of small grains. Paper No. 59-416. American Society of Agricultural Engineers. St. Joseph, Michigan. 1959.

(33) Mindlin, R. D. Compliance of elastic bodies in contact. Journal of Applied Mechanics, ASME. 71:259. 1949.

(34) Mindlin, R. D. and H. Deresiewicz. Elastic spheres in contact under varying oblique forces. Journal of Applied Mechanics, ASME. 75:327-344. 1953.

(35) Mindlin, R. D., W. P. Mason, T. F. Osner, and H. Deresiewicz. Effects of an oscillating tangential force on the contact surfaces of elastic spheres. Proceedings of the First National Congress of Applied Mechanics. pp. 203-208. 1951.

(36) Mohsenin, N. N. Physical Properties of Plant and Animal Materials: Parts I and II of Vol. I. The Pennsylvania State University. University Park, Pennsylvania. 1968.

(37) Murphy, G. Similitude in Engineering. The Ronald Press Co.: New York. 1950. Chapter 3.

(38) Narayan, C. V. and W. K. Bilanski. Behavior under high pressure of wheat grains in bulk. Paper No. 66-806. American Society of Agricultural Engineers. St. Joseph, Michigan. 1966.

(39) Natrella, M. G. Experimental Statistics. National Bureau of Standards Handbook No. 91. United States Department of Commerce. Washington, D. C. 1963.

(40) Orr, C., Jr. Particulate Technology. The MacMillan Company: New York. 1966.

(41) Riembert, M. and A. Riembert. Silos Traite Theorique et Pratique. Editions Eyrolles: Paris. 1956.

(42) Roscoe, K. H., A. N. Schofield and A. Thurairajah. Yielding of clays in states wetter than critical. Geotechnique. 13. 1963.

(43) Rowe, P. W. The stress-dilatancy relation for static equilibrium of an assembly of particles in contact. Proceedings, Royal Society of London, Series A. 269:174. 1963.

(44) Rowe, P. W. A stress-strain theory for cohesionless soil with application to earth pressure at rest and moving walls. Geotechnique. 4:2:70. 1954.

(45) Saada, A. S. Stress controlled apparatus for triaxial testing. Journal of the Soil Mechanics and Foundations Division, ASCE. 93:SM6:61-78. 1967.

(46) Saul, R. A. Measurement of grain pressures on bin walls and floors. Agricultural Engineering. 34:4:231-234. 1953.

(47) Shelef, L. and N. N. Mohsenin. Evaluation of the modulus of elasticity of wheat grain. Cereal Chemistry. 44:392. 1967.

(48) Shield, R. T. Mixed boundary value problems in soil mechanics. Quarterly Applied Mathematics. 11. 1953.

(49) Shpolyanskaya, A. L. Structural-mechanical properties of the wheat grain. Colloid Journal (English Translation.). 14:1:137-148. 1952.

(50) Stewart, B. R. Effect of moisture content and specific weight on the internal friction properties of sorghum grain. Paper No. 64-804. American Society of Agricultural Engineers. St. Joseph, Michigan. 1964.

(51) Stewart, B. R. Active and passive wall pressures induced by sorghum grain in a shallow bin. Paper No. 67-920. American Society of Agricultural Engineers. St. Joseph, Michigan. 1967.

(52) Terzaghi, K. Large retaining wall test: I. Pressure of dry sand. Engineering News-Record. 112:136-140. 1934.

(53) Terzaghi, K. Theoretical soil mechanics. Wiley and Sons: New York. 1965.

(54) Zoerb, G. C. and C. W. Hall. Some mechanical and rheological properties of grains. Paper No. 58-112. American Society of Agricultural Engineers. St. Joseph, Michigan. 1958.

(55) Zoerb, G. C. and C. W. Hall. Some mechanical and rheological properties of grains. Journal of Agricultural Engineering Research. 5:1:83-93. 1960.

APPENDIX A

STRESSES IN THE ORTHOGONAL PLANES
FOR SELECTED LOCATIONS
OF THE LOAD CYLINDER
ON THE STRESS PLATE
FOR A UNIT LOAD

APPENDIX A-I

STRESSES IN THE ORTHOGONAL PLANES FOR SELECTED LOCATIONS ON THE STRESS PLATE FOR UNIT LOAD

Angle θ (deg.)	Dist. r (in.)	Stresses[1] σ_1 (psi)	σ_2	σ_3	Stress Ratios σ_1/σ_3 (-)	σ_2/σ_3 (-)
0	0.00	0.33	0.33	0.33	1.00	1.00
	0.50	0.37	0.31	0.31	1.18	
	1.00	0.41	0.30	0.30	1.39	
	1.50	0.45	0.28	0.28	1.63	
	2.00	0.49	0.26	0.26	1.90	
	2.50	0.53	0.24	0.24	2.22	
	3.00	0.56	0.22	0.22	2.59	
30	0.50	0.37	0.33	0.30	1.22	1.11
	1.00	0.40		0.27	1.50	1.25
	1.50	0.43		0.23	1.86	1.43
	2.00	0.47		0.20	2.33	1.67
	2.50	0.50		0.17	3.00	2.00
	3.00	0.53		0.13	4.00	2.50
60	0.50	0.35	0.35	0.30	1.20	1.20
	1.00	0.37	0.37	0.26	1.45	1.45
	1.50	0.39	0.39	0.22	1.80	1.80
	2.00	0.41	0.41	0.18	2.29	2.29
	2.50	0.43	0.43	0.14	3.05	3.05
	3.00	0.45	0.45	0.10	4.38	4.38
90	0.50	0.33	0.37	0.30	1.00	1.22
	1.00		0.40	0.27	1.11	1.50
	1.50		0.43	0.23	1.43	1.86
	2.00		0.47	0.20	1.67	2.33
	2.50		0.50	0.17	2.00	3.00
	3.00		0.53	0.13	2.50	4.00

[1]Top cylinder stress $= \sigma_1 + \sigma_2 + \sigma_3 = 1.0$ psi.

APPENDIX B

DATA AND CORRECTION CURVE FOR THE VOLUMETRIC DEFORMATIONS DUE TO MEMBRANE INDENTATION AND COMPRESSION

APPENDIX B

DATA AND CORRECTION CURVE FOR THE VOLUMETRIC DEFORMATIONS DUE TO MEMBRANE INDENTATION AND COMPRESSION

Data are presented and the least squares best fit curve for those data is presented. The volumetric correction is for the indentation of the latex rubber membrane into the void spaces of a single layer of wheat grains. The correction term is equally valid in any of the three stress directions of a cubical element and is given in units of cu. cm. per sq. in. Thus, to apply the correction curve of Appendix B-II, the values must be multiplied by the area of the membrane.

APPENDIX B-I

REDUCED DATA FOR THE CORRECTION CURVE
FOR MEMBRANE INDENTATION
WITH WHEAT GRAINS

Stress σ_i (psi)	Volumetric Correction ΔV_{corr}/sq.in. (cu. cm./sq. in.)				
	Rep. 1	Rep. 2	Rep. 3	Rep. 4	Rep. 5
0	0.000	0.000	0.000	0.000	0.000
5	0.132	0.123	0.121	0.125	0.128
10	0.167	0.164	0.167	0.169	0.169
15	0.192	0.192	0.189	0.194	0.196
20	0.212	0.198	0.209	0.209	0.214
25	0.226	0.226	0.225	0.225	0.226
30	0.227	0.227	0.227	0.227	0.228
35	0.227	0.227	0.228	0.228	0.229
40	0.228	0.228	0.229	0.229	0.229
45	0.229	0.229	0.230	0.230	0.230

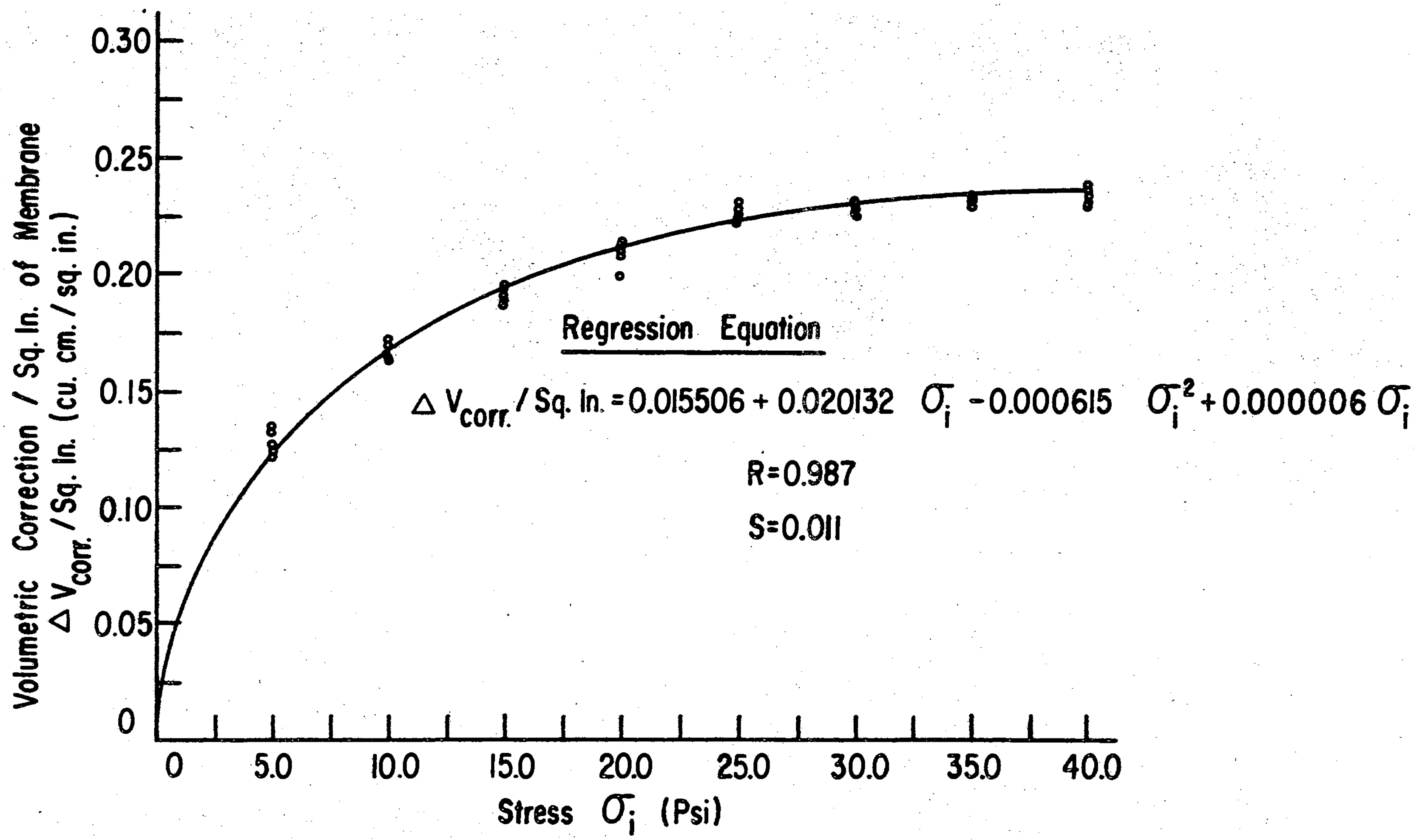

Appendix B-II. Correction Curve for Volumetric Deformation Due to Membrane Indentation

APPENDIX C

DATA FOR EVALUATION OF THE PHYSICAL PROPERTIES OF THE WHEAT GRAINS USED IN THE TESTING PROGRAM

TABLE C-I

AXIAL DIMENSIONS OF TWENTY-FIVE RANDOMLY SELECTED WHEAT GRAINS

Grain Identification	Maximum Dimension (mm x 40)	Intermediate Dimension (mm x 40)	Minimum Dimension (mm x 40)
A-1	315	170	150
A-2	310	150	135
A-3	290	150	130
A-4	315	155	140
A-5	305	150	145
B-1	300	140	135
B-2	320	165	145
B-3	305	145	125
B-4	295	155	140
B-5	310	150	140
C-1	305	150	140
C-2	320	155	145
C-3	290	145	130
C-4	305	145	130
C-5	315	145	140
D-1	260	110	105
D-2	310	160	145
D-3	295	145	135
D-4	295	145	130
D-5	300	150	135
E-1	295	160	150
E-2	305	150	145
E-3	305	160	145
E-4	285	145	130
E-5	290	155	135
Mean	$\bar{a}$ = 301.40	$\bar{b}$ = 150.00	$\bar{c}$ = 139.00
Std. deviation	13.05	10.96	9.56
Std. deviation of the mean	2.61	2.13	1.91

TABLE C-II

SELECTED PHYSICAL PROPERTIES OF WHEAT GRAINS USED IN THE TESTING PROGRAM

Sample	Specific Gravity (-)	Angle of Internal Friction (-)	Moisture Content (%)	Coef. of Static Friction Wheat on Latex Rubber (-)	Coef. of Static Friction Wheat on Aluminum (-)
A	1.400	24.8	10.85	0.480	0.260
B	1.388	25.4	12.00	0.478	0.253
C	1.398	25.0	12.15	0.462	0.247
D	1.355	24.6	10.90	0.500	0.260
E	1.441	25.2	11.00	0.464	0.245
Mean	1.396	25.0	11.38	0.477	0.253
Std. Dev.	0.030	0.3	0.64	0.015	0.007
Std. Dev. of Mean	0.013	0.1	0.28	0.007	0.003

APPENDIX D

REDUCED STRAINS FOR THE PRELIMINARY TESTS

APPENDIX D

REDUCED STRAINS FOR THE PRELIMINARY TESTS

I. Size Effects (Four Inch Stress Box).

II. Size Effects (Six Inch Stress Box).

III. Gravity Effects.

IV. Isotropy Studies.

V. Load Rate Study. Hydrostatic Compression.

VI. Load Rate Study. Deviatoric Stress State.

VII. Creep Test.

VIII. Cyclic Hydrostatic Compression.

IX. Cyclic Deviatoric Stress.

X. Superposition of a Deviatoric Stress State Upon a Hydrostatic Stress State.

XI. Superposition of a Hydrostatic Stress State Upon a Deviatoric Stress State.

XII. Cyclic Radial Stress State in which the Stress Ratio Varied During the Test.

TABLE D-I

STRESS-STRAIN DATA FOR THE SIZE EFFECT TESTS. HYDROSTATIC COMPRESSION TEST WITH THE FOUR INCH STRESS BOX

Stress	Strain								
	Rep 1			Rep 2			Rep 3		
	ϵ_1	ϵ_2	ϵ_3	ϵ_1	ϵ_2	ϵ_3	ϵ_1	ϵ_2	ϵ_3
(psi)	(in./in. x 10^2)			(in./in. x 10^2)			(in./in. x 10^2)		
0	0.0	0.0	0.0	0.0	0.0	0.0	0.0	0.0	0.0
1	0.286	0.286	0.206	0.753	0.715	0.618	0.543	0.477	0.445
2	0.496	0.496	0.282	0.868	0.820	0.553	0.810	0.829	0.597
3	0.601	0.591	0.304	0.934	0.877	0.705	0.944	0.963	0.662
5	0.677	0.658	0.250	1.001	0.944	0.716	0.972	1.011	0.640
8	0.915	0.877	0.358	1.278	1.211	0.911	1.249	1.278	0.814
11	1.163	1.106	0.477	1.430	1.364	1.030	1.402	1.449	0.987
14	1.297	1.203	0.553	1.630	1.554	1.161	1.592	1.678	1.074
17	1.468	1.487	0.629	1.754	1.688	1.258	1.754	1.812	1.161
20	1.592	1.545	0.716	1.888	1.821	1.367	1.897	1.916	1.226
17	1.592	1.506	0.640	1.869	1.783	1.302	1.878	1.878	1.150
14	1.564	1.468	0.618	1.821	1.735	1.248	1.821	1.850	1.117
11	1.478	1.402	0.532	1.754	1.669	1.161	1.774	1.792	1.041
8	1.449	1.364	0.477	1.688	1.602	1.063	1.659	1.688	0.922
5	1.306	1.211	0.314	1.583	1.506	0.965	1.545	1.564	0.792
3	1.344	1.259	0.358	1.621	1.535	0.987	1.592	1.621	0.846
2	1.249	1.163	0.293	1.392	1.373	0.879	1.364	1.487	0.748
1	1.106	1.011	0.217	1.287	1.182	0.781	1.421	1.449	0.748
0	0.753	0.753	0.087	0.915	0.744	0.705	0.810	0.648	0.477

TABLE D-II

STRESS-STRAIN DATA FOR THE SIZE EFFECT TESTS.
HYDROSTATIC COMPRESSION TESTS WITH
THE SIX INCH STRESS BOX

Stress	Strain								
	Rep 1			Rep 2			Rep 3		
	ϵ_1	ϵ_2	ϵ_3	ϵ_1	ϵ_2	ϵ_3	ϵ_1	ϵ_2	ϵ_3
(psi)	(in./in. x 10^2)			(in./in. x 10^2)			(in./in. x 10^2)		
0	0.0	0.0	0.0	0.0	0.0	0.0	0.0	0.0	0.0
1	0.458	0.443	0.231	0.508	0.545	0.440	0.305	0.314	0.298
2	0.698	0.684	0.381	0.613	0.624	0.504	0.604	0.616	0.437
3	0.805	0.794	0.458	0.664	0.675	0.523	0.653	0.667	0.455
5	0.825	0.814	0.529	0.763	0.763	0.553	0.723	0.740	0.461
8	1.054	1.037	0.689	1.006	1.006	0.701	0.975	0.992	0.600
11	1.234	1.223	0.833	1.144	1.144	0.790	1.138	1.161	0.713
14	1.384	1.367	0.969	1.325	1.322	0.907	1.288	1.311	0.753
17	1.494	1.472	1.107	1.455	1.446	0.984	1.418	1.444	0.895
20	1.633	1.602	1.175	1.556	1.554	1.061	1.534	1.556	0.969
17	1.619	1.596	1.107	1.562	1.548	1.018	1.548	1.559	0.938
14	1.571	1.548	1.027	1.528	1.520	0.981	1.523	1.526	0.898
11	1.514	1.523	0.935	1.466	1.455	0.904	1.452	1.452	0.858
8	1.444	1.424	0.824	1.418	1.412	0.858	1.412	1.415	0.830
5	1.356	1.339	0.716	1.294	1.288	0.750	1.305	1.314	0.689
3	1.364	1.348	0.726	1.266	1.266	0.753	1.297	1.308	0.704
2	1.308	1.291	0.673	1.172	1.181	0.720	1.243	1.249	0.673
1	1.113	1.088	0.566	1.031	1.048	0.695	1.141	1.147	0.649
0	0.774	0.743	0.443	0.667	0.698	0.673	0.729	0.746	0.600

APPENDIX D-III

REDUCED UNIT STRAINS FOR PRELIMINARY EXPERIMENT 3. GRAVITY EFFECT TESTS

Hydrostatic Stress Level (psi)	Unit Strain (in./in. x 10^2) Rep. 1 ϵ_1	Rep. 1 ϵ_2	Rep. 1 ϵ_3	Rep. 2 ϵ_1	Rep. 2 ϵ_2	Rep. 2 ϵ_3
0	0.00	0.00	0.00	0.00	0.00	0.00
1	0.77	0.70	0.58	0.58	0.62	0.47
2	1.02	0.91	0.64	0.84	0.90	0.67
3	1.18	1.07	0.69	0.95	1.01	0.73
4	1.32	1.18	0.75	1.07	1.12	0.81
5	1.42	1.27	0.78	1.20	1.25	0.88
6	1.59	1.36	0.88	1.28	1.32	0.92
9	1.75	1.57	0.94	1.46	1.51	1.04
12	1.90	1.72	1.05	1.64	1.68	1.13
15	2.05	1.82	1.19	1.78	1.79	1.23
18	2.19	1.96	1.28	1.91	1.92	1.33
21	2.32	2.08	1.28	--	--	--
18	2.29	2.06	1.27	--	--	--
15	2.28	2.05	1.27	1.90	1.91	1.30
12	2.24	2.03	1.29	1.89	1.90	1.28
9	2.21	2.01	1.31	1.86	1.91	1.24
6	2.16	1.98	1.26	1.82	1.87	1.16
5	2.10	1.92	1.27	1.78	1.83	1.13
4	2.05	1.89	1.25	1.74	1.78	1.07
3	1.98	1.84	1.24	1.68	1.74	1.01
2	1.81	1.73	1.24	1.61	1.67	0.96
1	1.70	1.53	1.07	1.43	1.49	0.81
0	1.08	0.87	0.64	0.94	1.02	0.40

APPENDIX D-IV

REDUCED UNIT STRAINS FOR PRELIMINARY EXPERIMENTS 3 AND 4. ISOTROPY AND LOAD RATE. ($\sigma_1:\sigma_2:\sigma_3$ = 2.33:1.67:1.00)

Cylinder Load[1] (psi)	Unit Strain (in./in. x 10^2)					
	Rep. 1			Rep. 2		
	ϵ_1	ϵ_2	ϵ_3	ϵ_1	ϵ_2	ϵ_3
	Experiment 3 (σ_1 is a horizontal stress)					
0	0.00	0.00	0.00	0.00	0.00	0.00
3	0.32	0.08	0.06	0.22	0.11	0.03
9	1.32	0.47	0.26	1.31	0.38	0.06
18	2.35	0.68	0.29	2.17	0.57	0.05
27	3.36	0.90	0.13	3.14	0.89	-0.33
36	4.00	0.96	-0.01	3.71	0.98	-0.49
45	4.60	1.02	-0.17	4.31	1.09	-0.69
36	4.63	1.07	-0.21	4.32	1.14	-0.69
30	4.63	1.09	-0.24	4.36	1.16	-0.70
20	4.63	1.07	-0.44	4.40	1.17	-0.70
9	4.55	1.04	-0.52	4.35	1.17	-0.71
3	4.31	0.99	-0.56	4.11	1.16	-0.66
0	4.02	0.88	-0.56	3.73	1.11	-0.61
	Experiment 4 (σ_1 is a vertical stress)					
0	0.00	0.00	0.00	0.00	0.00	0.00
3	0.35	0.36	0.03	0.14	0.24	0.09
9	1.10	0.77	0.06	0.75	0.72	0.14
18	1.80	1.24	0.08	1.37	1.10	0.20
27	2.47	1.57	-0.18	2.01	1.44	0.01
36	2.85	1.75	-0.19	2.39	1.61	-0.09
45	3.21	1.89	-0.27	2.73	1.78	-0.21
36	3.25	1.91	-0.27	2.77	1.82	-0.22
30	3.25	1.93	-0.27	2.80	1.81	-0.22
20	3.28	1.94	-0.26	2.81	1.80	-0.21
9	3.22	1.91	-0.26	2.76	1.79	-0.23
3	3.13	1.82	-0.26	2.62	1.69	-0.21
0	2.97	1.71	-0.26	2.44	1.61	-0.21

[1] Load = p = $\sigma_1 + \sigma_2 + \sigma_3$

APPENDIX D-V

REDUCED UNIT STRAINS FOR PRELIMINARY EXPERIMENTS 5, 6, AND 7. HYDROSTATIC LOAD RATE INVESTIGATIONS.

Stress[1] (psi)	Unit Strain ϵ_1 (in./in. x 10^2)	Unit Strain ϵ_2	Unit Strain ϵ_3	Unit Strain ϵ_1 (in./in. x 10^2)	Unit Strain ϵ_2	Unit Strain ϵ_3
	Load rate = 6 psi/min			Load rate = 3 psi/min		
0	0.00	0.00	0.00	0.00	0.00	0.00
2	0.31	0.33	0.29	0.33	0.33	0.29
4	0.66	0.69	0.66	0.75	0.73	0.66
8	1.12	1.16	0.92	1.10	1.13	0.84
16	1.62	1.64	1.13	1.60	1.62	1.08
24	1.99	2.01	1.31	2.01	2.03	1.27
32	2.35	2.37	1.53	2.30	2.33	1.47
40	2.62	2.66	1.72	2.61	2.63	1.66
32	2.54	2.58	1.67	2.56	2.58	1.61
24	2.48	2.50	1.54	2.48	2.49	1.51
16	2.38	2.41	1.45	2.40	2.41	1.44
8	2.32	2.35	1.37	2.33	2.35	1.39
4	2.21	2.25	1.33	2.27	2.28	1.40
2	2.11	2.15	1.28	2.09	2.11	1.27
0	1.92	1.96	1.19	1.94	1.96	1.19
	Load rate = 4.5 psi/min					
0	0.00	0.00	0.00			
2	0.35	0.33	0.20			
4	0.71	0.71	0.54			
8	1.14	1.13	0.75			
16	1.59	1.58	0.98			
24	2.05	2.06	1.18			
32	2.29	2.26	1.37			
40	2.61	2.58	1.59			
32	2.55	2.53	1.54			
24	2.44	2.42	1.43			
16	2.35	2.33	1.34			
8	2.30	2.27	1.26			
4	2.18	2.17	1.20			
2	2.06	2.07	1.16			
0	1.84	1.88	1.08			

[1]Hydrostatic stress level

APPENDIX D-VI

REDUCED UNIT STRAINS FOR PRELIMINARY EXPERIMENTS 8, 9, AND 10. DEVIATORIC STRESS LOAD RATE INVESTIGATIONS. ($\sigma_1 : \sigma_2 : \sigma_3 = 2.33 : 1.67 : 1.00$)

Cylinder Load[1] (psi)	Unit Strain					
	ϵ_1	ϵ_2	ϵ_3	ϵ_1	ϵ_2	ϵ_3
	(in./in. x 10^2)			(in./in. x 10^2)		
	Load rate = 3 psi/min			Load rate = 6 psi/min		
0	0.00	0.00	0.00	0.00	0.00	0.00
3	0.22	0.11	0.03	0.14	0.09	-0.01
9	1.31	0.38	0.06	1.14	0.51	-0.03
18	2.17	0.57	0.05	1.83	0.80	-0.06
27	3.14	0.89	-0.33	2.39	0.99	-0.14
36	3.71	0.98	-0.49	3.35	1.18	-0.58
45	4.31	1.09	-0.69	3.96	1.26	-0.85
36	4.32	1.14	-0.69	4.06	1.30	-0.87
27	4.40	1.16	-0.70	4.04	1.32	-0.86
18	4.40	1.17	-0.71	4.02	1.32	-0.87
9	4.33	1.18	-0.71	3.91	1.32	-0.87
3	4.11	1.16	-0.66	3.71	1.28	-0.87
0	3.73	1.11	-0.61	3.47	1.17	-0.88
	Load rate = 4.5 psi/min					
0	0.00	0.00	0.00			
3	0.07	0.12	0.01			
9	0.79	0.58	0.02			
18	1.87	0.93	0.01			
27	2.51	1.05	-0.09			
36	3.48	1.19	-0.50			
45	4.09	1.24	-0.74			
36	4.15	1.29	-0.76			
27	4.15	1.30	-0.76			
18	4.13	1.30	-0.76			
9	3.97	1.28	-0.76			
3	3.78	1.22	-0.74			
0	3.54	1.13	-0.73			

[1] Load = p = $\sigma_1 + \sigma_2 + \sigma_3$

APPENDIX D-VII

REDUCED UNIT STRAINS FOR PRELIMINARY EXPERIMENT 11. CREEP INVESTIGATIONS. ($\sigma_1 : \sigma_2 : \sigma_3 = 1:1:1$)

Elapsed Time (min.)	Unit Strain ϵ_1	ϵ_2 (in./in. x 10^2)	ϵ_3
	$\sigma_o = 20$ psi		
0	0.00	0.00	0.00
1	2.47	2.39	1.79
2	2.49	2.39	1.80
4	2.53	2.41	1.81
6	2.56	2.44	1.82
8	2.57	2.46	1.83
10	2.57	2.47	1.83
12	2.58	2.49	1.84
312	2.89	2.72	2.05
1080	3.13	2.97	2.25
1620	3.15	2.98	2.31

[1] Constant hydrostatic stress level = σ_o

APPENDIX D-VIII

REDUCED UNIT STRAINS FOR PRELIMINARY EXPERIMENT 12. CYCLIC HYDROSTATIC COMPRESSION TEST. ($\sigma_1:\sigma_2:\sigma_3 = 1:1:1$)

Stress[1] (psi)	Unit Strain ϵ_1 (in./in. x 10^2)	ϵ_2	ϵ_3	Stress[1] (psi)	Unit Strain ϵ_1 (in./in. x 10^2)	ϵ_2	ϵ_3
0	0.00	0.00	0.00	40	2.90	2.82	1.71
4	0.95	0.94	0.57	32	2.82	2.75	1.63
8	1.29	1.29	0.71	24	2.72	2.64	1.53
16	1.65	1.67	0.92	20	2.68	2.59	1.44
24	1.99	2.00	1.12	24	2.71	2.63	1.49
32	2.30	2.32	1.34	32	2.83	2.74	1.62
40	2.58	2.61	1.54	40	2.97	2.88	1.74
32	2.52	2.53	1.47	32	2.90	2.80	1.67
24	2.42	2.42	1.34	24	2.80	2.70	1.54
16	2.32	2.32	1.23	16	2.70	2.60	1.44
8	2.23	2.21	1.11	12	2.69	2.58	1.40
0	1.39	1.35	0.60	16	2.68	2.56	1.40
8	2.04	1.98	1.06	20	2.73	2.61	1.46
16	2.18	2.11	1.18	16	2.68	2.56	1.41
24	2.36	2.30	1.31	8	2.66	2.54	1.36
32	2.57	2.53	1.49	6	2.62	2.49	1.31
40	2.78	2.75	1.64	8	2.62	2.49	1.34
32	2.70	2.67	1.56	12	2.62	2.50	1.35
24	2.59	2.55	1.44	8	2.62	2.49	1.34
16	2.50	2.45	1.33	4	2.57	2.41	1.27
8	2.43	2.35	1.23	0	1.88	1.77	0.87
0	1.61	1.55	0.72	2	2.28	2.15	1.17
8	2.23	2.24	1.17	4	2.39	2.25	1.24
16	2.35	2.27	1.27	6	2.43	2.29	1.25
24	2.51	2.43	1.39	2	2.35	2.22	1.17
32	2.70	2.63	1.55	0	1.86	1.75	0.86

[1]Hydrostatic stress level

APPENDIX D-IX

REDUCED UNIT STRAINS FOR PRELIMINARY EXPERIMENT 13. CYCLIC DEVIATORIC STRESS TEST. ($\sigma_1:\sigma_2:\sigma_3$ = 2.33:1.67:1)

Cylinder Load[1] (psi)	Unit Strain ϵ_1 (in./in. x 10^2)	Unit Strain ϵ_2 (in./in. x 10^2)	Unit Strain ϵ_3 (in./in. x 10^2)	Cylinder Load[1] (psi)	Unit Strain ϵ_1 (in./in. x 10^2)	Unit Strain ϵ_2 (in./in. x 10^2)	Unit Strain ϵ_3 (in./in. x 10^2)
0	0.00	0.00	0.00	36	5.64	1.42	-1.68
3	0.11	0.07	0.03	27	5.65	1.41	-1.68
6	0.51	0.25	0.04	18	5.65	1.45	-1.66
9	0.92	0.43	0.03	9	5.55	1.45	-1.66
18	2.03	0.69	-0.04	0	5.10	1.39	-1.64
27	2.92	0.93	-0.44	9	5.05	1.38	-1.64
36	3.56	1.05	-0.67	18	5.25	1.41	-1.69
45	4.27	1.11	-1.02	27	5.45	1.40	-1.75
36	4.34	1.17	-1.05	36	5.66	1.42	-1.78
27	4.37	1.18	-1.06	45	5.94	1.42	-1.84
18	4.35	1.21	-1.04	36	5.95	1.47	-1.82
9	4.25	1.21	-1.09	30	5.96	1.48	-1.81
0	3.81	1.14	-1.04	36	5.96	1.46	-1.84
9	3.59	1.17	-1.09	45	6.08	1.45	-1.88
18	3.91	1.21	-1.13	36	6.07	1.50	-1.84
27	4.25	1.23	-1.23	27	6.08	1.50	-1.84
36	4.53	1.27	-1.30	18	6.06	1.54	-1.81
45	4.89	1.29	-1.41	15	6.04	1.54	-1.81
36	4.93	1.34	-1.43	18	6.03	1.54	-1.83
27	5.02	1.34	-1.44	27	6.01	1.48	-1.88
18	4.95	1.38	-1.43	30	6.04	1.49	-1.88
9	4.85	1.38	-1.44	27	6.04	1.51	-1.87
0	4.50	1.32	-1.45	18	6.07	1.54	-1.82
9	4.59	1.28	-1.47	9	5.97	1.55	-1.80
18	4.81	1.31	-1.50	0	5.47	1.47	-1.77
27	5.05	1.31	-1.57	9	5.46	1.51	-1.80
36	5.29	1.35	-1.62	15	5.62	1.53	-1.80
45	5.62	1.37	-1.67	9	5.67	1.55	-1.78
				0	5.48	1.51	-1.77

[1] Load = p = $\sigma_1 + \sigma_2 + \sigma_3$

APPENDIX D-X

REDUCED UNIT STRAINS FOR PRELIMINARY EXPERIMENT 15. DEVIATORIC STRESS STATE ($\sigma_1:\sigma_2:\sigma_3$ = 2.33:1.67:1.00) SUPERIMPOSED ON A HYDROSTATIC STRESS STATE ($\sigma_1:\sigma_2:\sigma_3$ = 1:1:1)

Cylinder Load[1] (psi)	Unit Strain ϵ_1 (in./in. x 10^2)	ϵ_2	ϵ_3
		Hydrostatic Component	
0	0.00	0.00	0.00
9	0.38	0.64	0.32
18	0.73	0.95	0.66
27	0.97	1.17	0.75
		Deviatoric Component Superimposed	
27 + 3[2]	1.03	1.19	0.79
27 + 6	1.11	1.22	0.79
27 + 12	1.41	1.33	0.79
27 + 18	1.67	1.38	0.78
27 + 24	1.88	1.47	0.76
27 + 18	1.95	1.51	0.78
27 + 12	1.97	1.53	0.79
27 + 6	1.95	1.55	0.80
		Unload Hydrostatic	
27	1.94	1.56	0.81
18	1.94	1.56	0.81
9	1.87	1.50	0.80
0	1.72	1.17	0.64
		Hydrostatic Component (2nd cycle)	
9	1.68	1.23	0.59
18	1.75	1.34	0.63
33	1.85	1.48	0.71
		Deviatoric Component Superimposed (2nd cycle)	
33 + 6	1.91	1.52	0.70
33 + 12	2.06	1.58	0.69
33 + 18	2.21	1.62	0.68
33 + 24	2.37	1.70	0.67
33 + 18	2.40	1.72	0.68
33 + 12	2.41	1.74	0.69
33 + 6	2.40	1.75	0.70
		Unload Hydrostatic (2nd cycle)	
33	2.38	1.74	0.71
18	2.39	1.74	0.72
9	2.33	1.71	0.70
0	2.17	1.44	0.60

[1]Load = p = $\sigma_1 + \sigma_2 + \sigma_3$

[2]First number is the hydrostatic stress level; the second is the deviatoric stress level.

APPENDIX D-XI

REDUCED UNIT STRAINS FOR PRELIMINARY EXPERIMENT 16.
HYDROSTATIC STRESS STATE ($\sigma_1:\sigma_2:\sigma_3 = 1:1:1$)
SUPERIMPOSED ON A DEVIATORIC STRESS
STATE ($\sigma_1:\sigma_2:\sigma_3 = 2.33:1.67:1.00$)

Cylinder Load[1] (psi)	Unit Strain (in./in. x 10^2) ϵ_1	ϵ_2	ϵ_3
		Deviatoric Component	
0 + 0[2]	0.00	0.00	0.00
0 + 3	0.16	0.10	0.05
0 + 6	0.69	0.22	0.05
0 + 12	1.69	0.45	0.08
0 + 18	2.23	0.52	0.06
0 + 24	2.91	0.61	-0.06
		Hydrostatic Component Superimposed	
9 + 24	3.33	0.67	-0.16
18 + 24	3.51	0.80	-0.17
27 + 24	3.65	0.95	-0.16
18 + 24	3.72	0.99	-0.12
9 + 24	3.75	1.02	-0.11
		Unload Deviatoric Component	
0 + 24	3.78	1.00	-0.12
0 + 18	3.82	1.00	-0.14
0 + 12	3.77	1.01	-0.15
0 + 6	3.63	0.94	-0.17
0 + 0	3.50	0.73	-0.18
		Load Deviatoric Component (2nd cycle)	
0 + 6	3.40	0.66	-0.19
0 + 12	3.50	0.72	-0.19
0 + 18	3.65	0.75	-0.21
0 + 24	3.81	0.77	-0.23
		Hydrostatic Component Superimposed (2nd cycle)	
9 + 24	3.90	0.84	-0.28
18 + 24	4.01	0.91	-0.27
27 + 24	4.10	1.00	-0.25
30 + 24	4.15	1.05	-0.23
27 + 24	4.17	1.06	-0.22
18 + 24	4.21	1.09	-0.18
9 + 24	4.23	1.09	-0.17
		Unload Deviatoric Component	
0 + 24	4.26	1.08	-0.19
0 + 18	4.31	1.08	-0.20
0 + 12	4.28	1.10	-0.20
0 + 6	4.21	1.02	-0.22
0 + 0	3.89	0.85	-0.22

[1] Load = $p = \sigma_1 + \sigma_2 + \sigma_3$

[2] The first number is the hydrostatic component; the second number is the deviatoric component.

APPENDIX D-XII

REDUCED UNIT STRAINS FOR PRELIMINARY EXPERIMENT 17.
RADIAL STRESS PATH WITH θ = 30 DEGREES.
R VARIED FROM 0 TO 3 INCHES.

Cylinder Load[1] (psi)	Distance[2] (in.)	Unit Strain ϵ_1 (in./in. x 10^2)	ϵ_2	ϵ_3
0	0	0.00	0.00	0.00
9		0.38	0.32	0.40
18		0.86	0.66	0.71
30		1.05	0.99	0.82
30	0.5	1.15	1.01	0.85
	1.0	1.35	1.03	0.81
	1.5	1.62	1.04	0.75
	2.0	2.12	1.04	0.70
	2.5	3.21	1.05	0.40
	3.0	3.50	1.02	-0.30
	2.0	3.63	1.08	-0.41
	1.0	3.64	1.10	-0.63
	0.0	3.64	1.12	-0.60
	0.5	3.63	1.12	-0.56
	1.0	3.66	1.13	-0.53
	1.5	3.66	1.14	-0.52
	2.0	3.71	1.14	-0.49
	2.5	3.87	1.14	-0.54
	3.0	4.47	1.15	-1.16
	2.0	4.64	1.14	-1.26
	1.0	4.65	1.17	-1.25
	0.0	4.65	1.18	-1.13
	0.5	4.61	1.20	-1.09
	1.0	4.71	1.20	-1.08
	1.5	4.76	1.20	-1.08
	2.0	4.83	1.19	-1.12
	2.5	4.96	1.18	-1.17
	3.0	5.43	1.17	-1.61
	2.0	5.52	1.17	-1.68
	1.0	5.56	1.18	-1.68
30	0.0	5.49	1.19	-1.50
18		5.46	1.26	-1.43
9		5.35	1.25	-1.40
0		5.08	1.06	-1.41
9		5.05	1.07	-1.39
18		5.09	1.12	-1.33
30		5.10	1.17	-1.24

APPENDIX D-XII (Continued)

Cylinder Load[1] (psi)	Distance[2] (in.)	Unit Strain ϵ_1 (in./in. x 10^2)	ϵ_2	ϵ_3
30	0.5	5.13	1.18	-1.21
	1.0	5.18	1.18	-1.20
	1.5	5.27	1.18	-1.23
	2.0	5.37	1.18	-1.29
	2.5	5.56	1.17	-1.44
	3.0	5.84	1.17	-1.67
	2.0	5.90	1.16	-1.74
	1.0	5.93	1.17	-1.75
	0.0	5.88	1.18	-1.64
	0.5	5.87	1.18	-1.61
	1.0	5.86	1.17	-1.59
	1.5	5.89	1.18	-1.58
	2.0	5.91	1.17	-1.50
	1.0	5.94	1.18	-1.64
30	0.0	5.91	1.19	-1.60
18		5.90	1.24	-1.53
9		5.81	1.26	-1.49
0		5.46	1.02	-1.50

[1]Load = p = $\sigma_1 + \sigma_2 + \sigma_3$

[2]Distance the load cylinder is located from the centroid of the stress plate.

APPENDIX E

DATA FOR THE VALIDATION TESTS

APPENDIX E-I

REDUCED UNIT STRAINS FOR THE VALIDATION EXPERIMENTS IN WHICH $\sigma_1:\sigma_2:\sigma_3 = 0.91:0.82:1.00$

Cylinder Load[1] (psi)	Unit Strain: Rep. 1 ϵ_1	ϵ_2	ϵ_3	Rep. 2 ϵ_1	ϵ_2	ϵ_3
	(in./in. x 10^2)			(in./in. x 10^2)		
0	0.00	0.00	0.00	0.00	0.00	0.00
3	0.19	0.12	0.10	0.18	0.15	0.11
6	0.48	0.31	0.25	0.44	0.33	0.27
12	0.87	0.57	0.52	0.83	0.60	0.55
18	1.10	0.73	0.68	1.06	0.73	0.73
24	1.25	0.81	0.82	1.24	0.84	0.89
30	1.40	0.88	0.92	1.38	0.91	1.00
36	1.51	0.94	1.03	1.49	0.98	1.10
42	1.62	0.98	1.11	1.58	1.06	1.19
48	1.72	1.04	1.20	1.69	1.10	1.27
54	1.81	1.10	1.27	1.78	1.16	1.36
60	1.90	1.15	1.36	1.87	1.20	1.44
54	1.91	1.18	1.36	1.89	1.23	1.45
48	1.91	1.19	1.34	1.89	1.24	1.44
42	1.91	1.19	1.33	1.88	1.25	1.43
36	1.91	1.21	1.34	1.89	1.24	1.42
30	1.91	1.20	1.32	1.89	1.25	1.41
24	1.90	1.21	1.29	1.88	1.25	1.39
18	1.89	1.20	1.27	1.86	1.25	1.35
12	1.86	1.19	1.23	1.84	1.23	1.31
6	1.80	1.14	1.17	1.76	1.16	1.23
3	1.74	1.11	1.12	1.71	1.13	1.17
0	1.59	1.01	0.97	1.57	1.03	1.04

[1] Load $= p = \sigma_1 + \sigma_2 + \sigma_3$

VITA

Harvey Bright Manbeck

Candidate for the Degree of

Doctor of Philosophy

Thesis: AN EXPERIMENTAL STUDY OF THE THREE DIMENSIONAL STRESS-STRAIN BEHAVIOR OF WHEAT EN MASSE

Major Field: Agricultural Engineering

Biographical:

Personal Data: Born in West Reading, Berks County, Pennsylvania, January 11, 1942, the son of Elias R. and Pearl M. Manbeck.

Education: Graduated from Conrad Weiser High School, in Robesonia, Pennsylvania, in 1959; graduated from Pennsylvania State University with a Bachelor of Science degree in Agricultural Engineering in 1963; received the Master of Science degree in Agricultural Engineering from Pennsylvania State University in 1965; completed the requirements for the Doctor of Philosophy degree from Oklahoma State University in July, 1970.

Professional Experience: Student Trainee with the Soil Conservation Service in Pennsylvania during the summers of 1962 and 1963; graduate research assistant in the Agricultural Engineering Department, Pennsylvania State University, 1964-1965; Instructor in Agricultural Engineering Department, Pennsylvania State University, 1966; graduate research assistant in the Agricultural Engineering Department, Oklahoma State University, 1966-1970.

Professional Organizations: Associate Member of the American Society of Agricultural Engineers.